



An Introduction to Satellite Laser Ranging Technology and its Applications: Part 1: Technology

Dr. John J. Degnan
SLR School
October 20, 2019
Stuttgart, Germany



PART 1: TECHNOLOGY OVERVIEW



- The Four Space Geodetic Techniques: SLR, VLBI, GNSS, DORIS
- Introduction to Satellite Laser Ranging (SLR)
- The SLR Ground Segment
 - Lasers
 - Detectors
 - Time Interval Units and Event Timers
 - Meteorological Subsystems: Surface pressure, temperature, humidity
- Accuracy Improvement: from meters to millimeters over 5 decades
- The Link Equation
- The SLR Space Segment: Retroreflector Arrays
- A Brief Introduction to Lunar Laser Ranging (LLR)
- Advantages of Single Photon Sensitivity and/or kHz Pulse Rates
- Interplanetary Laser Ranging via Transponders



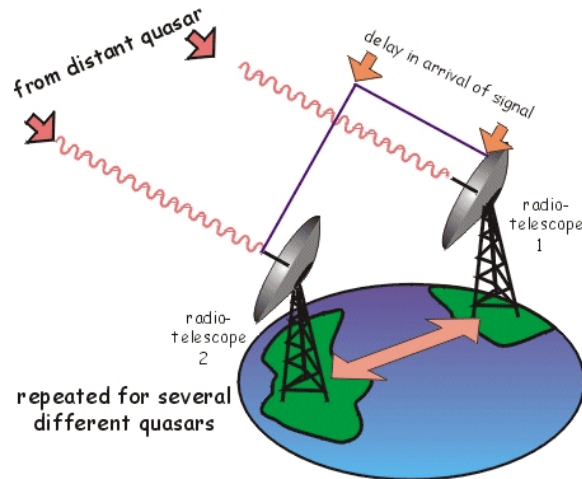
Space Geodetic Techniques



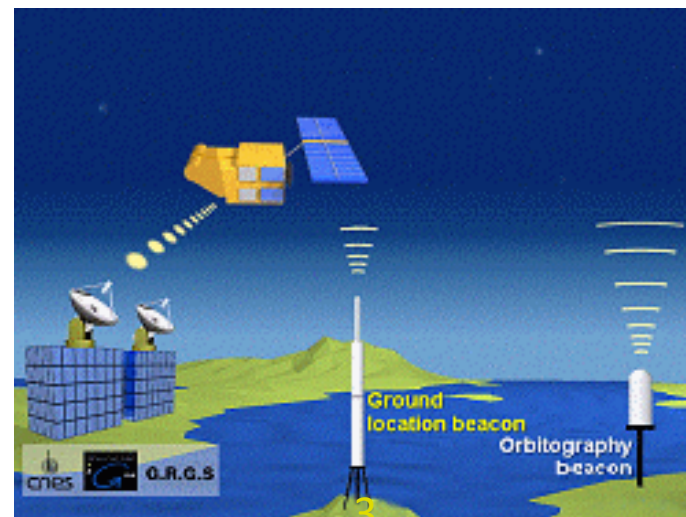
Satellite Laser Ranging



Very Long Baseline Interferometry



Global Navigation Satellite Systems (GNSS)
GPS(USA), GLONASS (Russia), Galileo (ESA)



DORIS (Doppler Orbitography and Radiopositioning Integrated by Satellite)

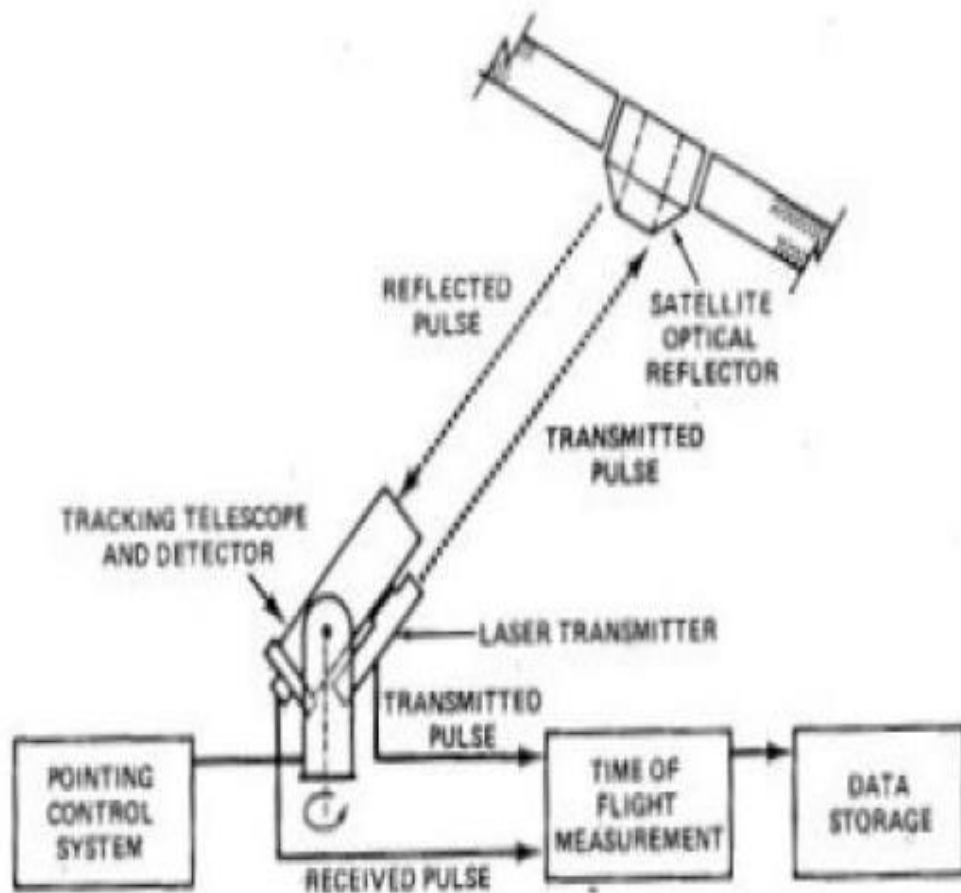


Fig. 1. Satellite laser ranging system concept.

The essential subsystems of an SLR station are:

A laser which generates a train of short pulses of light

A telescope, tracking gimbal and control system to point the laser beam at the satellite and collect the light from the retroreflectors.

A fast detector sensitive enough to see the weak signal return from the satellite retroreflector array.

A Time of Flight (TOF) receiver which records the times of departure and reception of the laser pulse using an accurate clock.

A meteorological station (not shown) to record local surface pressure, temperature, and relative humidity to be input to atmospheric models that provide TOF corrections.

A data storage unit to collect and store all of the above data.



SATELLITE LASER RANGING - 1964

Code 524 SLR Team

Dr. Henry H. Plotkin

Thomas S. Johnson*

Paul L. Spadin*

John E. Moye

Walter J. Carrion*

Nelson McAvoy*

Sol Howard Genatt*

Louis O. Caudill

Peter O. Minott

Herbert L. Richards*

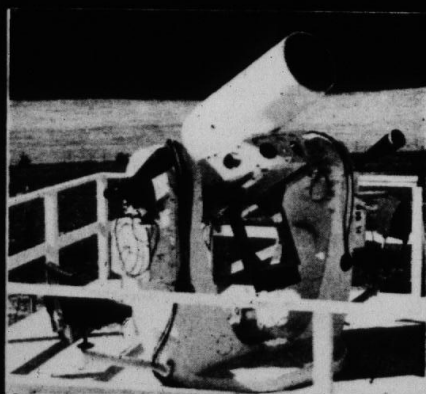
Michael W. Fitzmaurice

John J. Degnan

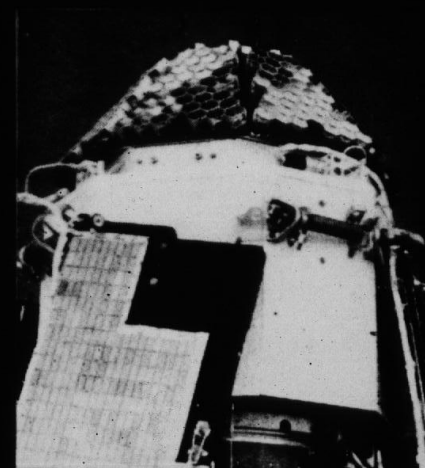
Ed Reid

Charles J. Peruso

Hal Walker*



TRANSMITTING LASER AND RECEIVING TELESCOPE, MOUNTED ON A MODIFIED NIKE-AJAX RADAR PEDESTAL.



THE BEACON EXPLORER-B SATELLITE WITH ARRAY OF CUBE-CORNER REFLECTORS.

*** Deceased**



SLR Technology in the 1960s



- Laser: Rotating Mirror Q-switched Ruby (694 nm –red beam)
 - Energy: 0.8 J
 - Pulwidth: 20 nsec
 - Repetition Rate:1 Hz
- Detector: 9558A Photomultiplier – standard dynode chain characterized by large variations in electron propagation paths and large transit time jitter which degraded range precision
- Telescope: 16 inch primary guided by two operators on elevation and azimuth joysticks following sunlit satellite image
- No daytime ranging until 1969 when GSFC's Don Premo introduced computer control of the tracking mount.
- Ranging Accuracy: 3 to 1 m (compared to 50 to 75 m for best microwave radars of the period)
- **First generation trailer-based Mobile Laser systems were developed by GSFC (MOBLAS 1 through 3)**



Maximizing the Range Accuracy



We maximize the individual range measurement accuracy by minimizing the variance in the pulse Time Of Flight (TOF) measurement which is the sum of the variances introduced by the individual subsystems, including the space target, and given by.

$$\sigma_{Total}^2 = \sigma_{Laser}^2 + \sigma_{Detector}^2 + \sigma_{Timer}^2 + \sigma_{Space}^2$$

Analysts determining the satellite orbits average over N individual “Full Rate Measurements” to form “Normal Points” for a segment of the orbital arc which have an improved range precision given by

$$\Delta R_{NP} = \frac{\sigma_{Total}}{\sqrt{N}}$$

Thus, as the laser pulse frequency increases, the faster we can achieve the desired normal point range precision. In addition, the resulting normal point represents a shorter orbital arc length and a higher resolution orbit.



Range Errors Caused by the Atmosphere

J. Degnan, Millimeter Accuracy Satellite Laser Ranging: A Review, Geodynamic Series Vol. 25, Contributions of Geodesy to Geodynamics, 1993



In addition to instrumental and satellite induced range errors, we have to compensate for few meter level changes in the measured range due to a decreasing atmospheric index of refraction n with altitude which results in changes in the pulse group velocity given by c/n and the deviation of the light path from a straight line. The Marini-Murray model assumes the atmosphere consists of thin spherical shells governed by the equations for hydrostatic equilibrium, the law of partial pressures, and the perfect gas law.

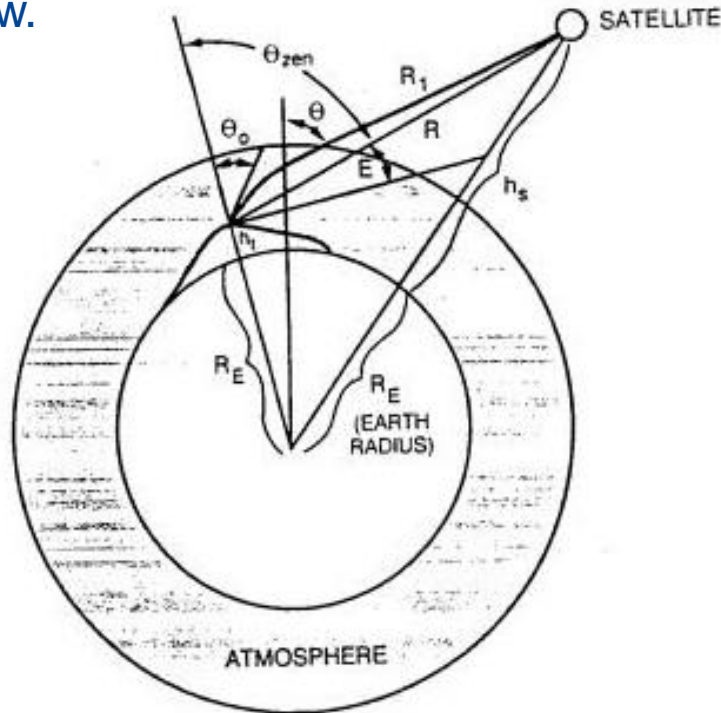


Fig. 15. Coordinate system used in the discussion of atmospheric refraction and the spherical shell model.

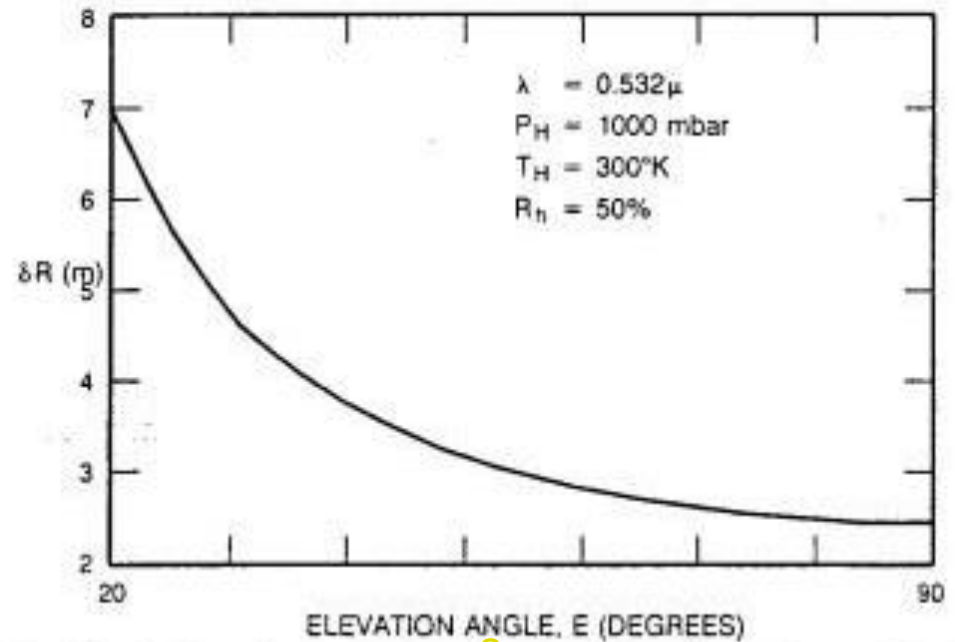


Fig. 16. Single color range correction versus elevation angle as predicted by the Marini-Murray spherical shell model for a wavelength of 532 nm and nominal surface meteorological parameters.



NGSLR Meteorological Station



Wind Monitor

- Belfort-Young Model 05103
- Wind speed -Range: 0 to 135 mph;
Accuracy: ± 0.6 mph
- Wind Direction: Range: 0 to 360°;
Accuracy: $+3^\circ$

Pressure/Temperature/Humidity Monitor

- Paroscientific MET3-1477-001
- Pressure:Range: 800 to 1100 mbar;
Accuracy: ~ 0.1 mbar; stability <0.1 mbar/yr
- Temperature: Range: -40 to 70
 $^\circ\text{C}$; Accuracy <0.5 $^\circ\text{C}$; Stability <0.1 $^\circ\text{C}/\text{yr}$;
- Relative Humidity: Range: 0 to 100%;
accuracy: $\pm 2\%$; stability: $<1\%/\text{yr}$

GPS Antenna

- Receives timing signals from GPS constellation to update Rubidium Frequency Standard and Station Clock

Security Camera



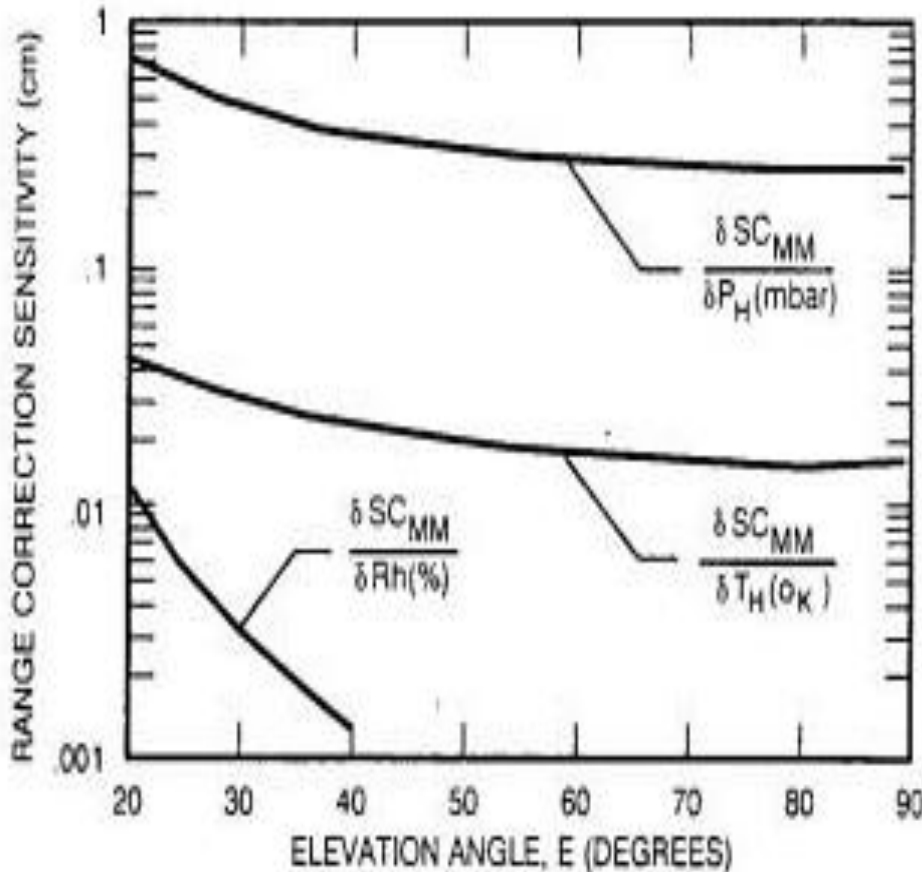


Fig 17. Sensitivity of the Marini-Murray range correction to measurement errors in surface pressure, temperature, and humidity.

Pressure/Temperature/Humidity Monitor

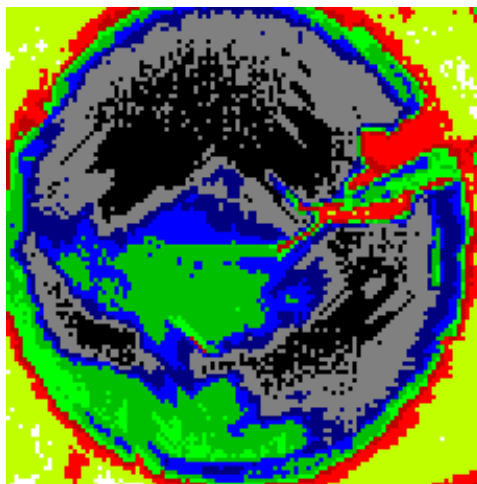
- Paroscientific MET3-1477-001

- Pressure:** Range: 800 to 1100 mbar; Accuracy: ~0.1 mbar (0.3mm to 0.7mm) ; stability<0.1 mbar/yr

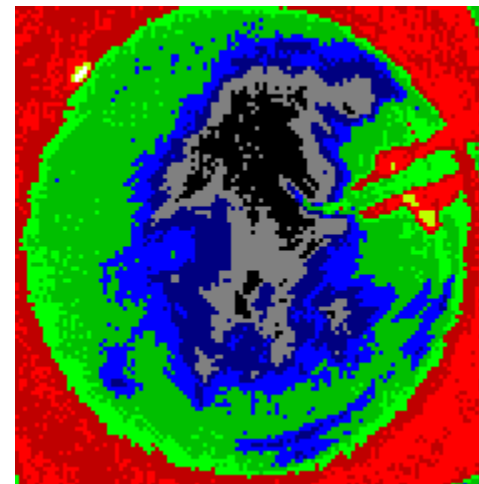
- Temperature:** Range: -40 to 70 °C; Accuracy<0.5 °C (0.008mm to 0.025mm); Stability accuracy:±2%(<0.2 mm) <0.1 °C/yr;

- Relative Humidity:** Range: 0 to 100%; stability: <1%/yr (<0.1mm/yr)

Uncooled IR Camera



Daytime thermogram shows clear (cooler) skies to the north and east. A cloud (warmer) covers zenith and extends to the southwest. The red object in the northeast is a support arm. Temperatures are 17 to 33 °C.



Nighttime thermogram reveals a large patch of clear sky at zenith, extending to the north and south. The east and west are cloudy. Temperature range is 4 to 21 °C.

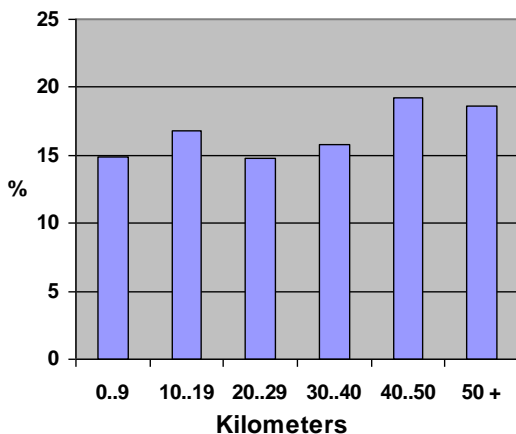
Color codes:

warmer = blue, green and red 11
cooler = gray and black.

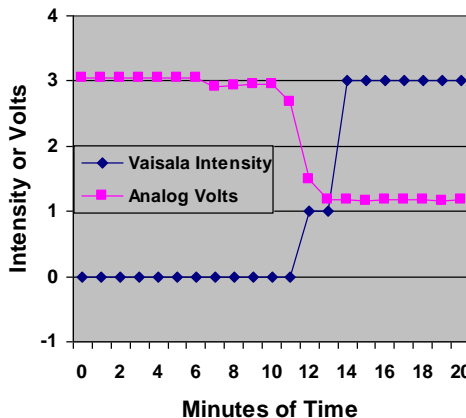


The Vaisala optics are comprised of an infrared beam and a detector aimed across the beam. Scattering particles in the intersection of the two paths reflect IR light to the detector. These reflections are analyzed and the particles are characterized. The CPU combines this information with temperature data, reports the type and intensity of precipitation, as well as the visibility, and decides whether the dome should be open or closed.

Histogram of Visibility



Precipitation Detection



The Vaisala reports precipitation within 2 to 3 minutes of its detection by a sensitive analog device, allowing time to close the dome and protect the equipment.

Visibility is defined as the distance that an observer can distinguish a black object against the horizon. At NASA/GSFC, the Vaisala instrument reports a fairly even distribution from 0 to 50 km over a year's time.



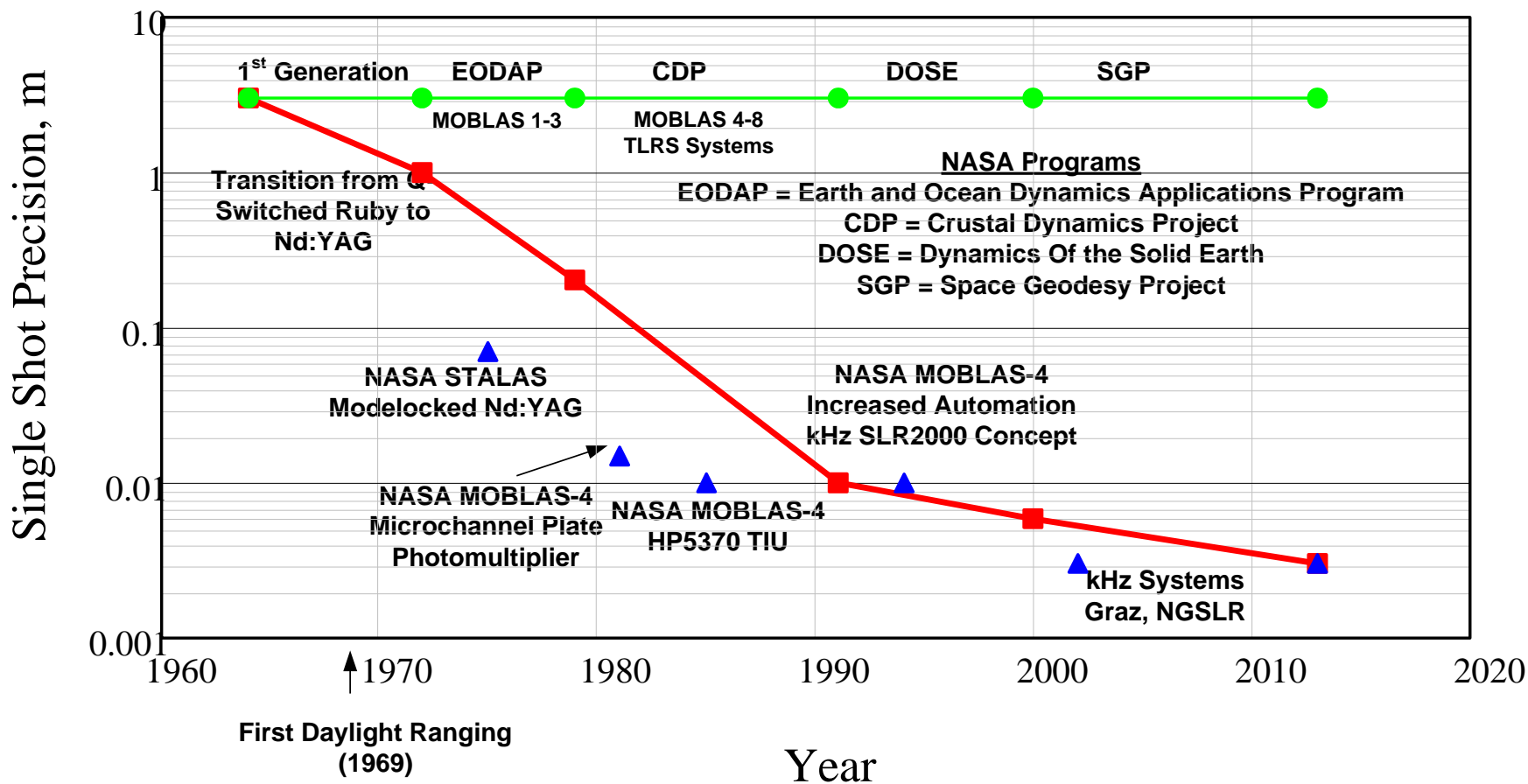
Maximizing Ground Segment Range Precision



- Minimize laser pulsewidth
 - 1964: Q-switched ruby lasers at 694.3 nm (red) with 20 nsec FWHM pulsewidth
 - 2019: Frequency-doubled modelocked Nd:YAG lasers at 532 nm (green) with FWHM pulsewidths <100 psec
- Increase laser pulse rate to accelerate accurate normal point generation and maximize satellite coverage
 - 1964: 1 Hz
 - 2019: 2000 Hz
- Use fast, low variance (<300 psec) detectors
 - 1964: Dynode Chain PhotoMultiplier Tubes (PMTs) had large electron path variations which degraded accuracy
 - 2019: Microchannel Plate PhotoMultiplier Tubes (MCP/PMTs), Single Photon Avalanche Photodiodes (SPADs), or Compensated SPADs (C-SPADs)
- Use high precision (few psec) timers with multistop capability
 - 1964: Single stop Time Interval Units (TIUs) could only make range measurements serially (i.e. single pulse in flight) and therefore limited the rate at which satellite normal point data could be acquired
 - 2019: Multistop Event Timers (ETs) allow rapid recording of overlapping start and stop events when multiple pulses are simultaneously in flight thereby permitting high altitude satellite tracking at kHz laser pulse rates and reducing the time required for high accuracy Normal Point generation
- Use optimized atmospheric models and high accuracy meteorological measurements (pressure, temperature, and humidity) as inputs for pulse TOF corrections as determined by the Marini-Murray model. More accurate atmospheric models exist for satellite elevation angles below 20 degrees.
 - 1964: Accuracy not particularly relevant due to large instrument errors in the 1 to 3 m range.
 - 2019: Essential to achieve current GGOS goal of 1 mm accuracy normal points



Representative SLR Precision vs Time



Red Curve = nominal best International SLR Network accuracies vs time

Blue Triangles = key station experiments that eventually led to improved network range performance



SLR Link Equation



$$n_s = \frac{E_t}{h\nu} \eta_t \frac{2}{\pi(\theta_d R)^2} \exp\left[-2\left(\frac{\Delta\theta_p}{\theta_d}\right)^2\right] \left[\frac{1}{1 + \left(\frac{\Delta\theta_j}{\theta_d}\right)^2} \right] \left(\frac{\sigma A_r}{4\pi R^2} \right) \eta_r \eta_c T_a^2 T_c^2$$

n_s = detected satellite photoelectrons per pulse

E_t = laser pulse energy

$h\nu$ = laser photon energy = 3.73×10^{-19} J @ 532 nm (Doubled Nd:YAG)

η_t = transmitter optical throughput efficiency

θ_d = Gaussian beam divergence half angle

R = slant range between station and satellite (signal decreases as $1/R^4$)

$\Delta\theta_p$ = laser beam pointing error

$\Delta\theta_j$ = RMS tracking mount jitter

σ = satellite optical cross-section = sole link contribution of space segment

A_r = Telescope Receive Area.

η_r = receiver optical throughput efficiency

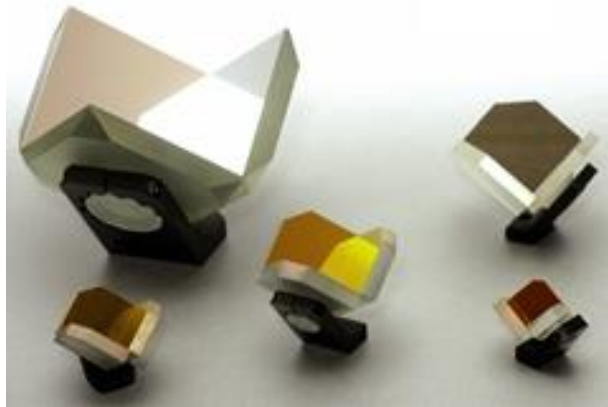
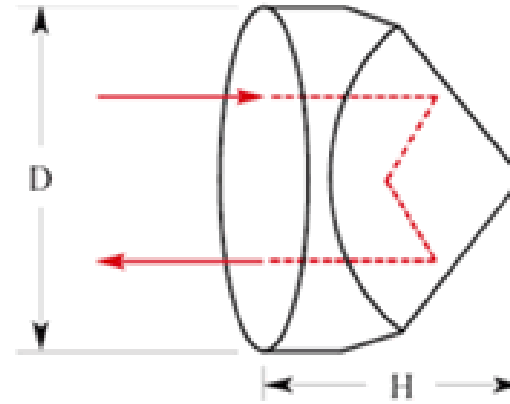
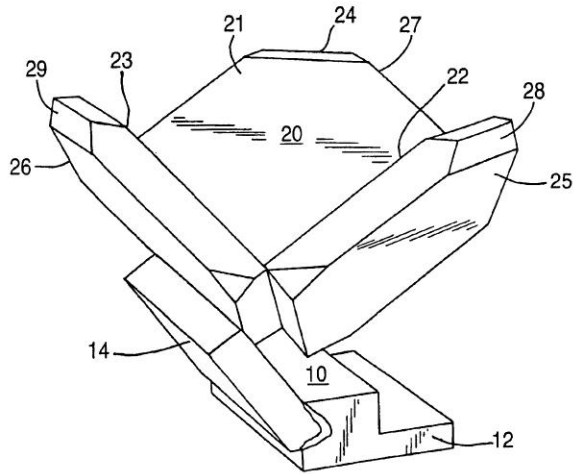
η_c = detector counting efficiency

T_a = one way atmospheric transmission

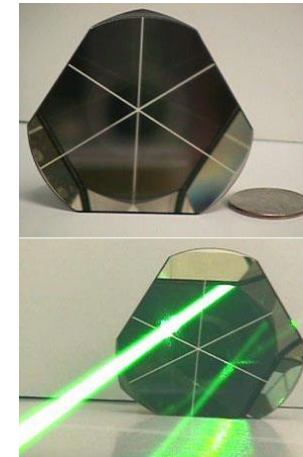
T_c = one way cirrus cloud transmission

To maintain the same signal strength, the satellite cross-section must increase as R^4

*Reference: J. Degnan, "Millimeter Accuracy Satellite Laser Ranging: A Review", in Contributions of Space Geodesy to Geodynamics: Technology Geodynamics, 25, pp. 133-162, 1993.



Hollow Cube Corner



Solid Cube Corner

Cube corner retroreflectors reflect light back to the point of origin in a narrow beam. Increasing the size and/or number of reflectors increases the return signal strength.



Three Types of Cube Corners



Type	Al Back-Coated Solid	Uncoated Solid (TIR)	Hollow
Frequency of Use	Most Common	Occasional Use	Not currently used in the visible
Satellite Examples	Most satellites	Apollo, LAGEOS, AJISAI, ETS-VIII	ADEOS RIS, REM, TES
Reflectivity, ρ	0.78	0.93	Can approach 1.0
Polarization Sensitive	No	Yes	No – metal coating Yes-dielectric coating
Weight	Heavy	Heavy	Light
Far Field Pattern	Wide	Wide	Narrow
Issues	Metal coatings absorb sunlight and create thermal gradients. Not as well shielded at high orbital altitudes.	Fewer thermal problems but TIR “leaks” at incidence angles $> 17^\circ$. Polarization effects reduce cross-section by factor of 4.	Thermal heating and gradient effects on joints



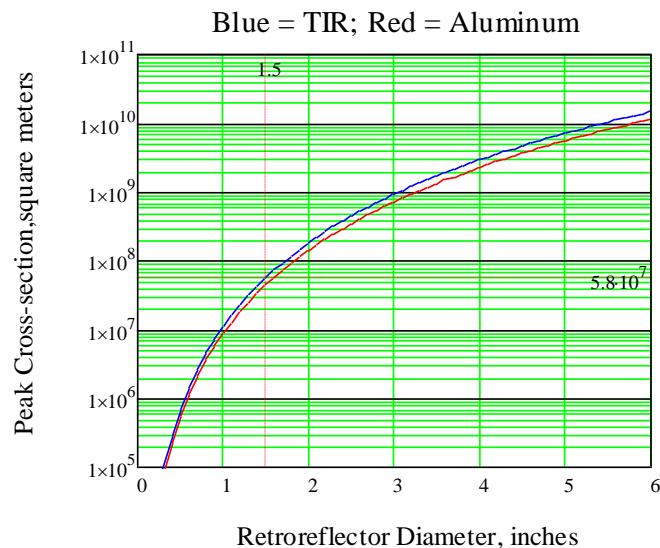
Peak Cross-Section of a Perfect Cube Corner



For normally incident light, a single unspoiled retroreflector (cube corner) has a peak, on-axis, optical cross-section defined by

$$\sigma_{cc} = \rho A_{cc} \left(\frac{4\pi}{\Omega} \right) = \rho \left(\frac{4\pi A_{cc}^2}{\lambda^2} \right) = \frac{\pi^3 \rho D^4}{4\lambda^2}$$

where the reflectivity of the cube corner, ρ , is typically equal to 0.78 or 0.93 for aluminum-coated back faces and uncoated Total Internal Reflection (TIR) surfaces respectively, A_{cc} is the collecting aperture of the corner cube, D is the cube diameter, and $4\pi/\Omega$ is the on-axis reflector gain and Ω is the effective solid angle occupied by the Far Field Diffraction Pattern (FFDP) of the retroreflector.



The peak optical cross-section rises rapidly as the retroreflector diameter to the fourth power. For the popular 1.5 in (38 mm) diameter cube with a physical cross-section of 0.001m², the peak optical cross-section is about 5.8 x 10⁷ m², an increase of over ten orders of magnitude.



Retroreflector Far Field Diffraction Pattern(FFDP)



For a uniformly illuminated circular aperture, the FFDP of the reflected wave is the familiar Airy Function given by

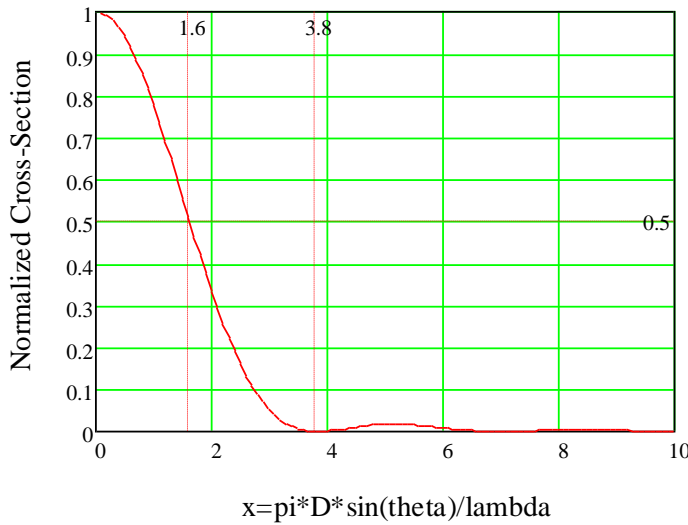
$$\sigma(x) = \sigma_{cc} \left[\frac{2J_1(x)}{x} \right]^2$$

where $J_1(x)$ is a Bessel function and the argument x is related to the off-axis angle θ by

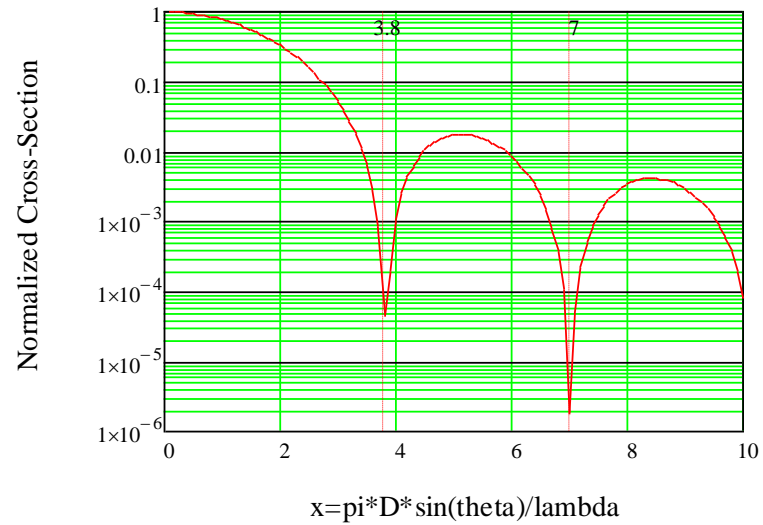
$$x = \frac{\pi D}{\lambda} \sin \theta$$

$\lambda = 532 \text{ nm}$ is the most widely used SLR laser wavelength, and D is the cube aperture diameter.

Normalized Cross-Section vs Angle Theta



Normalized Cross-Section vs Angle Theta



The half-power and first null occur at $x = 1.6$ and 3.8 respectively. For the popular 1.5 in (38 mm) diameter cube at 532 nm, this corresponds to $\theta = 7.1$ and 16.9 microradians (1.5 and 3.5 arcsec) respectively.



Peak Cross-Section vs Incidence Angle (Hollow Cube vs Coated Fused Silica)



At arbitrary incidence angle, θ_{inc} , the effective area of the cube is reduced by the factor

$$\eta(\theta_{inc}) = \frac{2}{\pi} (\sin^{-1} \mu - \sqrt{2} \tan \theta_{ref}) \cos \theta_{inc}$$

where θ_{inc} is the incidence angle and θ_{ref} is the internal refracted angle as determined by Snell's Law, i.e.

$$\theta_{ref} = \sin^{-1} \left(\frac{\sin \theta_{inc}}{n} \right)$$

where n is the cube index of refraction. The quantity μ is given by the formula

$$\mu = \sqrt{1 - \tan^2 \theta_{ref}}$$

Thus, the peak optical cross-section in the center of the reflected lobe falls off as

$$\sigma_{eff}(\theta_{inc}) = \eta^2(\theta_{inc}) \sigma_{cc}$$

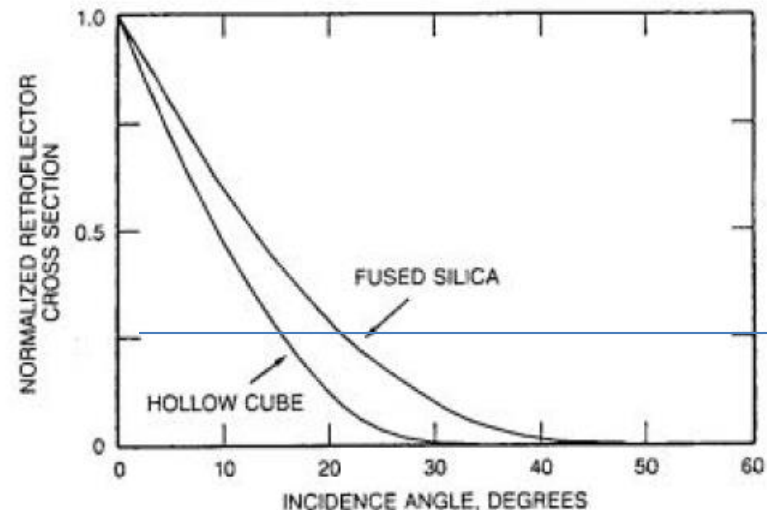


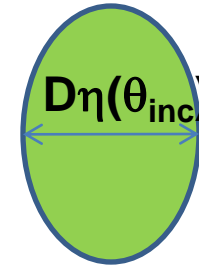
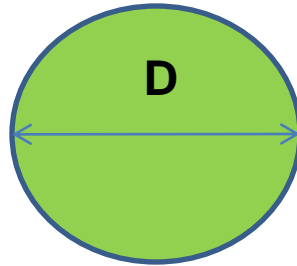
Fig. 23. Normalized cross-section as a function of incidence angle for hollow and fused silica retroreflectors.

- The 50% and 0% efficiency points for fused silica ($n=1.455$) are 13° and 45° respectively.
- The 50% and 0% efficiency points for a hollow cube ($n=1$) are 9° and 31° respectively.
- In short, hollow cubes have a narrower angular response range than solid cubes.

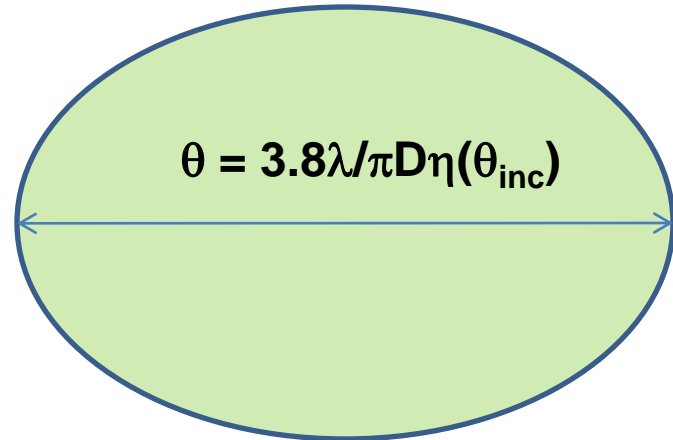
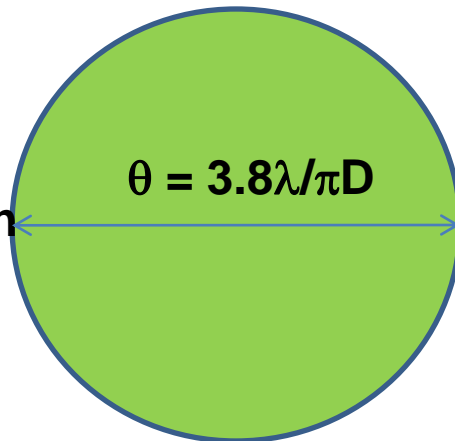
Normal Incidence

Non- Normal Incidence

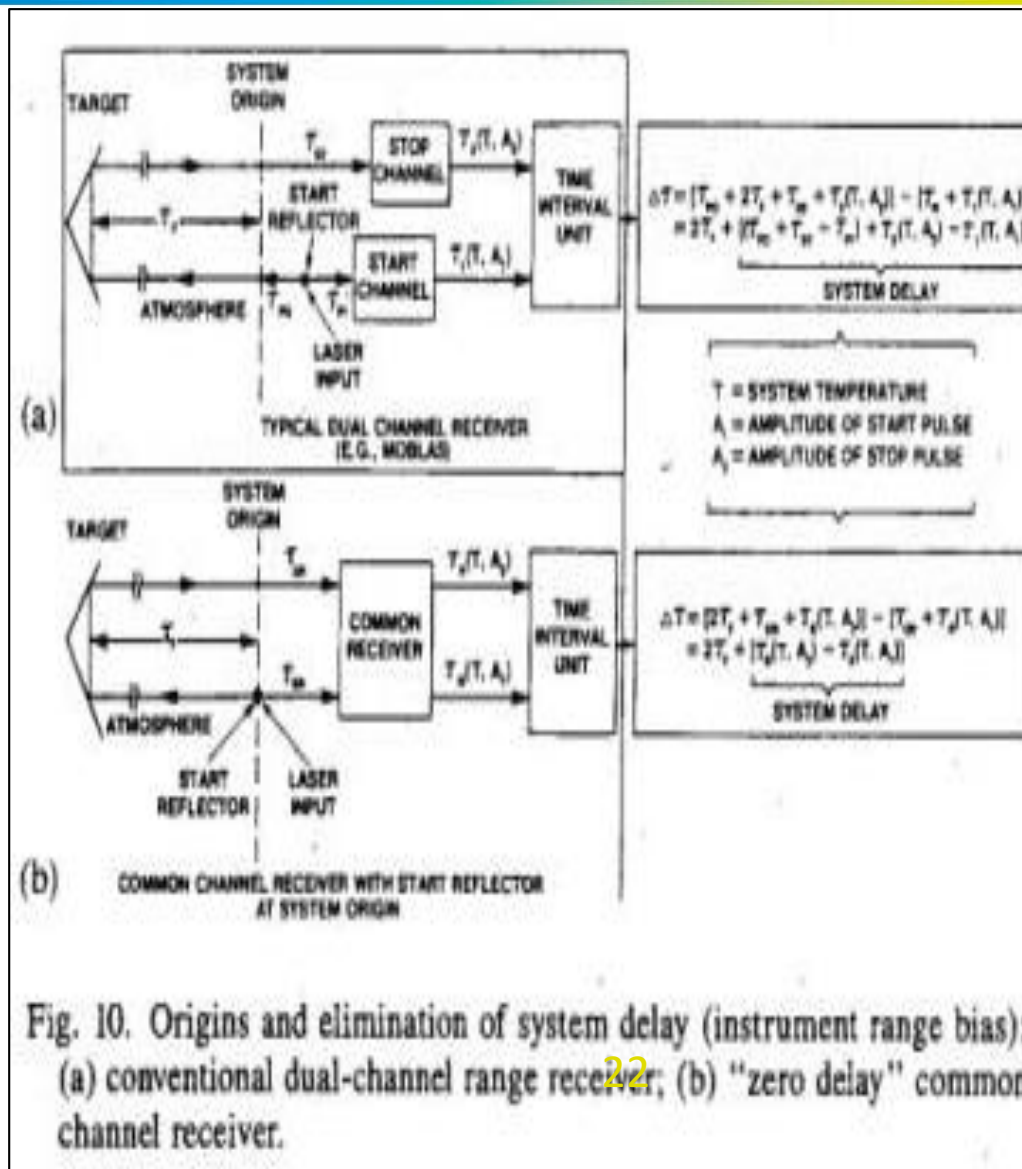
Retro Face Seen by Incident Radiation



Far Field Diffraction Pattern



All SLR stations make use of a calibration scheme to initially determine, and then monitor changes in, optical and/or electronic system delays that might be caused by changes in hardware or environmental conditions (e.g. temperature). The most common approach is to place a single retroreflector at some carefully measured distance from the system “invariant point”, defined as the intersection of the elevation and azimuth axes of the telescope assembly. The retro acts as a point source with a delta function response. This distance is usually measured at the 1 or 2 mm level using accurate ground surveying techniques. Subtracting the known target range from the measured range provides a “range correction” which is then applied to all future satellite measurements. For maximum accuracy, calibrations are typically performed hourly.





Starlette and LAGEOS*



Since, for maximum accuracy orbit determination, the distance of the effective light reflection point from the satellite center of mass is ideally independent of the viewing angle, geodetic satellites are typically spheres embedded with retros. Furthermore, since the signal strength decreases with satellite range as $1/R^4$, the sphere diameter is increased to accommodate more retros and meet cross-section (signal strength) requirements.



Starlette

CNES, France

Launch: 1975

Diameter: 24 cm

Number of Retros: 60



LAGEOS

NASA, USA

Launch: 1976

Diameter: 60 cm

Number of Retros: 426 (4 Ge for NIR)

* LAGEOS-2 (Italy) was launched from the NASA Space Shuttle in 1992.

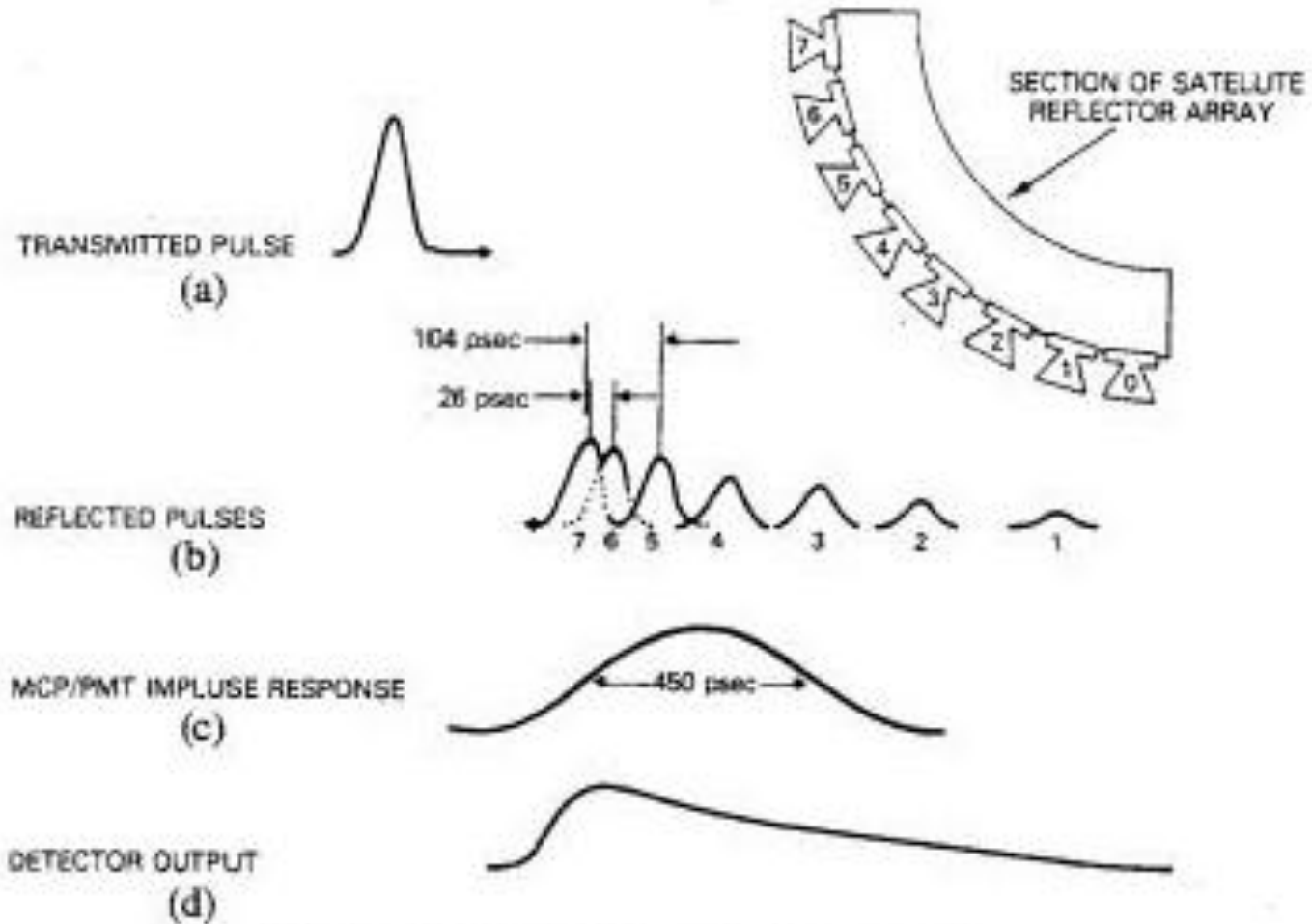


Fig. 9. LAGEOS induced pulse spreading.

Note that the satellite impulse response (range variance) will vary slightly depending on where the line of sight between the station and the satellite CoM falls within the array.

In the following graph, τ is a time normalized to the time it takes a light pulse to travel the diameter of the satellite, i.e. $2R_s/c$. Increasing the radius of the satellite to make it appear flatter will increase the cross-section but broaden the impulse response. However, narrowing the incidence angle response by using hollow cubes or recessing the solid cubes reduces the width of the satellite impulse response (range variance) and improves range accuracy. However, the larger satellite radius increases the number of retros illuminated by the laser and hence the effective cross-section.

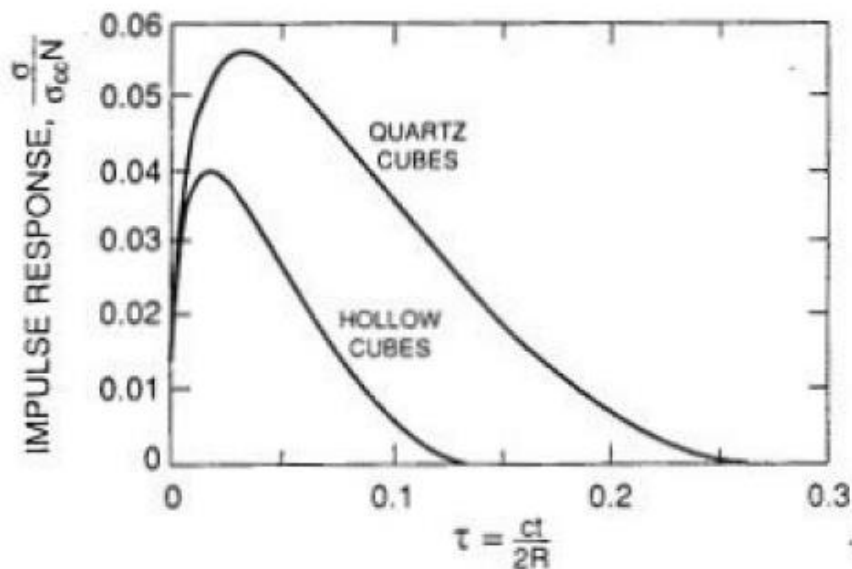
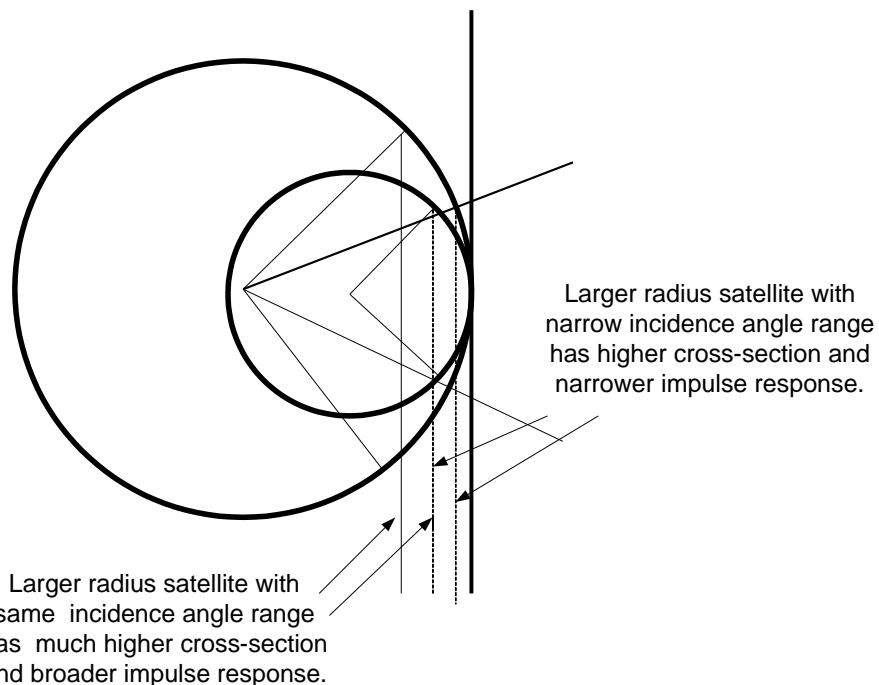
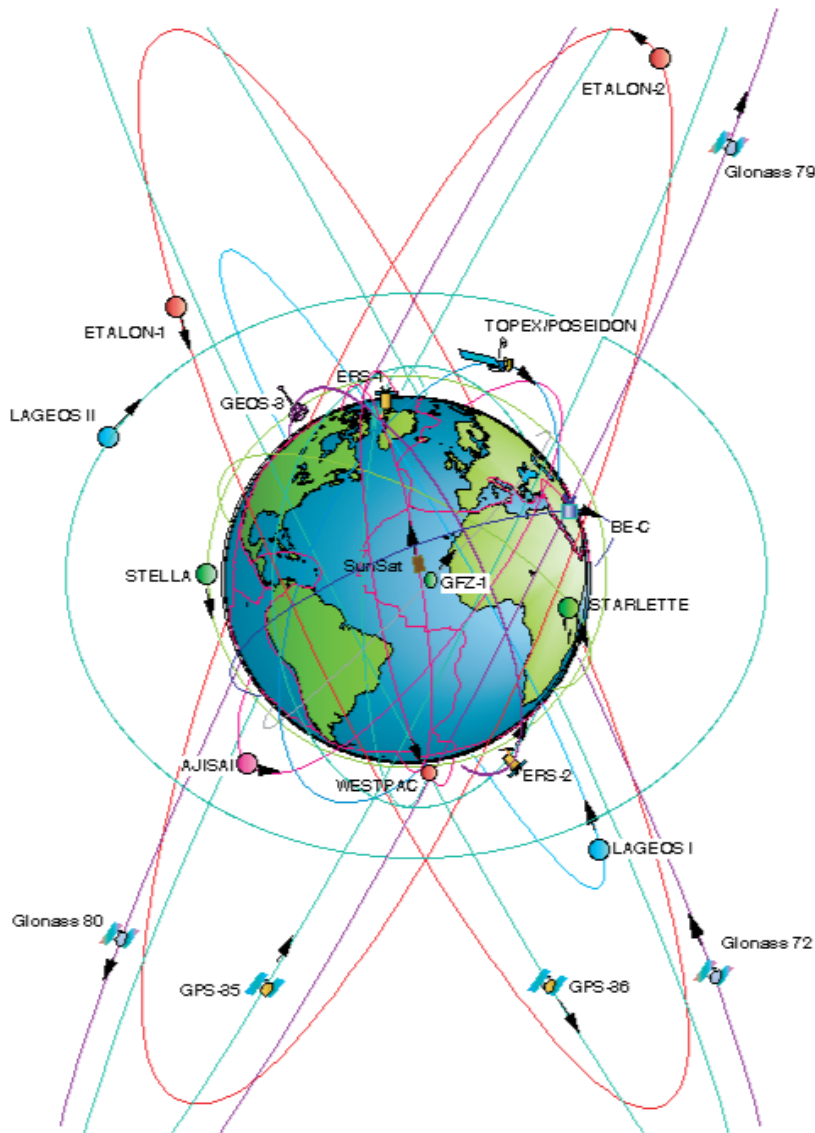


Fig. 27. Impulse response in the large satellite limit ($R_s \gg nL$) for both hollow and solid quartz cube corners.



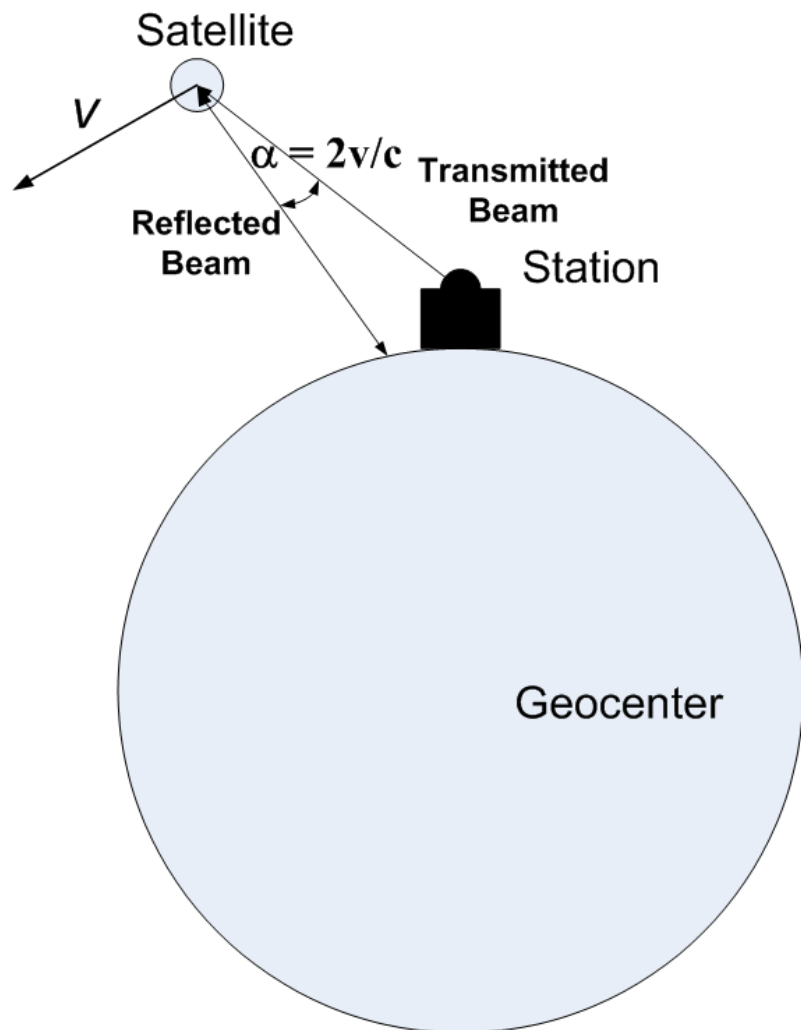


SLR Missions and Orbits



The current SLR constellation spans a wide range of altitudes (500 km to 36,000 km) and inclinations and each retroreflector array has to be designed accordingly based on orbital altitude, mission goals, desired signal strength, etc. The satellites typically fall into four altitude realms with very different science goals:

1. Low Earth Orbiting (LEO: $h < 1,500$ km)
Higher Order Gravity Field Studies
Spaceborne Radar/Lidar Orbital Support for observing terrain, sea/ice levels, etc.
2. Medium Earth Orbiting (MEO: $h \sim 6,000$ km)
Low drag MEO satellites such as LAGEOS 1 and 2 are ideal for observing relative station positions, tectonic plate motion, regional crustal deformation, etc.
3. Global Navigation System Satellites (GNSS: $h \sim 20,000$ km)
SLR provides Orbital support to International Navigation Constellations such as GPS (US), GLONASS (Russia), GALILEO (EU), COMPASS/BeiDou (China), etc and enhances the accuracy of GNSS orbits and ground networks
4. Geosynchronous (GEO: $h \sim 36,000$ km)



- If there is no relative velocity between the station and satellite, the beam reflected by the retroreflector will fall directly back onto the station .

- However, a relative velocity, v , between the satellite and station causes the reflected beam to be angularly deflected from the station in the forward direction of the satellite motion by an angle

$$\alpha = 2v/c.$$

- Since small diameter cubes have small optical cross-sections but large angle FFDPs , the signal at the station is not significantly reduced by velocity aberration.

- On the other hand, large diameter cubes with high cross-sections have small angle FFDPs, and the signal at the station is therefore substantially reduced by velocity aberration.

- In general, the signal is reduced by half or more if the cube diameter, D_{cc} , satisfies the inequality

$$D_{cc} > D_{1/2} = \frac{1.6\lambda}{\pi\alpha} = \frac{0.8\lambda c}{\pi v}$$



Velocity Aberration vs Orbital Altitude



J. Degnan, Contributions of Space Geodesy to Geodynamics: Technology, Geodynamics 25, pp. 133- 162 (1993)

If there is a relative velocity between the satellite and the station, the coordinates of the FFDP are translated in the direction of the velocity vector. The magnitude of the angular displacement in the FFDP is given by

$$\alpha(h_s, \theta_{zen}, \omega) = \alpha_{\max}(h_s) \sqrt{\cos^2 \omega + \Gamma^2(h_s, \theta_{zen}) \sin^2 \omega}$$

where the maximum and minimum values are given by

$$\alpha_{\max}(h_s) = \alpha(h_s, 0, 0) = \frac{2v_s}{c} = \frac{2}{c} \sqrt{\frac{gR_E^2}{R_E + h_s}}$$

$$\alpha_{\min}(h_s) = \alpha(h_s, 70^\circ, 90^\circ) = \alpha_{\max}(h_s) \Gamma(h_s, 70^\circ)$$

$$\Gamma(h_s, \theta_{zen}) = \sqrt{1 - \left(\frac{R_E \sin \theta_{zen}}{R_E + h_s} \right)^2} < 1$$

$$\omega = \cos^{-1} \left[\left(\hat{r} \times \hat{p} \right) \cdot \hat{v} \right]$$

v_s = satellite velocity at altitude h_s

R_E = Earth radius = 6378 km

g = surface gravity acceleration = 9.8m/sec²

h_s = satellite height above sea level

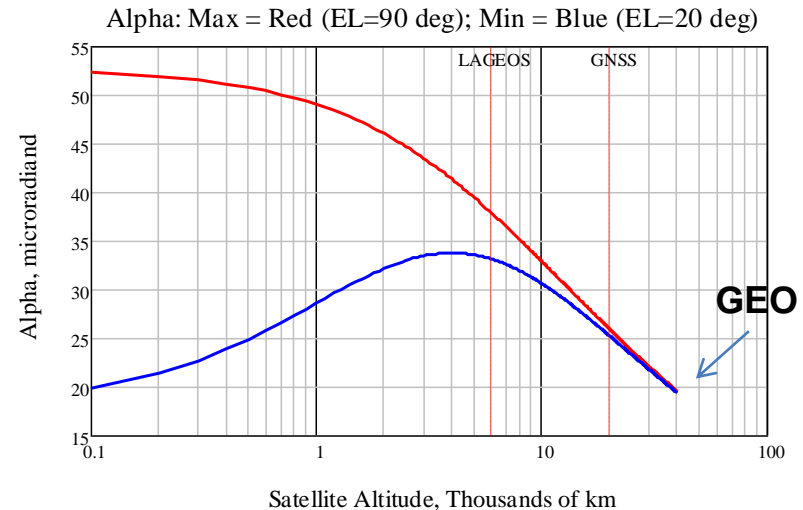
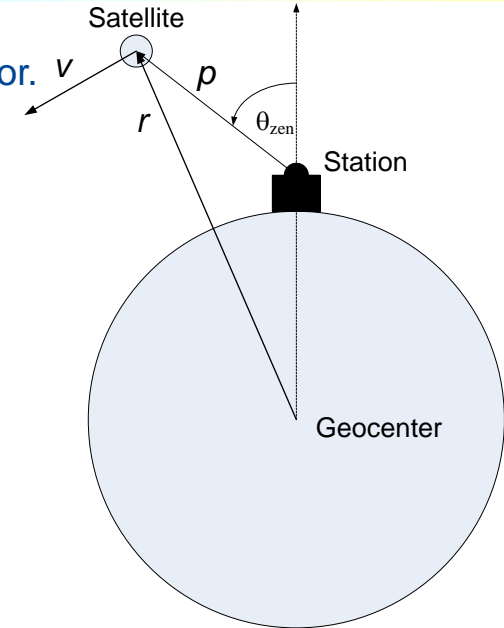
c = velocity of light = 3x10⁸ m/sec

θ_{zen} = largest satellite zenith angle for tracking = 70°

r = unit vector to satellite from the geocenter

p = unit vector from station to satellite

v = unit vector in direction of satellite velocity





“Spoiled” Retroreflectors



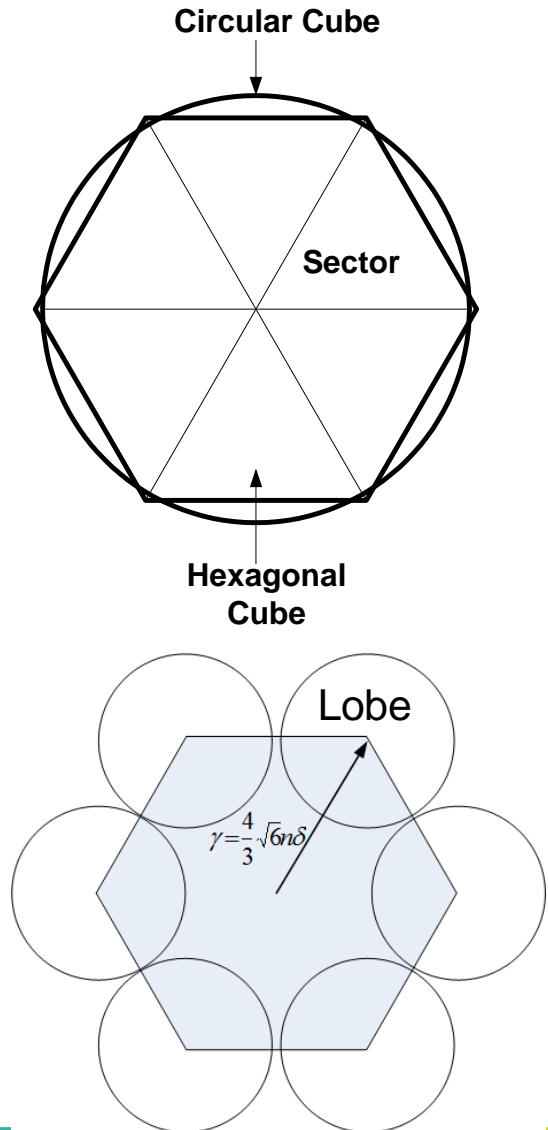
- “Spoiling” is used to compensate for velocity aberration and improve the signal return from the satellite.
- If we offset one or more ($N = 1$ to 3) of the cube dihedral angles from 90° by an amount δ , the central lobe of the FFDP splits into $2N$ spots.
- If n is the cube index of refraction, the mean angular distance of the lobe from the center of the original Airy pattern increases linearly with the dihedral angle offset, δ , according to

$$\gamma = \frac{4}{3} \sqrt{6} n \delta = 3.27 n \delta$$

- As before, the angular size of any given lobe decreases as the cube diameter gets larger.
- The FFDP of each lobe is the 2D Fourier transform of an individual 60° sector. The energy distribution is complex but has hexagonal symmetry if all three δ s are equal.
- Furthermore, the effective area and peak cross-section of each lobe is reduced to

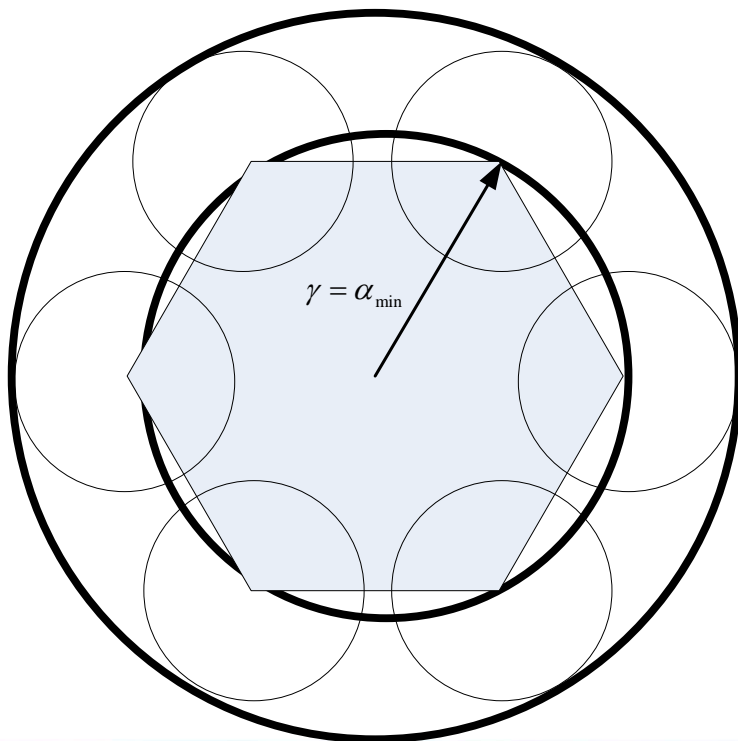
$$A_{eff} = \eta(\theta_{inc}) \frac{A_{cc}}{2N}$$

$$\sigma_{peak} = \eta^2(\theta_{inc}) \frac{\sigma_{cc}}{(2N)^2}$$

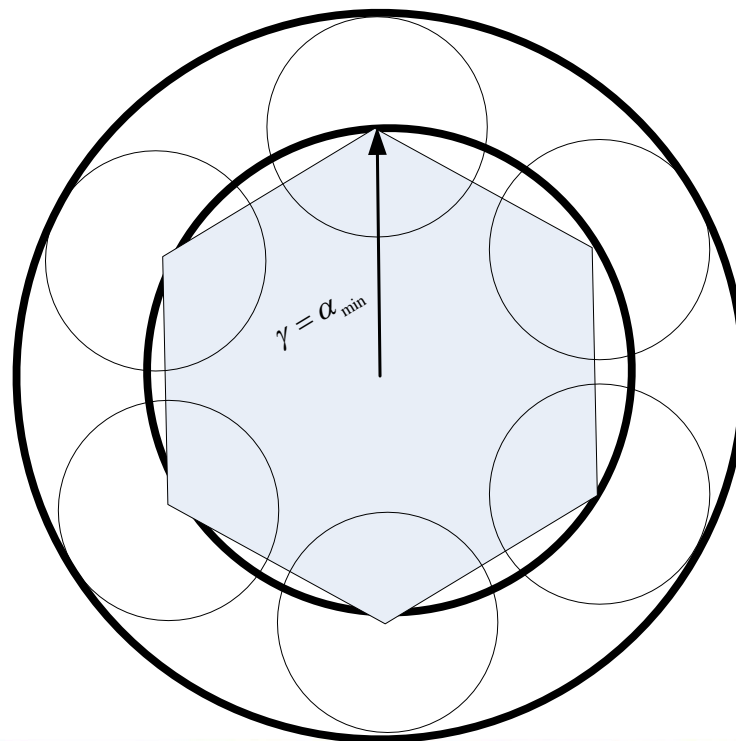


Since the return signal is weakest at the lowest elevation tracking angle, choosing $\gamma = \alpha_{\min}$ places the peak of the lobe there but any lobe energy inside the inner dark ring is wasted. Filling in circumferential gaps between lobes can be accomplished by rotating an adjacent cubes by an angle equal to 60° divided by an integer greater than 1. A smaller lobe diameter will reduce the spillover into the region outside the outermost dark circle but will also create a larger gap between lobes which in turn requires more clocking positions.

0° Clocking



30° Clocking

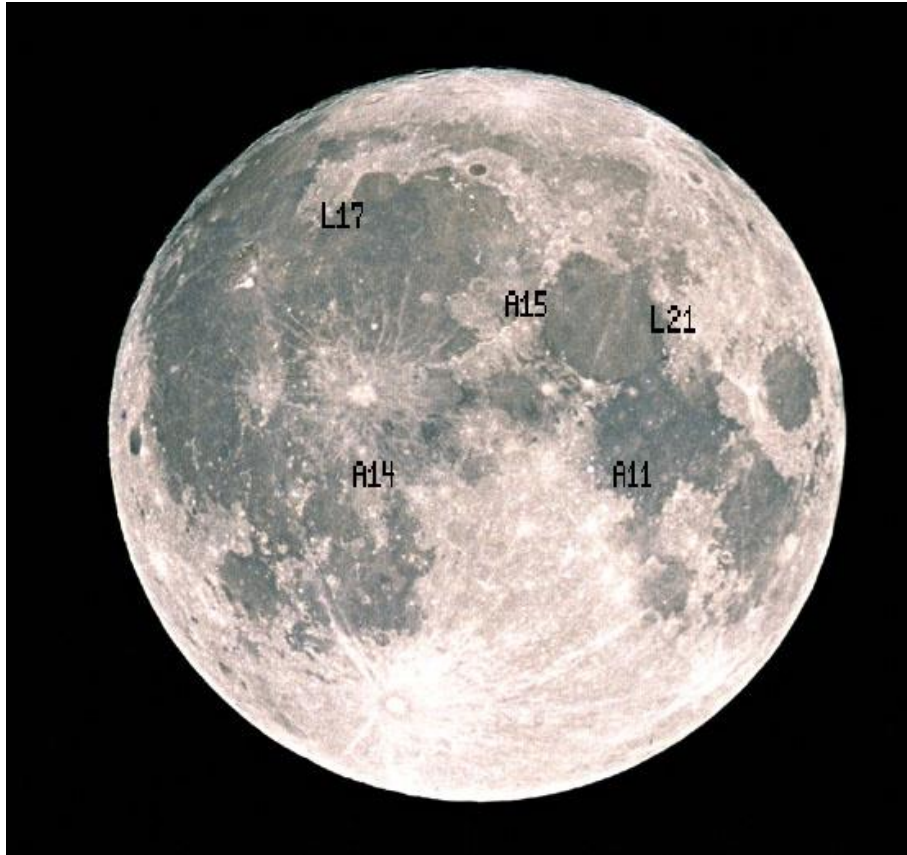




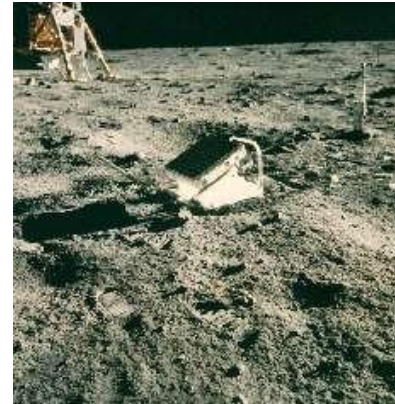
Lunar Retroreflector Arrays



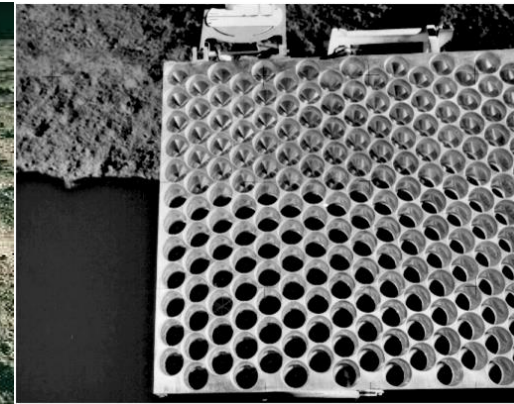
Five retroreflector arrays were placed on the lunar surface beginning with Apollo 11 in 1969. Two other manned Apollo missions (14 and 15) also left arrays with Apollo 15 being the largest (300 vs 100 cubes) to strengthen the return signal. Two unmanned Soviet Lunakhod (17 and 21) missions landed additional arrays provided by France. Because the Moon is so far away and maintains a fairly constant angular orientation with respect to the Earth, flat reflector panels could be used.



Retroreflector Array Sites

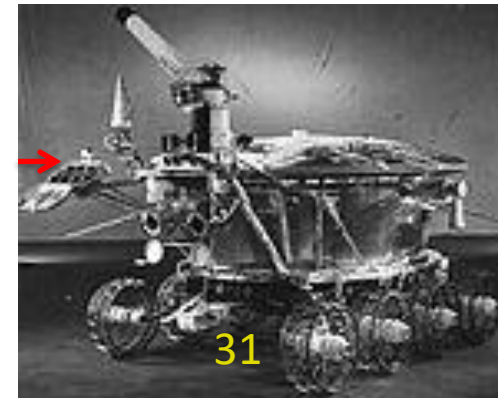


Apollo 11, 1969



Apollo 15

Array



Lunakhod



Apollo 15 Lunar Example



Earth-Moon Distance : $R_{EM} = h + R_E = 384.4 \times 10^6$ m. From the previous equations

$\alpha_{max} = 6.74 \mu\text{rad}$ or 1.40 arcsec

$\alpha_{min} = 6.68 \mu\text{rad}$ or 1.39 arcsec at an elevation angle of 20 degrees

v = relative velocity between target and station due to lunar orbital motion = 1 km/sec

However, the latter equations ignore the small contribution of station motion due to Earth rotation (~ 0.46 km/sec) to the relative velocity which typically reduces α to 4 or 5 μrad for LLR but is negligible for LEO to GEO satellites.

If the Apollo reflector arrays are pointed at the center of the Earth, the maximum beam incidence angle on the array from any Earth station (ignoring lunar libration) is

$$\theta_{inc} = a \tan\left(\frac{R_E}{R_{EM}}\right) = 0.95 \text{ deg}$$

The unspoiled cube diameter for which the cross-section falls to half its peak value is

$$D_{1/2} = 40.6 \text{ mm} = 1.6 \text{ in}$$

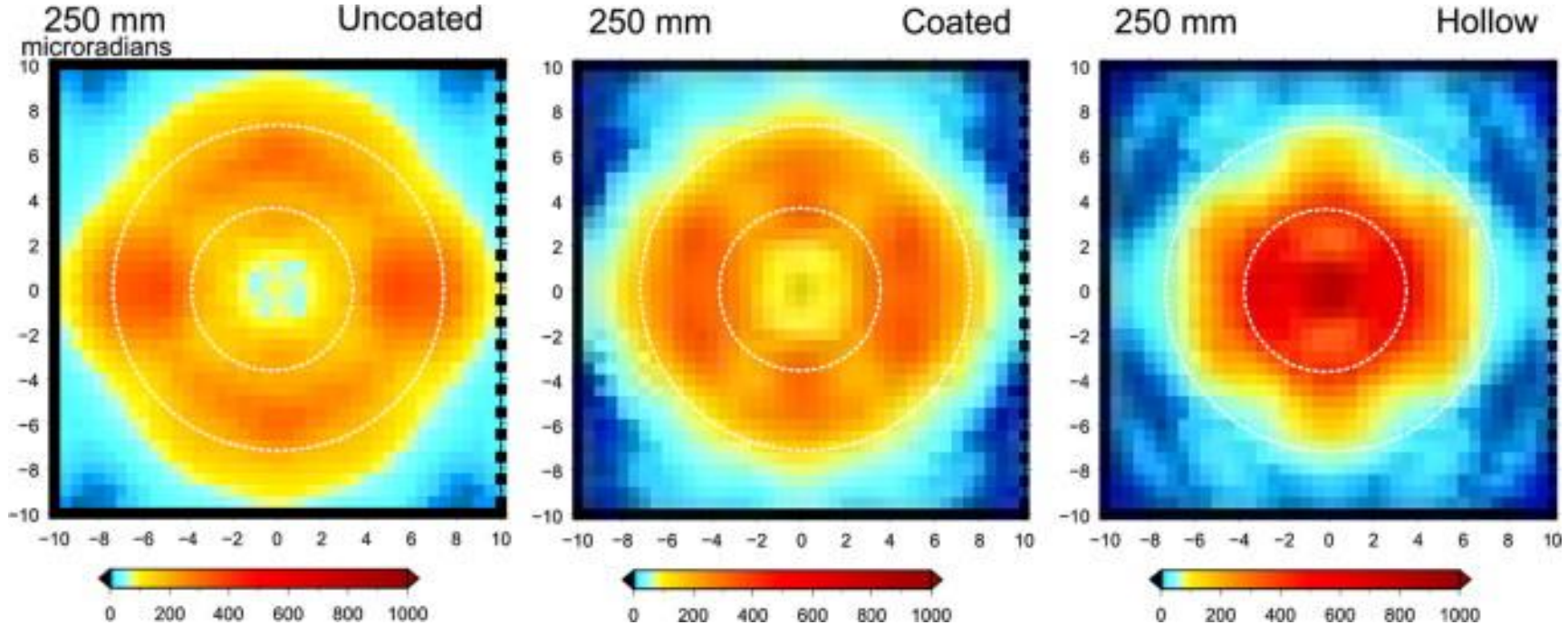
Typical manufacturing tolerances are 0.5 arcsec for dihedral angles and $\lambda/10$ for surface flatness.



Apollo 15 has a flat array of 300 38 mm fused quartz cubes each with an unspoiled peak cross-section of $5.8 \times 10^7 \text{ m}^2$. Thus, the theoretical array cross-section, ignoring manufacturing tolerances and local environment effects, is $\Sigma \cong 300(0.5)(5.8 \times 10^7 \text{ m}^2) = 8.7 \times 10^9 \text{ m}^2$. According to Dave Arnold, polarization losses due to uncoated TIR faces reduce cross-section by factor of 4, leaving $\Sigma \sim 2.2 \times 10^9 \text{ m}^2$. The tabulated ILRS value is $1.4 \times 10^9 \text{ m}^2$.

Otsubo et al, *Advances in Space Research*, Vol. 45, pp. 733-740, 2010.

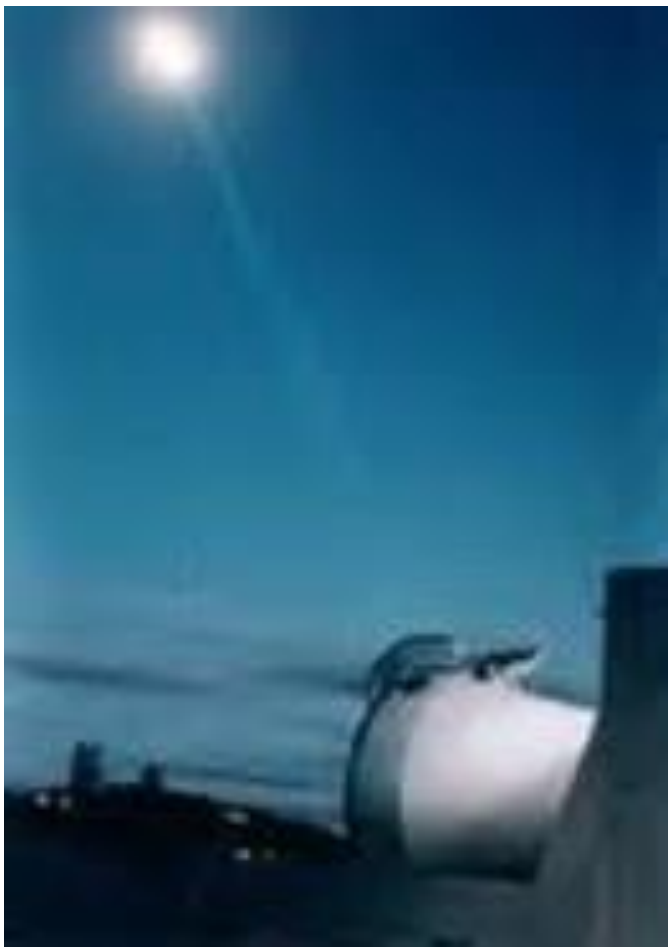
According to the authors, simulations indicate that a single reflector with a diameter of 150 to 250 mm has similar performance to Apollo arrays. No dihedral angle is required for small diameter reflectors (<150 mm for coated and <100 mm for uncoated and hollow reflectors). Larger diameters required dihedral angles of 0.20, 0.25, and 0.35 arcsec for coated, uncoated, and hollow reflectors respectively.



250 mm reflectors with 0.25 arcsec dihedral angles, incidence angle = 6 degrees



Lunar Laser Ranging

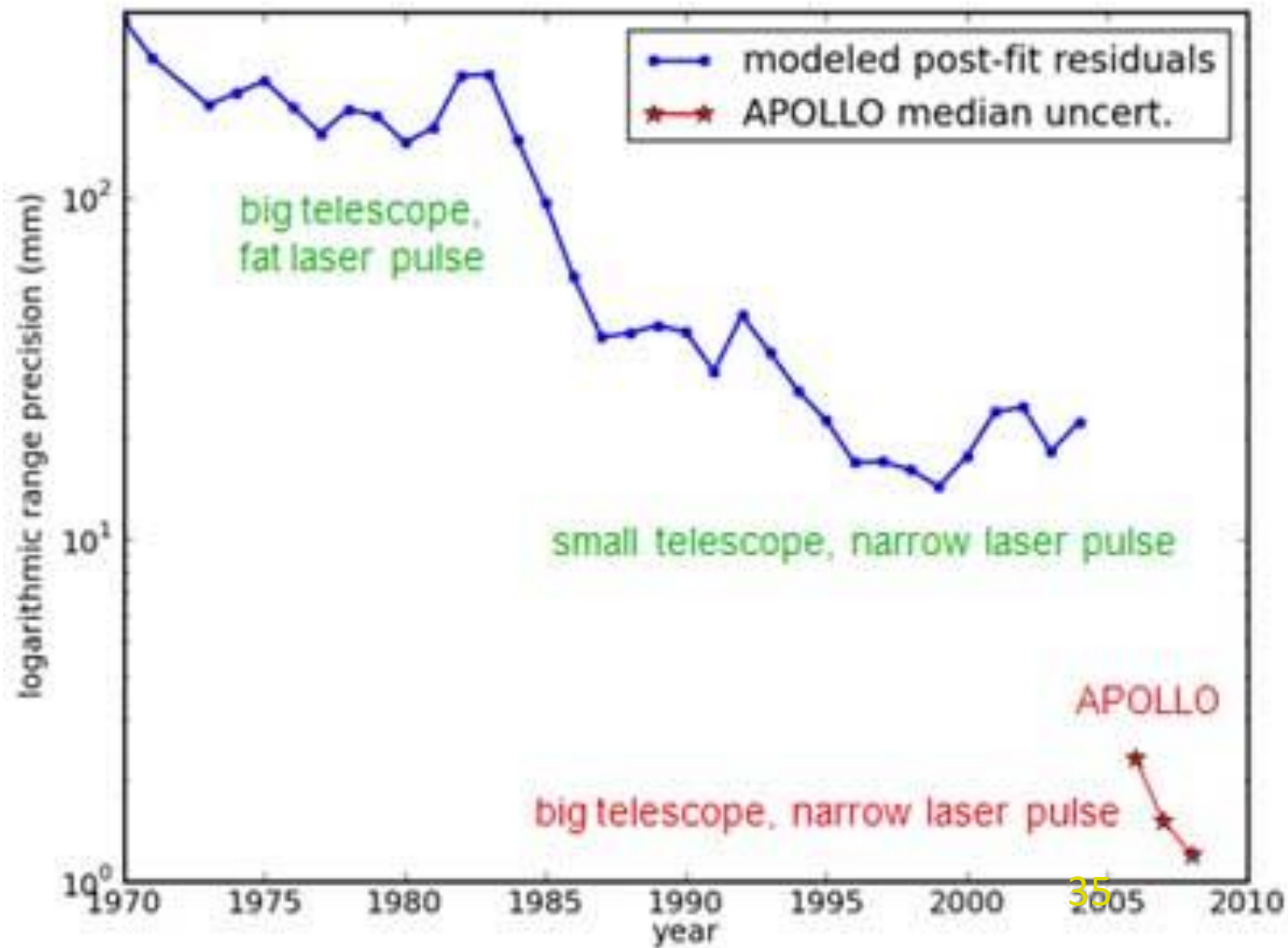


MLRS ranging to the Moon

- **Currently five passive retroreflector arrays were landed on the Moon by**
 - 3 NASA manned Apollo missions (11,14, and 15)
 - 2 Soviet Lunakhod missions (1 and 2)
- **For over 30 years, the LLR data set was provided by only three sites:**
 - MLRS, McDonald Observatory, Texas, USA
 - CERGA LLR, Grasse, France
 - Mt. Haleakala, Hawaii, USA (decommissioned in 1992)
- **New LLR systems have since come online:**
 - MLRO, Matera, Italy
 - Apollo, Apache Point, New Mexico, USA (multiphoton, 3.5 m telescope)



LLR Range Precision vs Time





GNSS and Geostationary Satellites



GNSS and Geosynchronous Satellites have some features in common with LLR:

1. Their orbital altitudes correspond to several Earth radii
2. They generally perform a utilitarian function (e.g. Earth observation, communications, navigation, etc.) which keeps the nadir side of the satellite approximately facing the Earth CoM

Their differences from LLR are :

1. The range in velocity aberration, $\Delta\alpha = \alpha_{\max} - \alpha_{\min}$, is 4 to 5 times larger (20 to 25 μrad)
2. For a maximum zenith tracking angle of 70° , beam Incidence angles can vary from 0 to β where

$$\beta = a \sin \left[\frac{R_E}{R_E + h} \sin(110^\circ) \right] \quad \begin{aligned} &= 13.1 \text{ deg for GNSS satellites at 20,000 km} \\ &= 8.2 \text{ deg for GEO satellites at 36,000 km} \end{aligned}$$

The smaller range of incidence angles ensures: (1) near maximum strength returns from a planar array; and (2) limited pulse spreading, especially if the array is compact in size and the retros are densely packed together to achieve the required cross-section.

Nevertheless, the maximum flat panel induced spreading per linear foot of array due to zenith tracking angle is still 474 psec (7 cm) and 292 psec (4.4 cm) for GNSS and GEO satellites respectively. This spreading can increase further if satellite attitude deviations from true nadir extend the range of incidence angles. Furthermore, the temporal response of a flat rectangular or square panel varies with both satellite zenith and azimuthal angle



Space Segment Summary



mm Accuracy LEO to MEO Geodetic Satellites

- Use large radius spherical satellites to:
 - better match the incoming plane wave and minimize pulse spreading
 - allow more reflectors within the active area to increase cross-section
- Reduce range of accepted incidence angles to minimize satellite impulse response width via
 - Hollow cubes or
 - Recessed hollow or solid cubes
- Also incidence angles $< 17^\circ$ do not leak light in solid TIR reflectors
- Selection of cube diameters and clocking to best match the “ α annulus” while favoring the response at high zenith (low elevation) angles is key to efficient array design

GNSS and GEO Satellites

- Typically have a nadir face pointed near Earth center due to other functions (Earth observation, communications, navigation, etc.)
- Flat panels OK but still several hundred psecs of temporal spread at lower satellite elevation angles. Flat circular (rather than rectangular) arrays would reduce azimuthal range biases.
- Range accuracy would further benefit from replacing flat panels by segments of a large sphere to eliminate satellite zenith angle variations.

LLR

- Characterized by small incidence angles (< 1 deg ignoring lunar librations) and velocity aberrations (< 1.0 arcsec) suggest the possible use of large diameter cubes provided thermal issues on the lunar surface can be resolved.



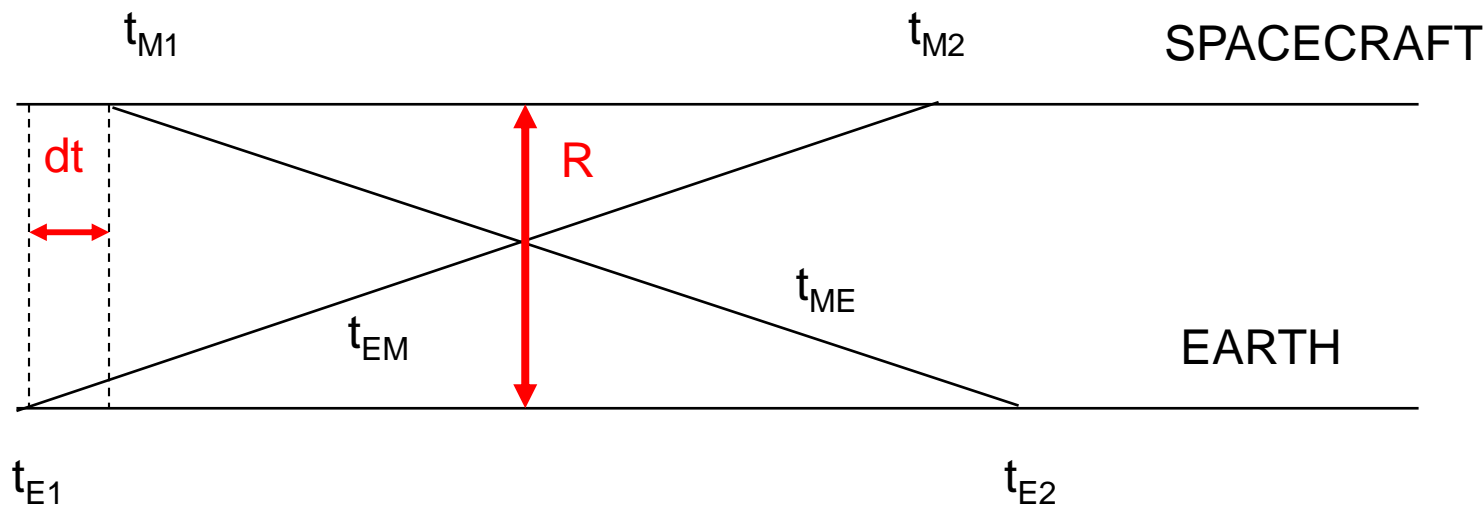
Laser Transponders: Laser Ranging Beyond the Moon



- Given the current difficulty of laser ranging to passive reflectors on the Moon, conventional single-ended ranging to passive reflectors at the planets is unrealistic due to the R^{-4} signal loss in the link equation.
- Since double-ended laser transponders have active transmitters on both ends of the link, signal strength falls off only as R^{-2} making precise interplanetary laser ranging and time transfer possible. Furthermore, since most of the link burden (laser power, telescope aperture) can be carried by the Earth station, the space terminal can be relatively modest in size, weight, and power consumption.



Asynchronous Ranging and Time Transfer*



Range $R = c(t_{ME} + t_{EM})/2 = c [(t_{E2} - t_{E1}) + (t_{M2} - t_{M1})]/2$

Clock Offset $dt = [(t_{E2} - t_{E1}) - (t_{M2} - t_{M1})]/[2(1 + \dot{R}/c)]$

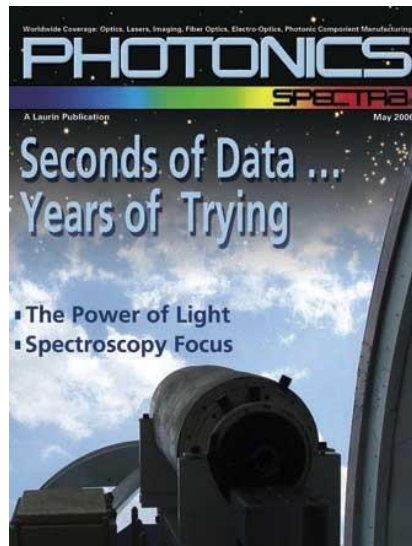
*J. Degnan, J. Geodynamics, 34, pp. 551-594 (2002).



Two-Way Transponder Experiment to the Messenger Spacecraft (May/June 2005)*



GSFC 1.2 Meter Telescope



Messenger Laser Altimeter (MLA) enroute to Mercury



24.3 Million Km
Range Accuracy <20 cm

Ground Station

Xiaoli Sun Jan McGarry
Tom Zagwodzki John Degnan
D. Barry Coyle

Science/Analysis/Spacecraft

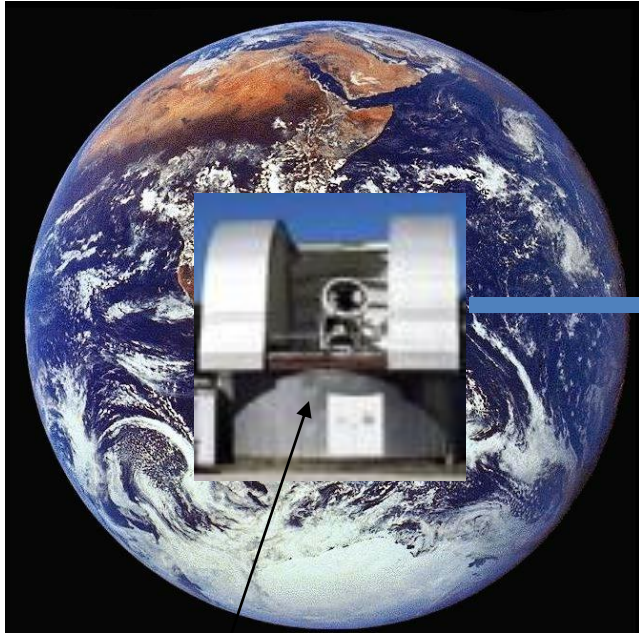
David Smith Maria Zuber
Greg Neumann John Cavanaugh

40

*D. E. Smith et al, *Science*, January 2006.

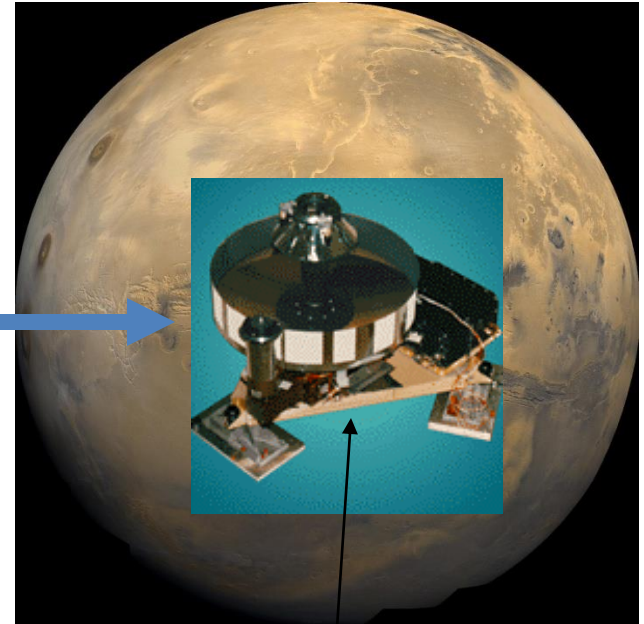


One-Way Earth-to-Mars Laser Transponder Experiment (Sept. 2005)



80 Million Km!

~500 laser pulses observed at Mars!



GSFC 1.2 Meter Telescope

Ground Station

Xiaoli Sun	Jan McGarry
Tom Zagwodzki	John Degnan

MOLA at Mars

Science/Analysis/Spacecraft

David Smith	Maria Zuber
Greg Neumann	Jim Abshire



Transponder Link Parameters*



Experiment	MLA (cruise)		MOLA (Mars)
Range (10^6 km)	24.3		~80.0
Wavelength, nm	1064		1064
	Uplink	Downlink	Uplink
Pulsewidth, nsec	10	6	5
Pulse Energy, mJ	16	20	150
Repetition Rate, Hz	240	8	56
Laser Power, W	3.84	0.16	8.4
Full Divergence, μ rad	60	100	50
Receive Area, m^2	.042	1.003	0.196
EA-Product, $J\cdot m^2$	0.00067	0.020	.0294
PA-Product, $W\cdot m^2$	0.161	0.160	1.64

Table 1: Summary of key instrument parameters for recent deep space transponder experiments at 1064 nm.

Note that the PA-product for the MLA space and Earth terminals are roughly the same and most of the link burden for the uplink and downlink is borne by the Earth terminal.

42

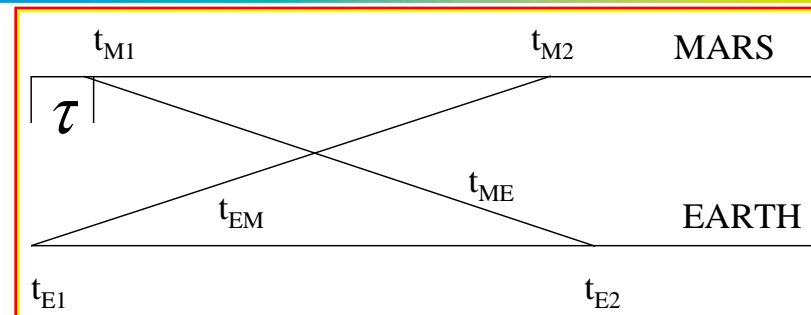
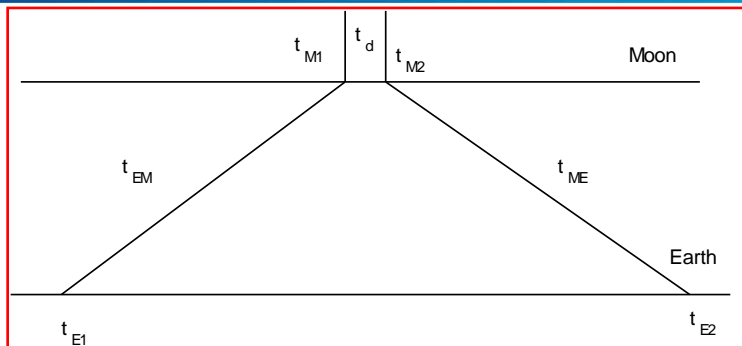
*J. Degnan, Int. J. Modern Physics D, 16, pp. 1-14 (2007).



Backup Slides



Two Way Transponders*



- **Echo Transponders ($R \ll 1$ AU)**

- Spacecraft transponder detects pulses from Earth and fires a reply pulse back to the Earth station.
- To determine range, the delay t_d must be known a priori (or measured onboard and communicated back to Earth) and subtracted from the measured round-trip time-of-flight at the Earth station.
- Works well on “short” links (e.g. to the Moon) where the round trip transit time is short (~ 2.5 sec) and the single shot detection probability at both terminals is high.

- **Asynchronous Transponders ($R > 1$ AU)**

- Transmitters at opposite terminals fire asynchronously (independently).
- Signal from the opposite terminal must be acquired autonomously via a search in both space and time (easier when terminals are on the surface or in orbit about the planet)
- The spacecraft transponder measures both the local transmitter time of fire and any receive “events” (signal plus noise) on its own time scale and transmits the information back to the Earth terminal via the spacecraft communications link. Range and clock offsets are then computed.
- This approach works well on “long” links (e.g., interplanetary) even when the single shot probability of detection is relatively small

*J. Degnan, J. Geodynamics, 34, pp. 551-594 (2002).



Laser vs Microwave Transponders



- **Laser Advantages**

- Ranging/timing instrumentation is more precise (~ 1 mm) due to availability of picosecond transmitters, detectors, and timers in the optical regime
- Divergence of transmitted optical beam is 4-5 orders of magnitude smaller than microwaves for a given transmit aperture ($\sim \lambda/D$)
 - More energy focused at the opposite receiver
 - Smaller antennas (telescopes) and transmitters, more lightweight, less prime power
- Charged particles cannot follow optical frequencies so
 - no propagation delays due to Earth's ionosphere or the interplanetary solar plasma
 - no need for solar plasma models or correction via dual wavelength methods
- Optical atmospheric propagation delay uncertainties are typically at the sub-cm level with ground measurements of pressure, temperature, and relative humidity, as in SLR.

- **Laser Disadvantages**

- Requires more precise pointing knowledge and control (but well within SOA)
- Link availability affected by weather and clouds but can be $> 99\%$ by utilizing several globally distributed ground sites or three orbiting terminals
- As with any new technology, lasers have not yet demonstrated space heritage, lifetime and reliability comparable to more mature microwave transponders but several laser altimeters have already operated in Earth, Lunar, Mars, and Mercury orbits.



The Road Forward



- **Messenger and MOLA were experiments of opportunity rather than design.**
 - Since the spacecraft had no ability to lock onto the opposite terminal or even the Earth image, the spaceborne lasers and receiver FOV's were scanned across the Earth terminal providing only a few seconds of data.
 - Detection thresholds were relatively high due to the choice of wavelength (1064 nm) and the use of analog multiphoton detectors
 - Precision was limited to roughly a decimeter or two by 2nd generation SLR technology onboard the spacecraft, i.e. 6 nsec laser pulsewidths and comparable receiver bandwidths.
- **The physical size, weight, and accuracy of future interplanetary transponder experiments will benefit from current SLR photon counting technology, such as:**
 - Multi-kHz, low energy, ultrashort pulse lasers (10 to 50 psec)
 - Single photon sensitivity, picosecond resolution range receivers
 - Autonomous tracking with transmitter point ahead and receiver pointing correction via pixellated single photon detectors.
- **We will now demonstrate that the SLR satellite constellation can accurately mimic interplanetary links (including effects of the Earth's atmosphere) for inexpensive, pre-mission testing of both laser transponder and communications concepts.**



Simulating Interplanetary Laser Ranging and Communications using the SLR Constellation*



*J. Degnan, Int. J. Modern Physics D, 16, pp. 1-14 (2007).

Transponder Link Equations for Station A (Earth) to Station B (another planet)

Transponder/Lasercom System:

$$n_T^{AB} = \frac{4\eta_q^B \eta_t^A \eta_r^B T_A^{\sec\theta_A} T_B^{\sec\theta_B}}{h\nu_A (\theta_t^A)^2 (4\pi)} \frac{E_t^A A_r^B}{R_T^2}$$

One/Two-Station Ranging to a Satellite:
One Station implies B = A

$$n_R^{AB} = \frac{4\eta_q^B \eta_t^A \sigma_s \eta_r^B T_A^{2\sec\theta_A}}{h\nu_A (\theta_t^A)^2 (4\pi)^2} \frac{E_t^A A_r^B}{R_R^4}$$

Setting $n_T^{AB} = n_R^{AB}$ gives us an equivalent transponder range for the two-station SLR experiment

$$R_T(h, \theta_A, \sigma_s) = R_R^2(h, \theta_A) \sqrt{\frac{4\pi}{\sigma_s} \left(\frac{T_B^{\sec\theta_B}}{T_A^{\sec\theta_A}} \right)}$$

$$\cong R_R^2(h, \theta_A) \sqrt{\frac{4\pi}{\sigma_s} \frac{1}{T_A^{\sec\theta_A}}}$$

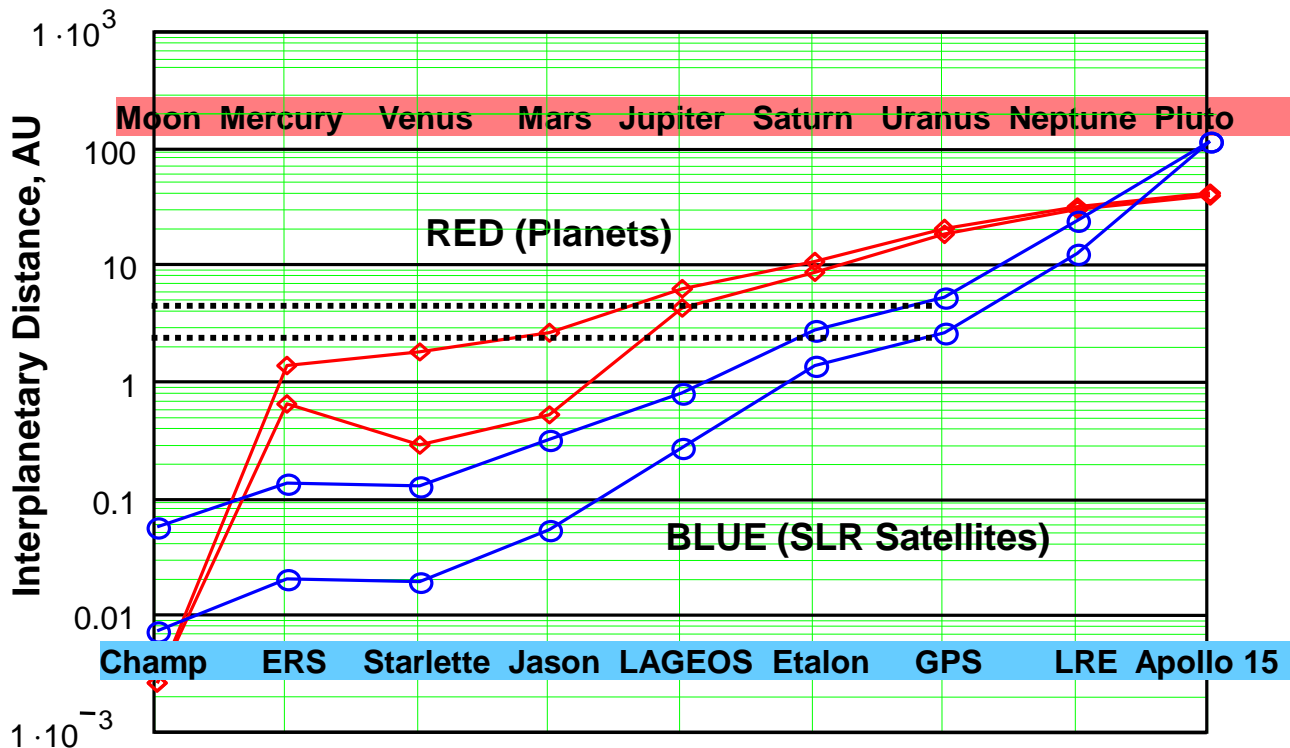
Simulations can be carried out from either a single SLR station (e.g. Wettzell, Germany) or two adjacent stations (e.g. GSFC 1.2 m and SGSLR in the USA) located within the far field pattern of the retroreflector array.



Planet/Satellite Equivalence*



1 AU = 150 million km



Red curves bound the Earth-planetary distance
Blue curves bound the equivalent transponder range
at satellite elevations of 90 and 20 degrees respectively.

*J. Degnan, Int. J. Modern Physics D, 16, pp. 1-14 (2007).



Summary of Equivalent Links



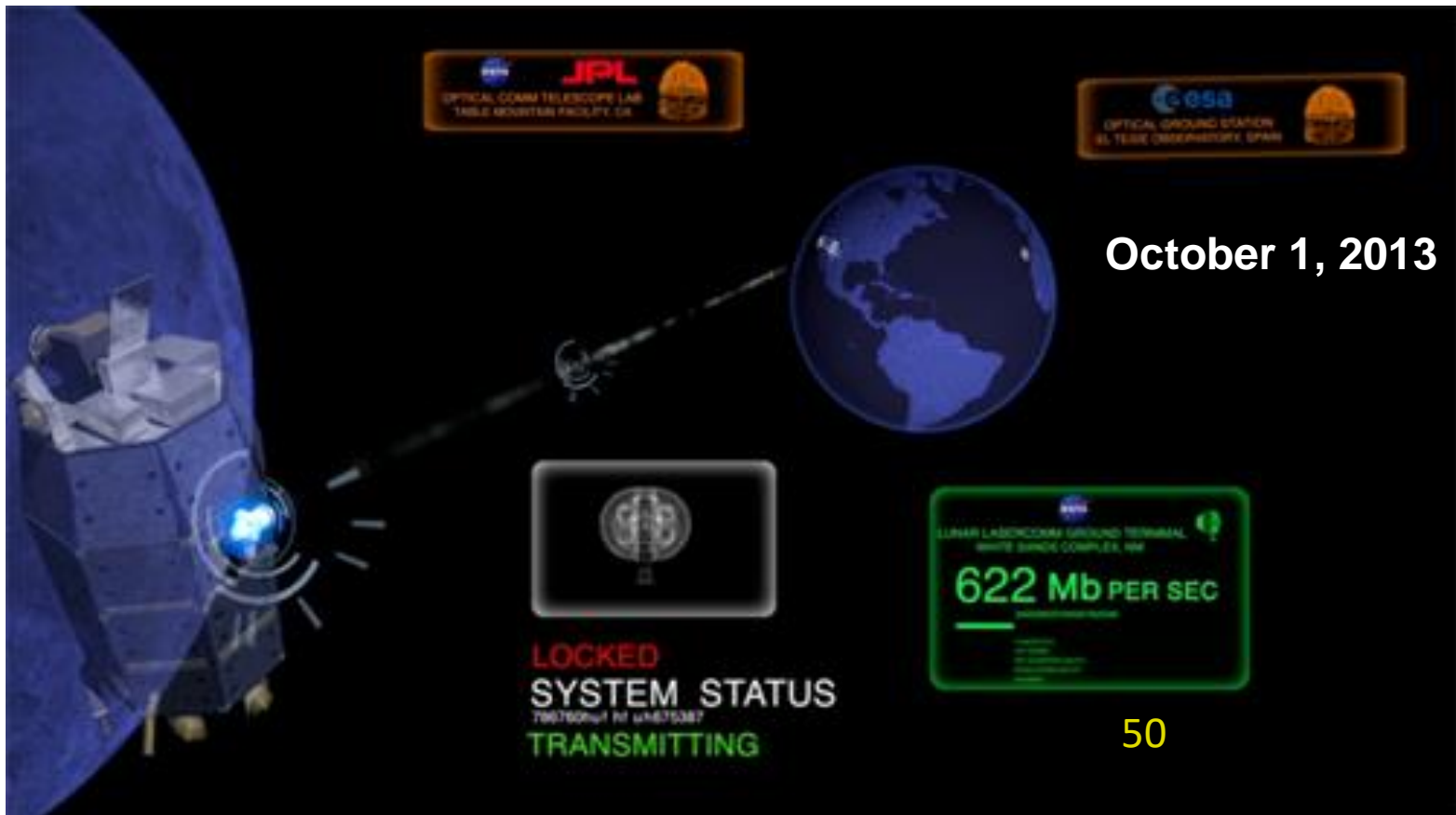
- Moon (~ 0.0026 AU) and Trans-lunar
 - Champ, ERS, Starlette, Jason
- Mercury, Venus, Mars (0.28 to 2.52 AU)
 - LAGEOS (near planetary PCA)
 - Etalon, GPS-35, 36 (Full planetary synodic cycle)
- Jupiter, Saturn, Uranus (4.2 to 18.2 AU)
 - GPS-35, 36 (Jupiter PCA); LRE @25,000 km
- Neptune, Pluto, Kuiper Belt (30 to 50 AU)
 - Future retro-equipped GEO satellites?
- Beyond our Solar System (~ 100 AU)
 - Apollo 15 lunar array



Lunar Laser Communications Demonstration (LLCD)



Over the past two decades, there have been several high bandwidth lasercom experiments between Earth-orbiting spacecraft or between spacecraft and a ground station carried out or currently planned by various countries. A low bandwidth link between LOLA/LRO and NGS LR successfully transmitted an image of the Mona Lisa from lunar orbit, but the LLCD on the lunar LADEE mission recently demonstrated a bandwidth of 622 Mbps!





An Introduction to Satellite Laser Ranging Technology and its Applications: Part 2: Applications

**Dr. John J. Degnan
SLR School
October 20, 2019
Stuttgart, Germany**



Part 2 Overview



- ILRS Station Network
- SLR Earth Science Products
 - Precise Orbit Determination (POD) and Geopotential Model
 - Terrestrial Reference Frame (Center of Mass and Scale)
 - Tectonic Plate Motion and Regional Crustal Deformation
 - Polar Motion and Length of Day
- Earth Observation Satellites Equipped with Microwave or Laser Altimeters
 - Global Sea Level and Ocean Currents
 - Seafloor Topography
 - ICESat-1 and 2
- Global Laser Time Transfer
- Science Contributions of Lunar Laser Ranging (LLR)
 - Earth/Moon Dynamics
 - Tests of General Relativity
- Using the SLR satellite constellation to simulate interplanetary
 - Ranging
 - Time Transfer
 - Communications



Current SLR Network

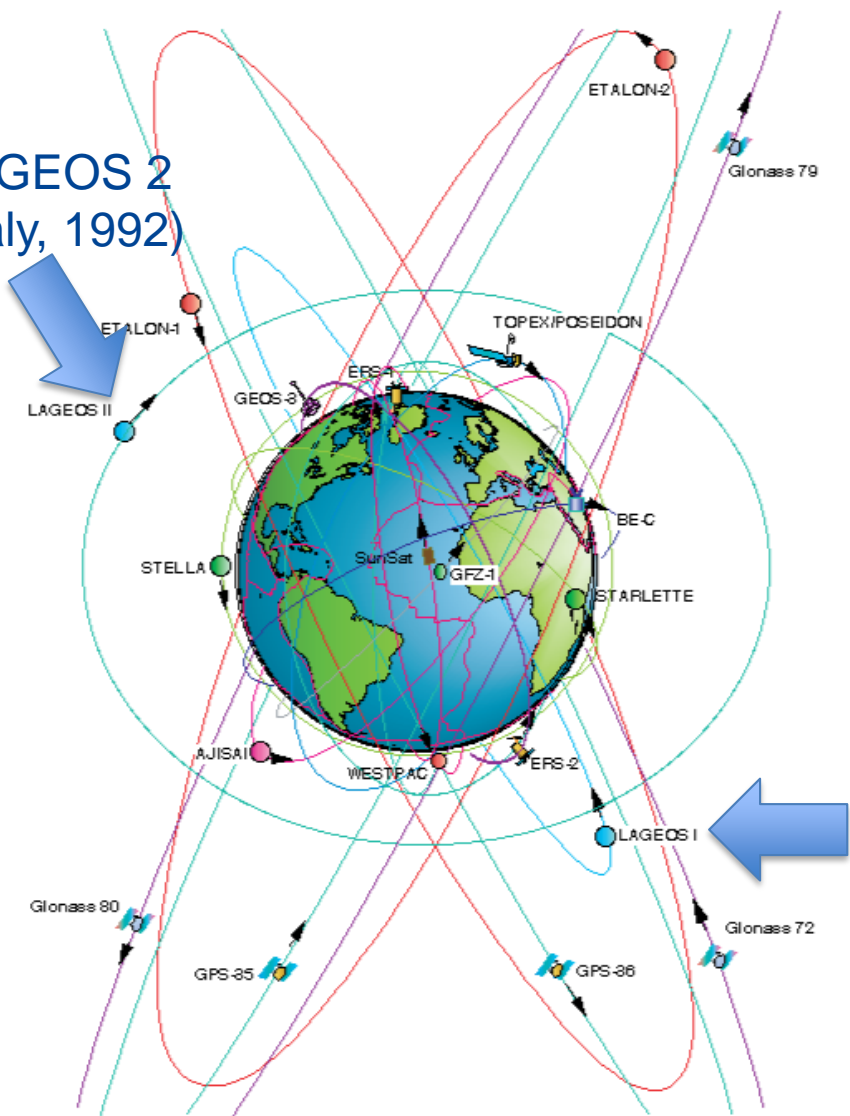




SLR Missions and Orbits



LAGEOS 2
(Italy, 1992)



- The SLR constellation spans a wide range of altitudes and inclinations.
- The LAGEOS 1 and 2 geodetic satellites are in stable, low drag, 6000 km high orbits and define the Terrestrial Reference Frame (TRF)
- Low Earth Orbiting (LEO) satellites are more sensitive to higher order variations in the Earth's gravity field resulting from non-uniform mass distributions and migrations.
- SLR also provides cm precision orbits to the Global Navigation System Satellites (GNSS) such as GPS, GLONASS, GALILEO, etc to correct for biases and further improve their ground geolocation performance.

LAGEOS I
(USA, 1976)



TRF and Geopotential



- The Earth's Center of Mass (CoM) serves as the origin of the 3-dimensional Terrestrial Reference Frame(TRF).
- The Scale Factor, GM , is the product of Newton's Universal Gravitational Constant, G , and the Earth Mass, M .
- The gravitational field of an object with distributed mass density $\rho(x',y',z')$ is given by

$$W_a(x, y, z) = G \iiint_v \frac{\rho(x', y', z')}{\sqrt{(x - x')^2 + (y - y')^2 + (z - z')^2}} dx' dy' dz'$$

and can be expressed in spherical coordinates as a sum of orthogonal spherical harmonics

$$W_a(r, \lambda, \varphi) = \frac{GM}{r} \sum_{\ell=0}^{\ell_{\max}} \sum_{m=0}^{\ell} \left(\frac{R}{r}\right)^{\ell} P_{\ell m}(\sin \varphi) (C_{\ell m}^W \cos m\lambda + S_{\ell m}^W \sin m\lambda)$$

- r, λ, φ - spherical geocentric coordinates of computation point (radius, longitude, latitude)
- R - reference radius
- GM - product of gravitational constant and mass of the Earth
- ℓ, m - degree, order of spherical harmonic
- $P_{\ell m}$ - fully normalised Legendre functions
- $C_{\ell m}^W, S_{\ell m}^W$ - Stokes' coefficients (fully normalised)

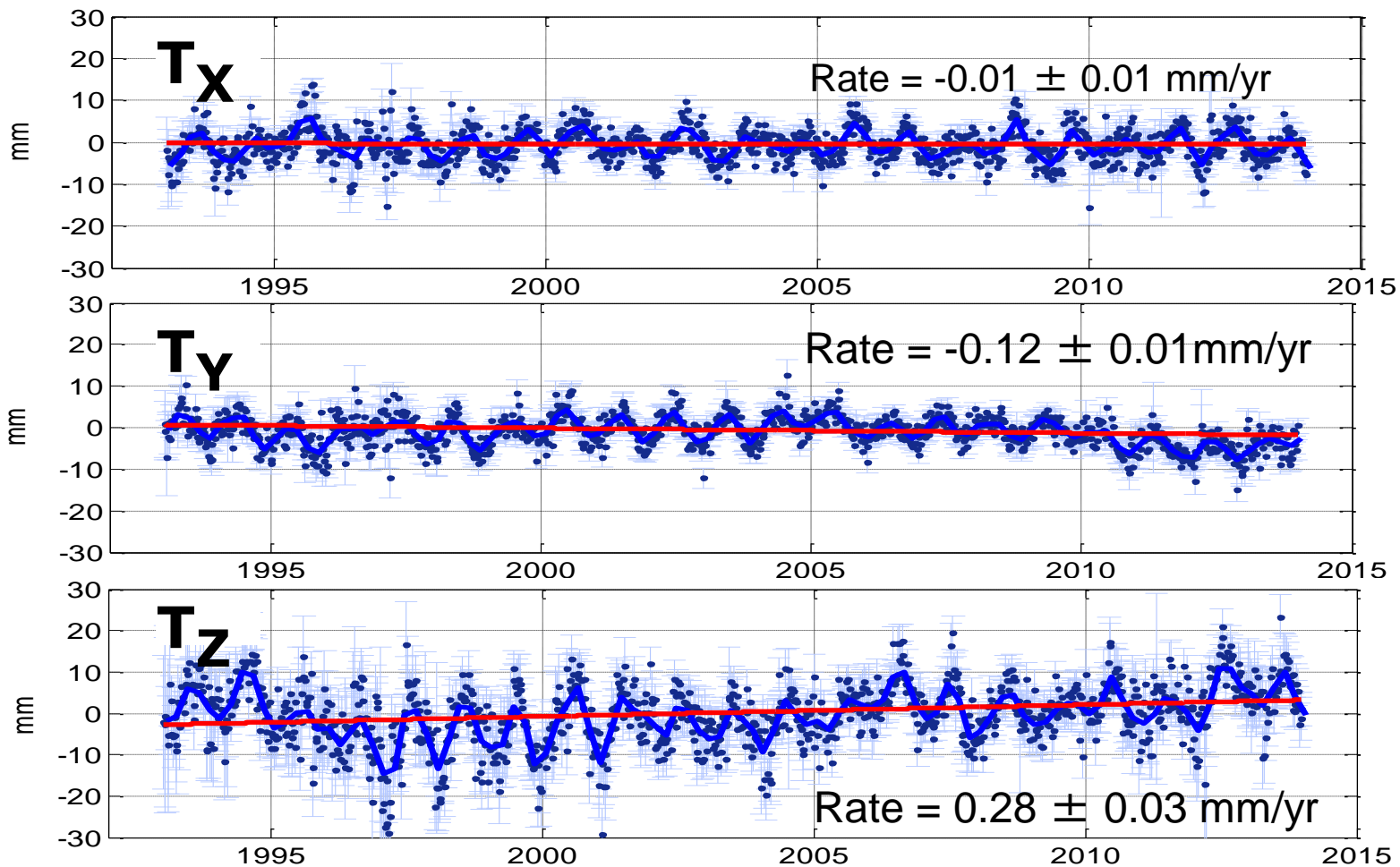


SLR TRF Origin (ITRF2013)*



* Courtesy, Erricos Pavlis, UMBC/GSFC

SLR defines the origin of the Terrestrial Reference Frame (TRF), i.e., the Earth Center of Mass (Geocenter) and monitors its movement over time.



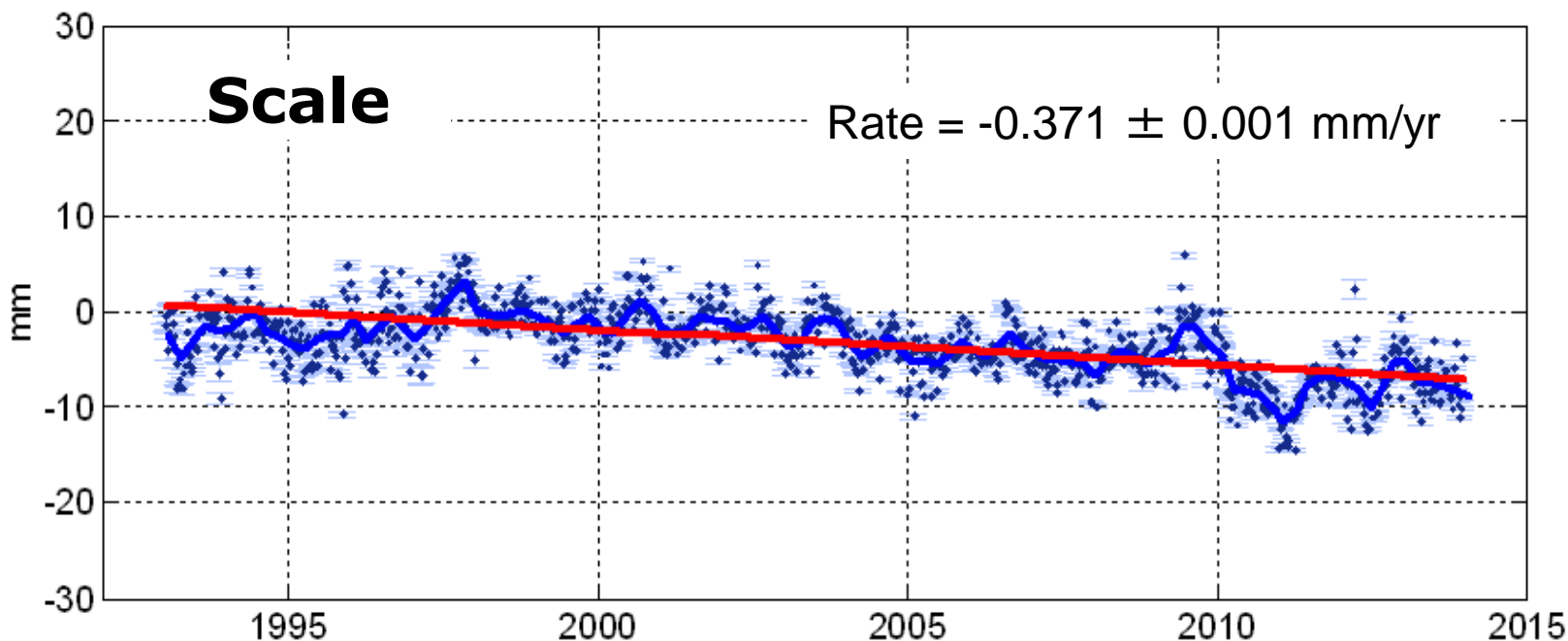


SLR TRF Scale (ITRF2013)

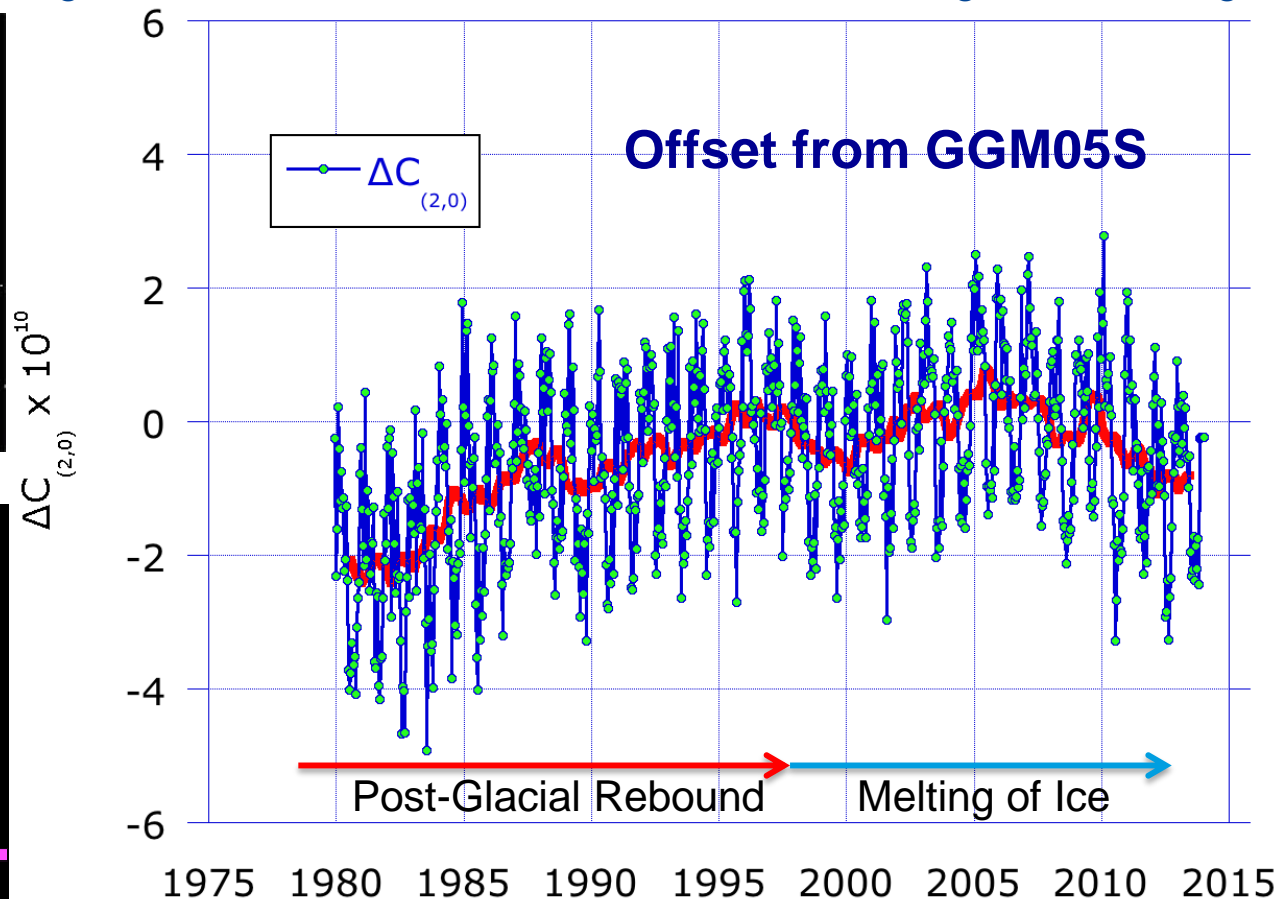
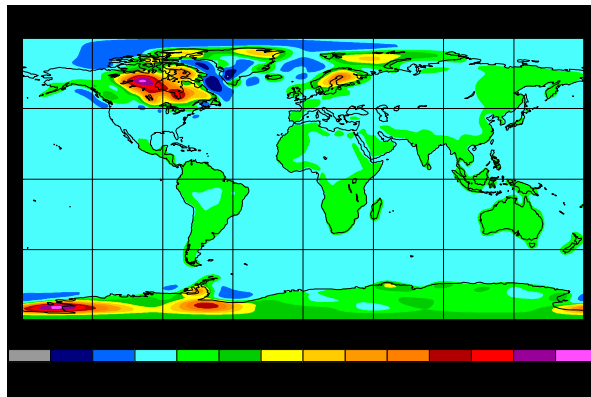
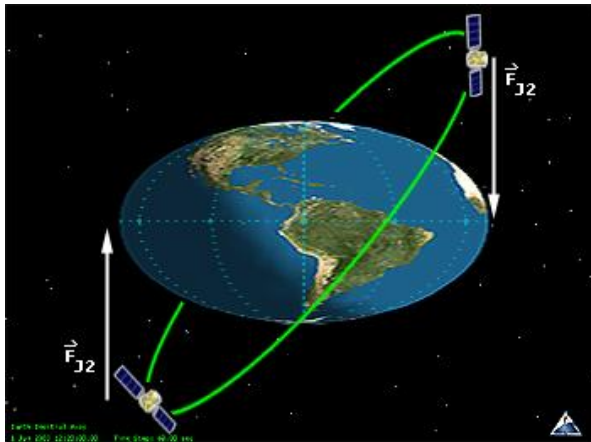


* Courtesy, Erricos Pavlis, UMBC/GSFC

TRF Scale is defined as the product GM where G is the gravitational constant and M is the mass of the Earth. Scale is also a measure of the positional stability of the overall SLR network.

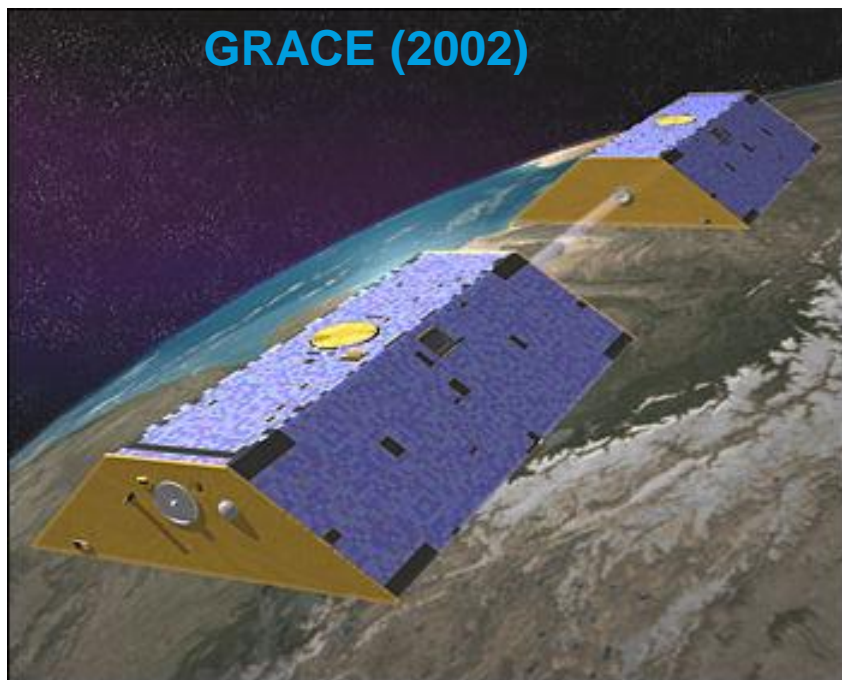


$C_{2,0}$ is a coefficient for one of the lowest order terms in the spherical harmonic model of the Earth's gravity field which measures "roundness" or "oblateness". Until about the late 1990s, the increase in roundness was attributed to post-glacial rebound in Canada following the last ice age. However, as we approached the millennium, the direction of the coefficient changed sign which scientists attributed to the melting of ice and redistribution of water mass due to global warming.





Gravity Recovery and Climate Experiment (GRACE)



GRACE (2002)

- Two identical spacecraft (GRACE A&B) in polar orbit at 500 km altitude are tracked by GPS and SLR
- Separation (~220 km) measured by K-band microwave link
- Observed changes to separation provide high spatial frequency components in the gravity field whereas SLR does a better job measuring low frequency components.

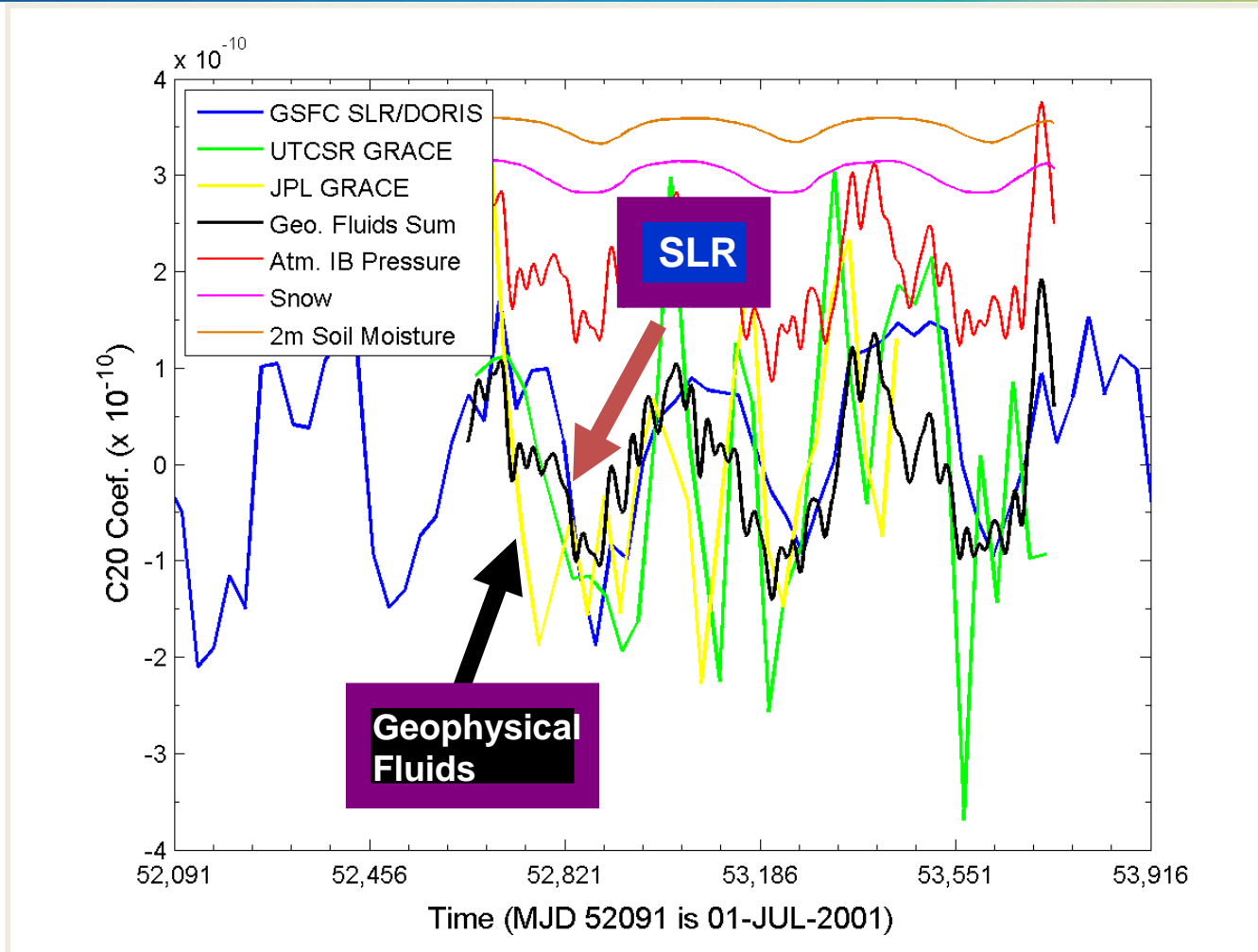
- Goals:
 - Map gravity field and changes with time
 - create a better profile of the Earth's atmosphere.
- The gravity variations that GRACE studies include:
 - changes due to surface and deep currents in the ocean
 - runoff and ground water storage on land masses
 - exchanges between ice sheets or glaciers and the oceans*
 - variations of mass within the Earth..

**Estimated Ice Mass Loss:
100 Gigaton/yr in Antarctica
200 Gigaton/yr in Greenland**



C_{2,0}: Comparison: SLR vs GRACE monthly

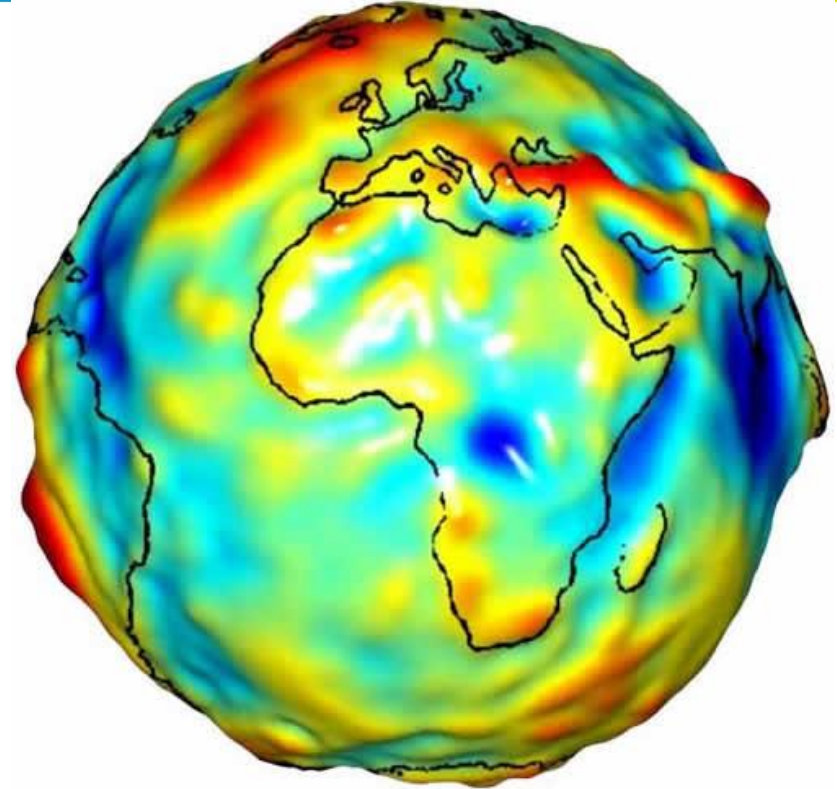
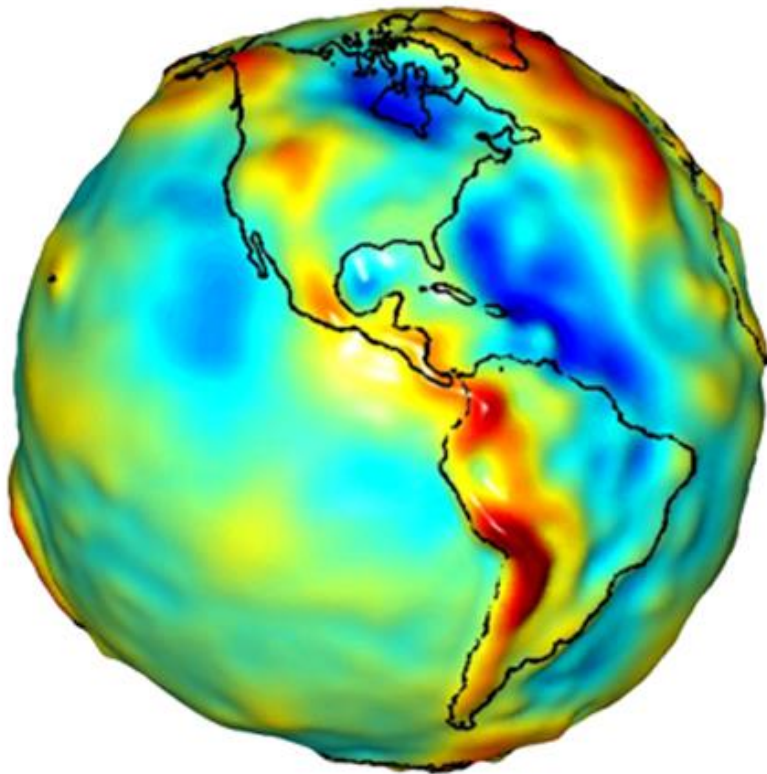
Courtesy: Frank Lemoine, NASA/GSFC



As our knowledge of the Earth gravity field improved, analysts were also able to better model non-conservative forces affecting satellite orbits, such as atmospheric drag and radiation pressures (Sun and Earth albedo).



Global Gravity Field from GRACE Mission



The images show the regions of strong (red, raised) and weak (blue, depressed) gravitational acceleration as measured by the GRACE mission. SLR is still the best source for the low order spherical harmonic coefficients.

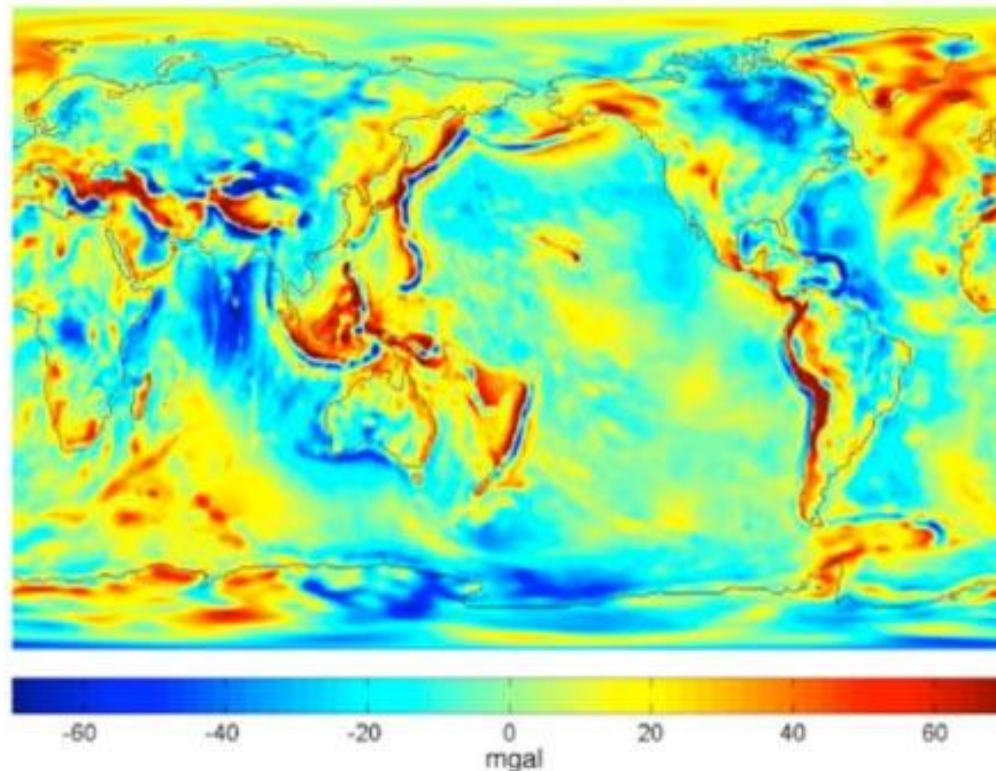
A companion satellite with similar goals, the Gravity field and steady-state Ocean Circulation Explorer (GOCE) was launched by ESA on March 19, 2009 and ran out of fuel in 2013. The joint NASA-ESA GRACE-FO mission was launched in June 2019.



Mean Gravity Anomalies



A **gravity anomaly** is the difference between the observed acceleration of a planet's gravity and a value predicted from a global model, expressed as a sum of spherical harmonics. A location with a positive anomaly exhibits more gravity than predicted, while a negative anomaly exhibits a lower value than predicted.



A milligal is a convenient unit for describing variations in gravity over the surface of the Earth. 1 milligal (or mGal) = 0.00001 m/s^2 , which can be compared to the total gravity on the Earth's surface of approximately 9.8 m/s^2 . Thus, a milligal is about 1 millionth of the standard acceleration on the Earth's surface.

NGS Definition of “geoid”: “The equipotential surface of the Earth's gravity field which best fits, in a least squares sense, global mean sea level “The Geoid is a surface to which the force of gravity is everywhere perpendicular (but not equal in magnitude).

$$W_a(r, \lambda, \varphi) = W_0$$

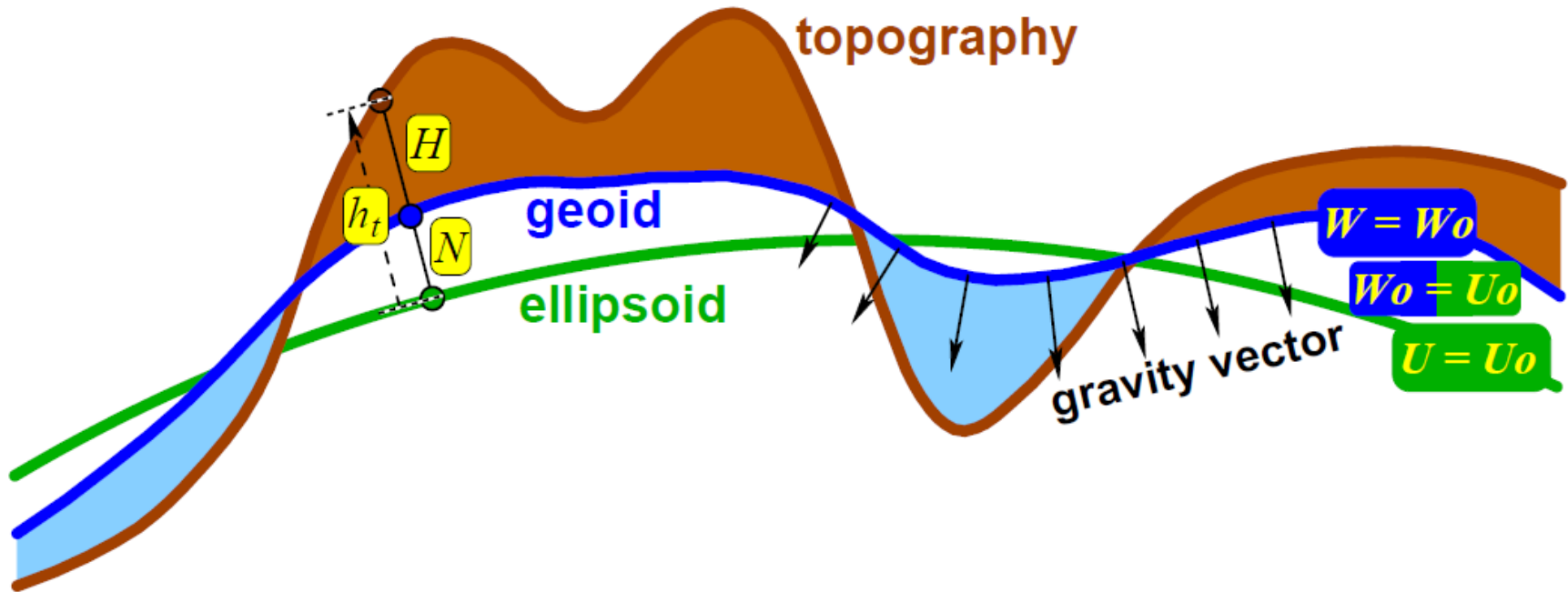


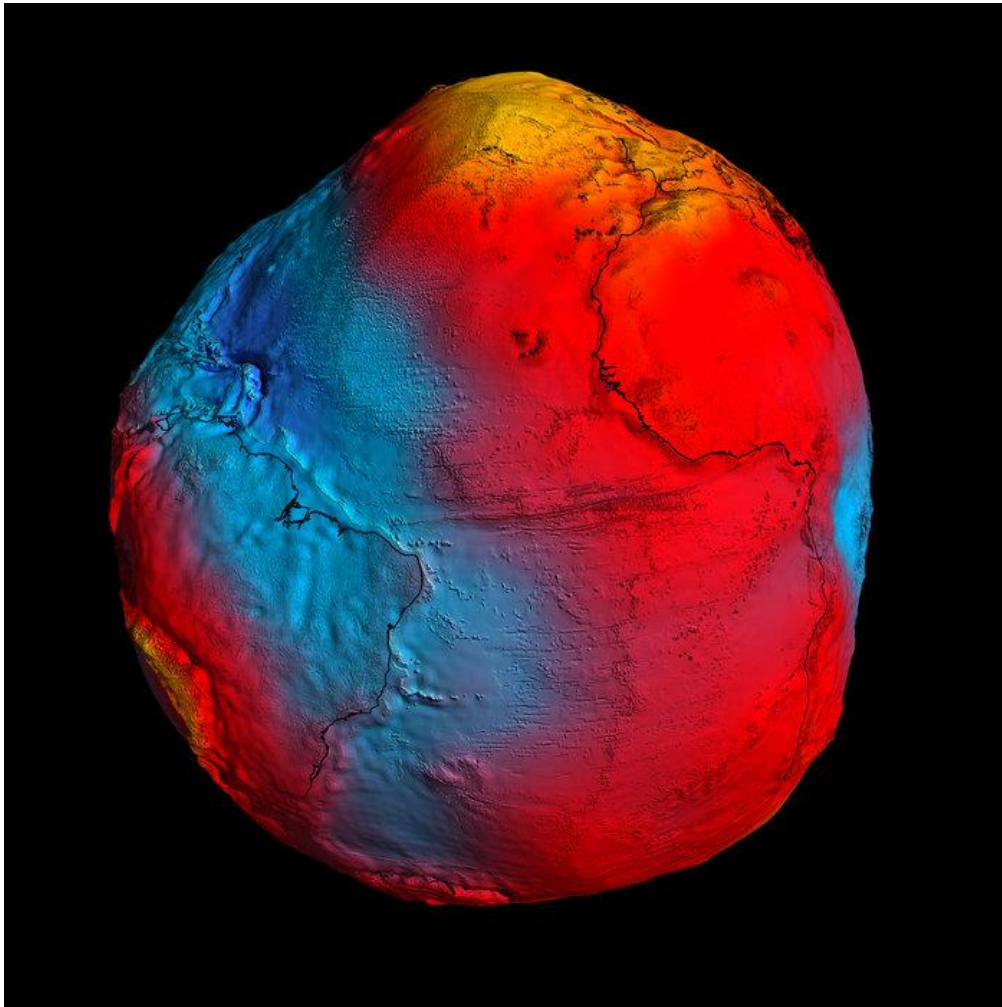
Figure 1: The ellipsoid, the geoid and the topography



GOCE Earth Geoid



NGS Definition of “geoid”: “The equipotential surface of the Earth's gravity field which best fits, in a least squares sense, global mean sea level “

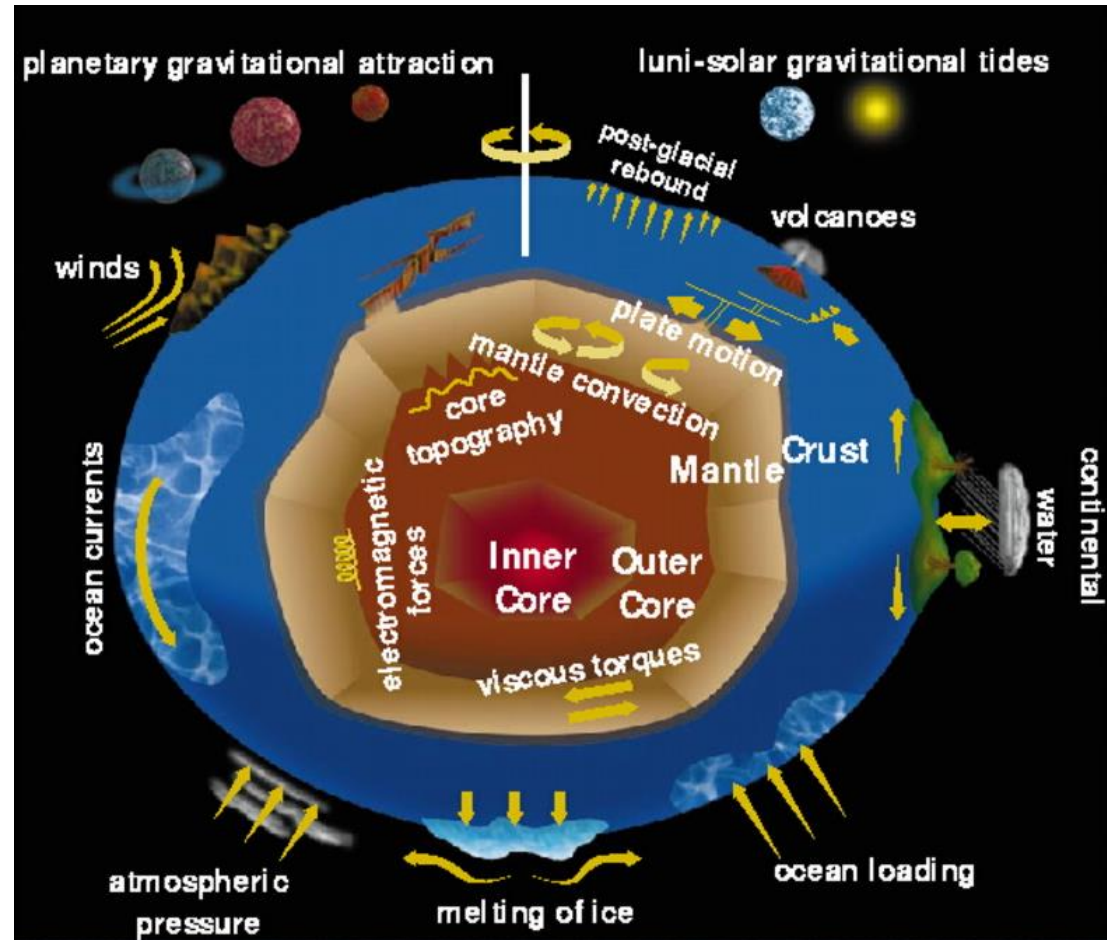


ESA GOCE Mission: The colors in the image represent deviations in height (– 100 m to +100 m) from an ideal geoid. The blue shades represent low values and the reds/yellows represent high values.

A precise model of Earth's geoid is crucial for deriving accurate measurements of ocean circulation, sea-level change and terrestrial ice dynamics. The geoid is also used as a reference surface from which to map the topographical features on the planet. In addition, a better understanding of variations in the gravity field will lead to a deeper understanding of Earth's interior, such as the physics and dynamics associated with volcanic activity and earthquakes.



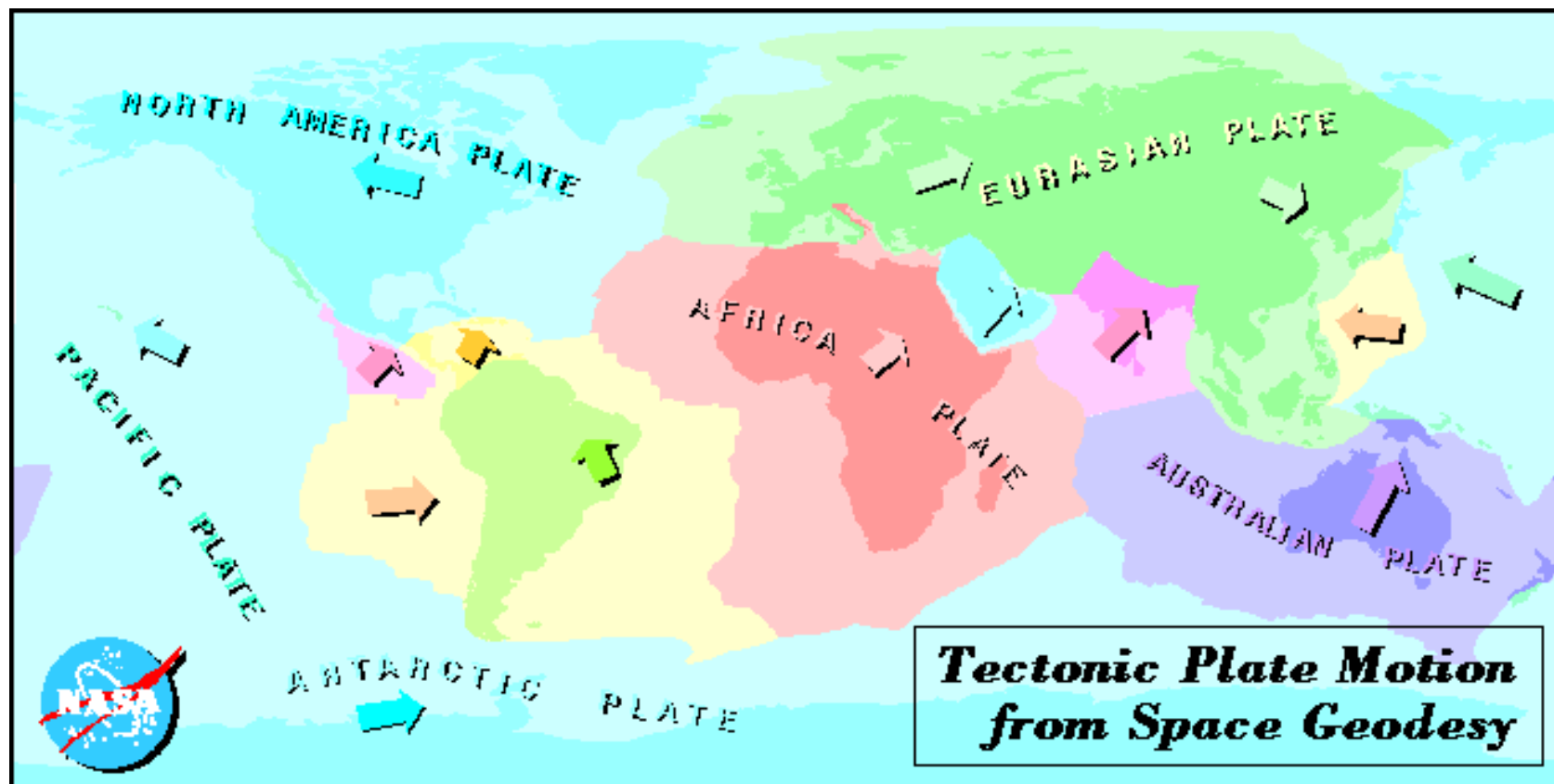
International Earth Rotation Service



Earth Orientation Parameters (EOP)
 Polar motion (Chandler Wobble has 435 day period)
 Length of Day (LOD)
 High frequency Universal Time (UT1)

VLBI, working with distant quasars in the Celestial Reference Frame, is the only source of UT1, but SLR interpolated the wobble and LOD results between VLBI campaigns. These interpolations are now augmented by GNSS techniques.

High, low drag satellites, like LAGEOS in a 6000 km high orbit, provide a stable inertial reference frame which allow us to see changes in relative positions of SLR stations that track them and thereby monitor tectonic plate motion.



Length of the arrows are an indication of relative velocity.



Transportable SLR Stations



MOBLAS 3 thru 8
(MOBILE LASer)
NASA, USA



TLRS 1 thru 4
Transportable Laser Ranging
System
NASA, USA



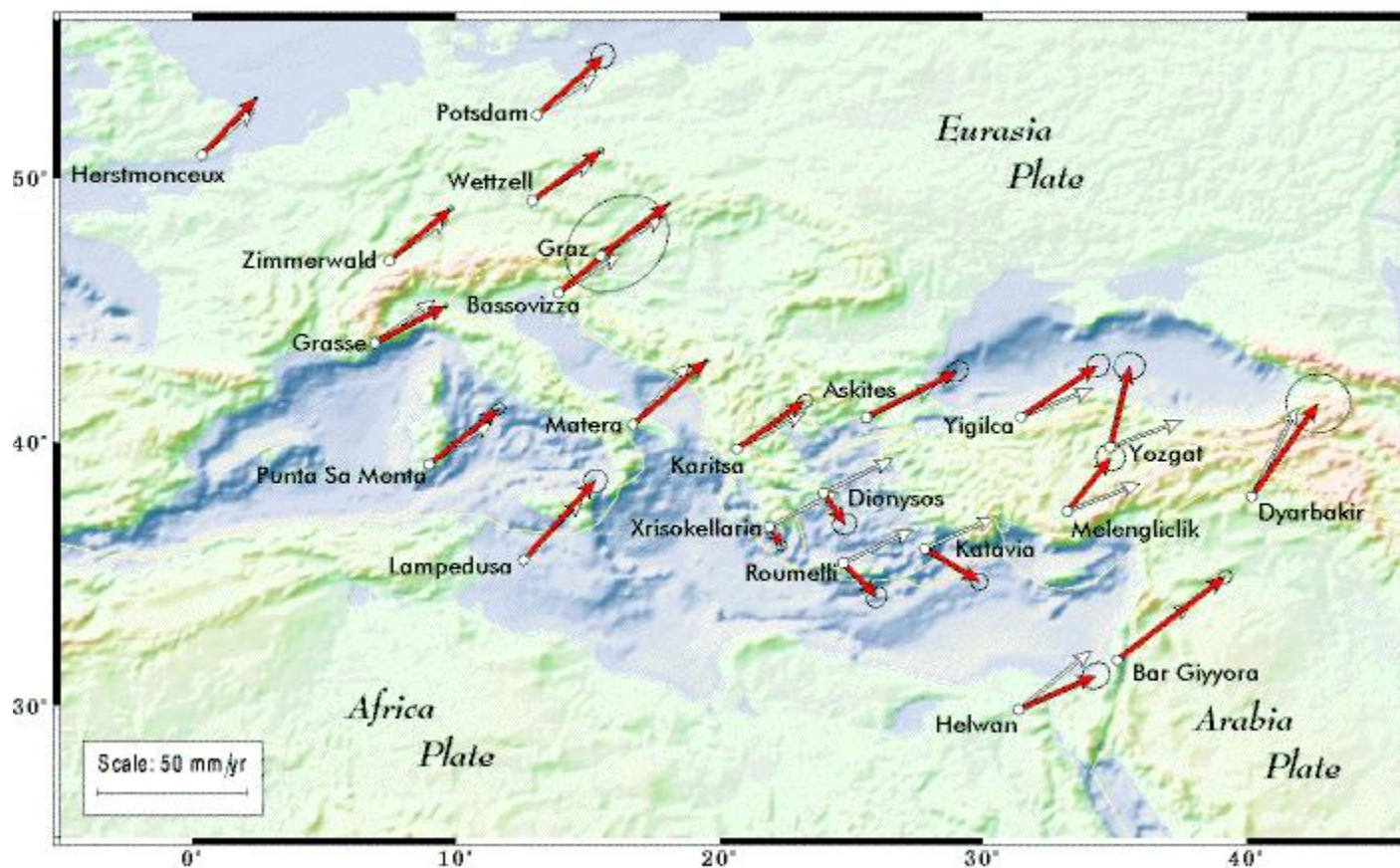
MTLRS 1 & 2
Modular Transportable
Laser Ranging System
Germany, Netherlands

The transportable systems allowed SLR measurements to be carried out from several sites during campaigns in Europe and North America during the 1970s and 1980s. With the advent of GNSS networks (GPS, GLONASS, GALILEO, etc), the transportables have since been retired or assigned to permanent locations.

SLR Site Motion in Europe

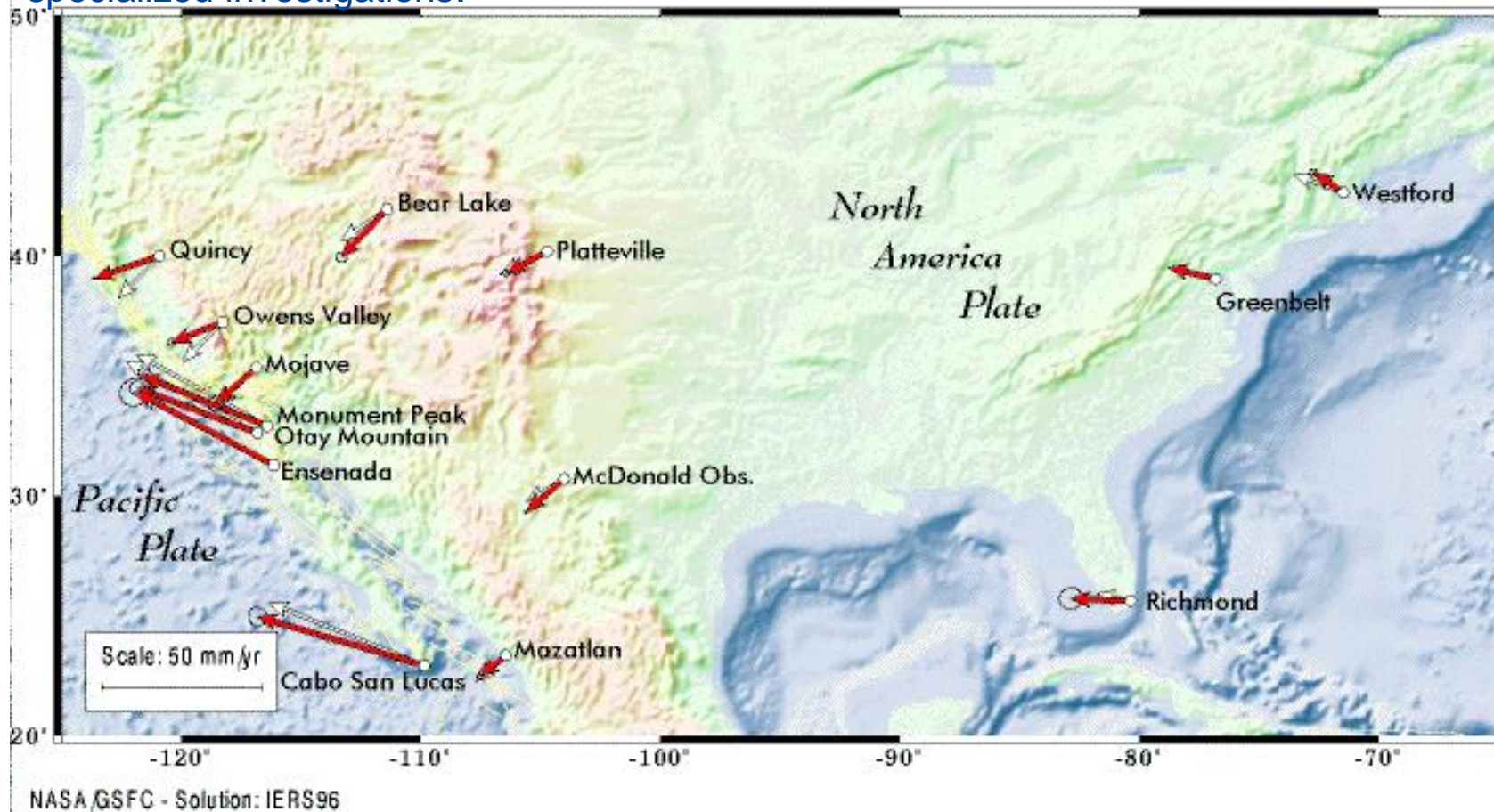
CDP/WEGENER-MEDLAS Campaigns

US and European SLR transportables routinely alternated between sites in the Western US and the Mediterranean to monitor the complex motions near major fault lines.



CDP/WEGENER Campaigns

Regional deformation measurements were enabled by the development of highly transportable SLR stations in the US and Europe. This function has since been largely taken over by GPS with most SLR transportables now either in fixed locations or doing specialized investigations.

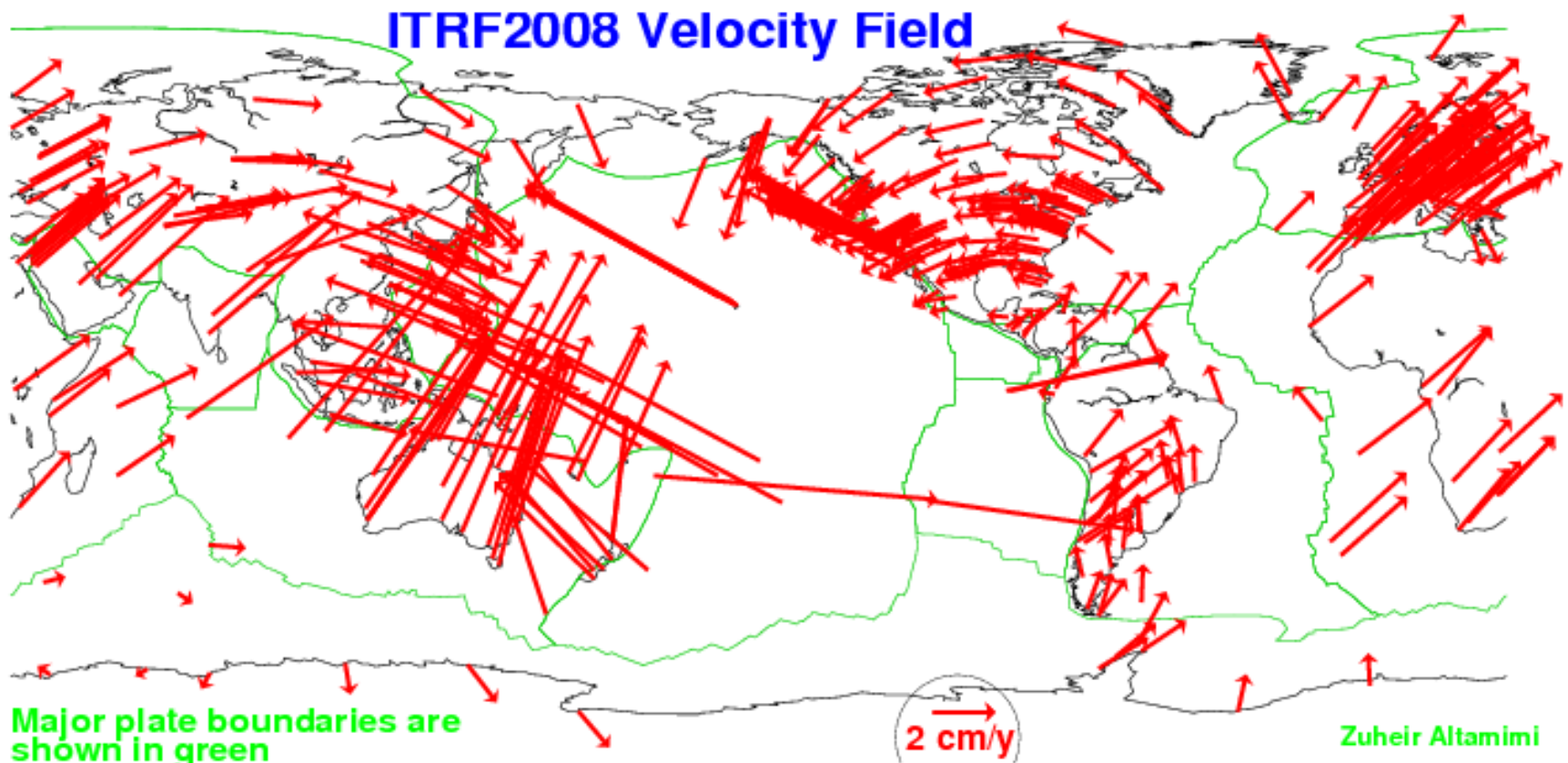




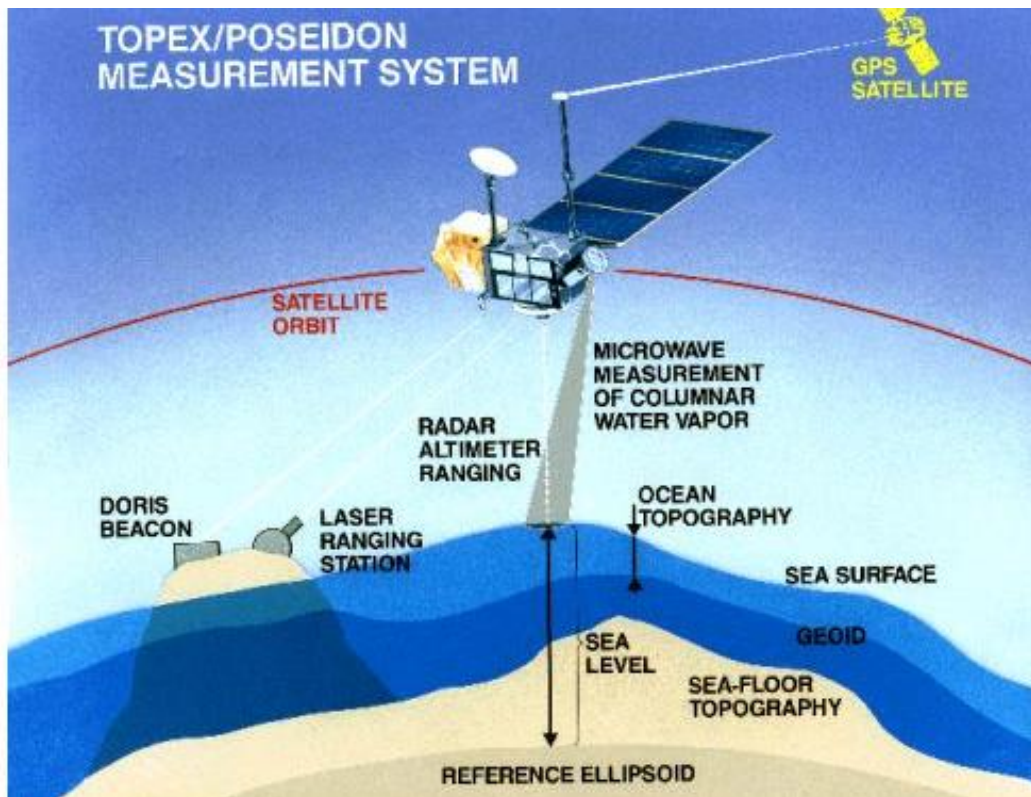
Global Tectonic Plate Motion



The addition of relatively inexpensive GNSS ground networks (GPS, GLONASS, Galileo, etc.) and DORIS to the earlier SLR and VLBI networks over the past two decades has greatly densified the measurement of global tectonic plate motion and associated regional crustal deformation near plate boundaries.



Radar altimetry on GeoSat, ERS-1, TOPEX/Poseidon, ERS-2, GFO, and JASON satellites, all tracked by SLR



- “Ocean Topography” (OT) is defined as the height difference between the sea surface and the geoid (sum of gravity and Earth rotation effects)
- In the Northern hemisphere, currents flow CW around topographic highs and CCW around lows. The reverse is true in the Southern Hemisphere
- Height of the OT is proportional to the speed of the surface currents.
- Radar altimeter measures the distance between the sea surface and the spacecraft on a global scale
- SLR provides:
 - Cm accuracy SLR station locations relative to Geocenter
 - Moderate to long wavelength geoid surface relative to geocenter
 - Cm accuracy positioning of the TOPEX/Poseidon satellite in geocentric reference frame

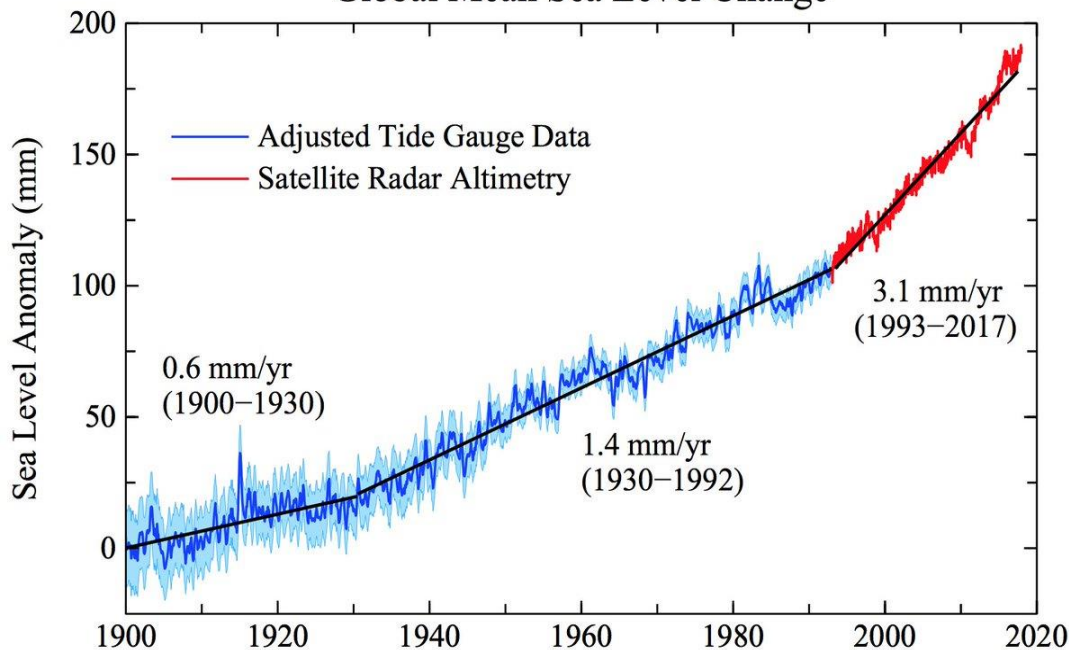
$$OT = \text{Satellite Distance from Geocenter (SLR)} - \text{Local Geoid (SLR/Alt)} - \text{Altimeter Range}$$



Global Mean Sea Level Rise



Global Mean Sea Level Change



Contributors to Sea Level Change

- variations in sea water temperature and salinity at all depths
- Tectonic changes to the water basin “shape”
- change of the ocean mass as a result of exchanges of water with the other surface reservoirs (atmosphere, continental waters, melting glaciers and ice sheets).

SLR tracking of radar altimetry satellites (Topex/Poseidon, Jason-1, and Jason-2) since 1992

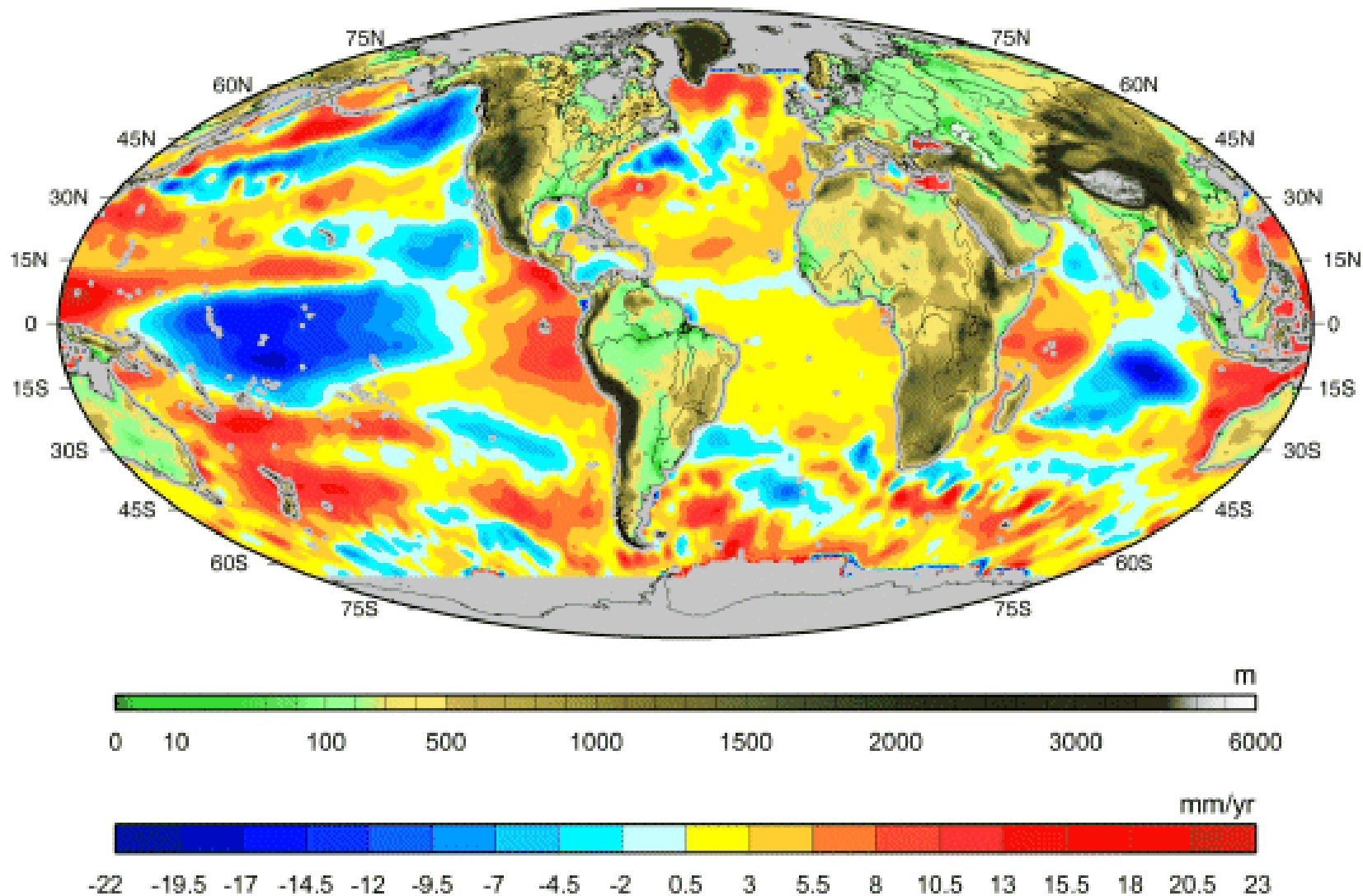
70 mm rise in Mean Sea Level from 1992 to 2014 (22 years) yields rate of 3.17 ± 0.4 mm/yr

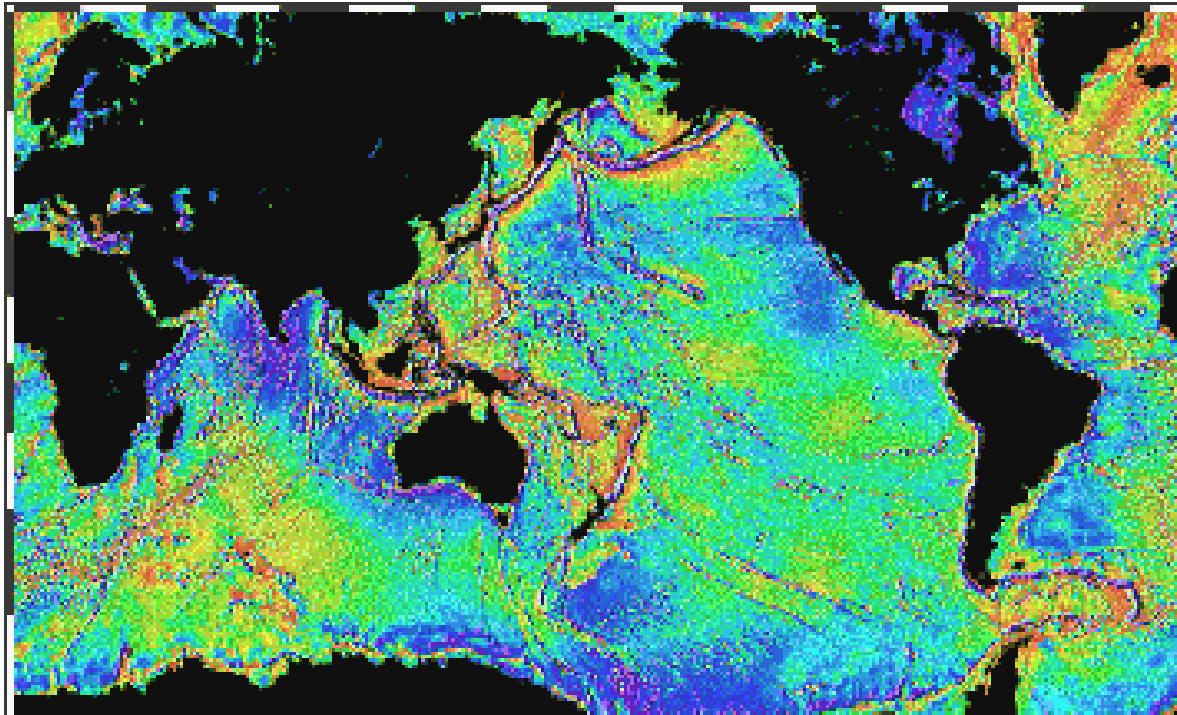
Tide Gauge Drawbacks

- Prior to the launch of the oceanographic satellites, tide gauges were used to estimate sea level rise
- Sparse geographical distribution provides very poor sampling of the ocean basins,
 - They measure sea level relative to the land, hence recording vertical crustal motions that may be of the same order of magnitude as the sea level variation.

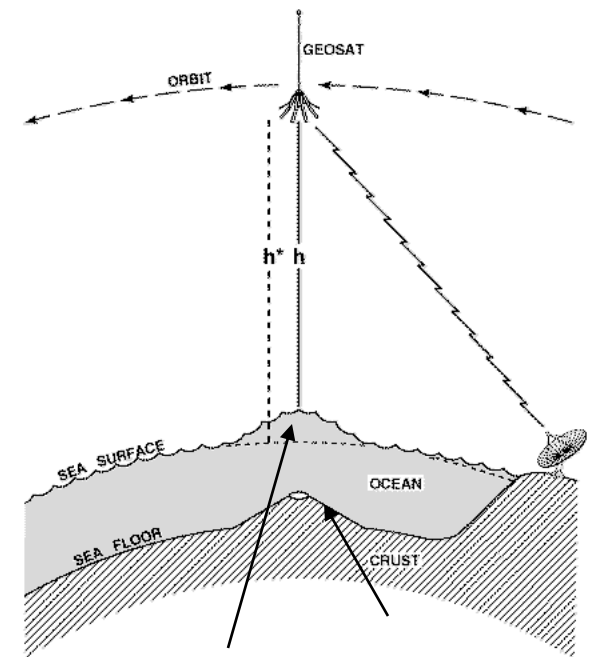


Spatially Resolved Global Sea Level Rise





Ocean floor topography from Geosat and ERS-1 radar altimetry obtained with SLR tracking only
(David Sandwell and Walter Smith)



Approximately 1000:1
ratio in heights
(1 km sea mount creates
~1 m bump in sea level)



Spaceborne Laser Altimetry

(adapted from J. B. Abshire, GSFC)



Compared to microwave altimeters, lasers have much better spatial resolution and range precision. Until the launch of ICESat-2 by NASA in September 2018, spaceborne laser altimeters utilized 2nd generation SLR technology.

Apollo, - Moon
NASA (1971-1972)
Ruby laser,
5,000 shots



Clementine - Moon
LLNL/NRL (1994)
Nd:YAG laser,
~72,000 shots



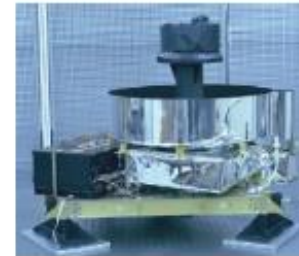
SELENE/LALT - Moon
Japan (2007-present)
Nd:YAG laser,



Chang'E - Moon
China (2007-present)
Nd:YAG laser



MGSMOLA - Mars
NASA GSFC (1992,
1996 -2000)
Nd:YAG laser,
670 Million shots



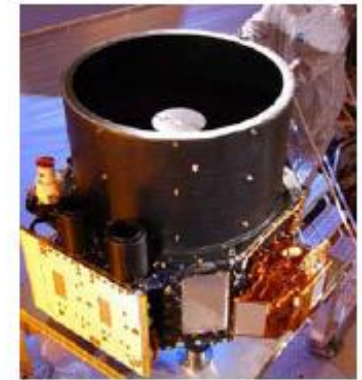
NEAR/NLR - Eros
JHU/APL (96-2001)
Nd:YAG laser,
11 Million shots



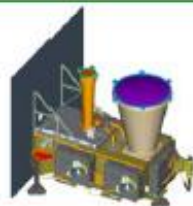
MESSENGER/MLA - Mercury
NASA GSFC (2004-2012)
Nd:YAG laser,
12M shots (planned)



CALIPSO/CALIOP - Earth
NASA LaRC/ Ball Aerospace
(2006-present)
2 Nd:YAG lasers,
> 2B shots to date

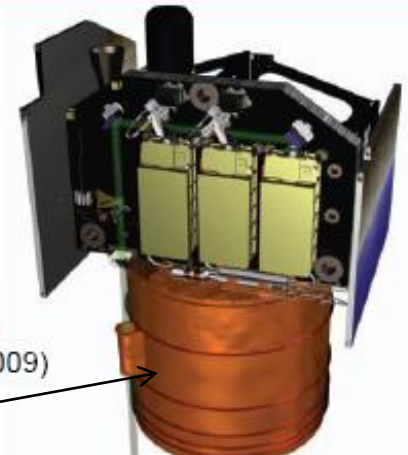


LRO/LOLA - Moon
NASA GSFC (2008-now)
Nd:YAG laser,
>1 Billion shots



Hayabusa -Itokawa
Japan (2003)

ICESat/GLAS - Earth
NASA GSFC (2003-2009)
3 Nd:YAG lasers
1.98 Billion shots



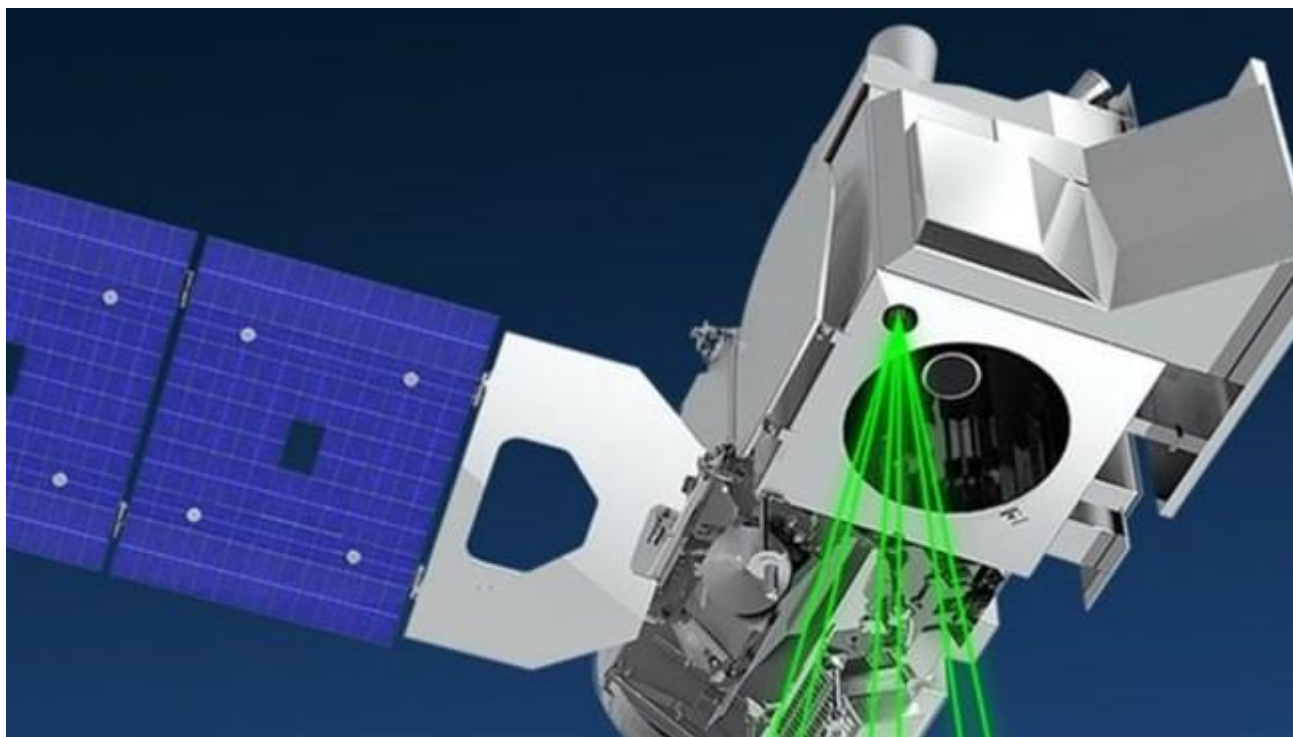


NASA ICESat-2



Advanced Topographic Laser Altimeter System (ATLAS) on ICESat-2 (NASA- Launched into Earth orbit September 2018)

- 6 beams @ 10 kHz = 60,000 surface measurements per second compared to 40/sec for ICESat-1
- Tracked by SLR and has already made over 1 trillion surface measurements

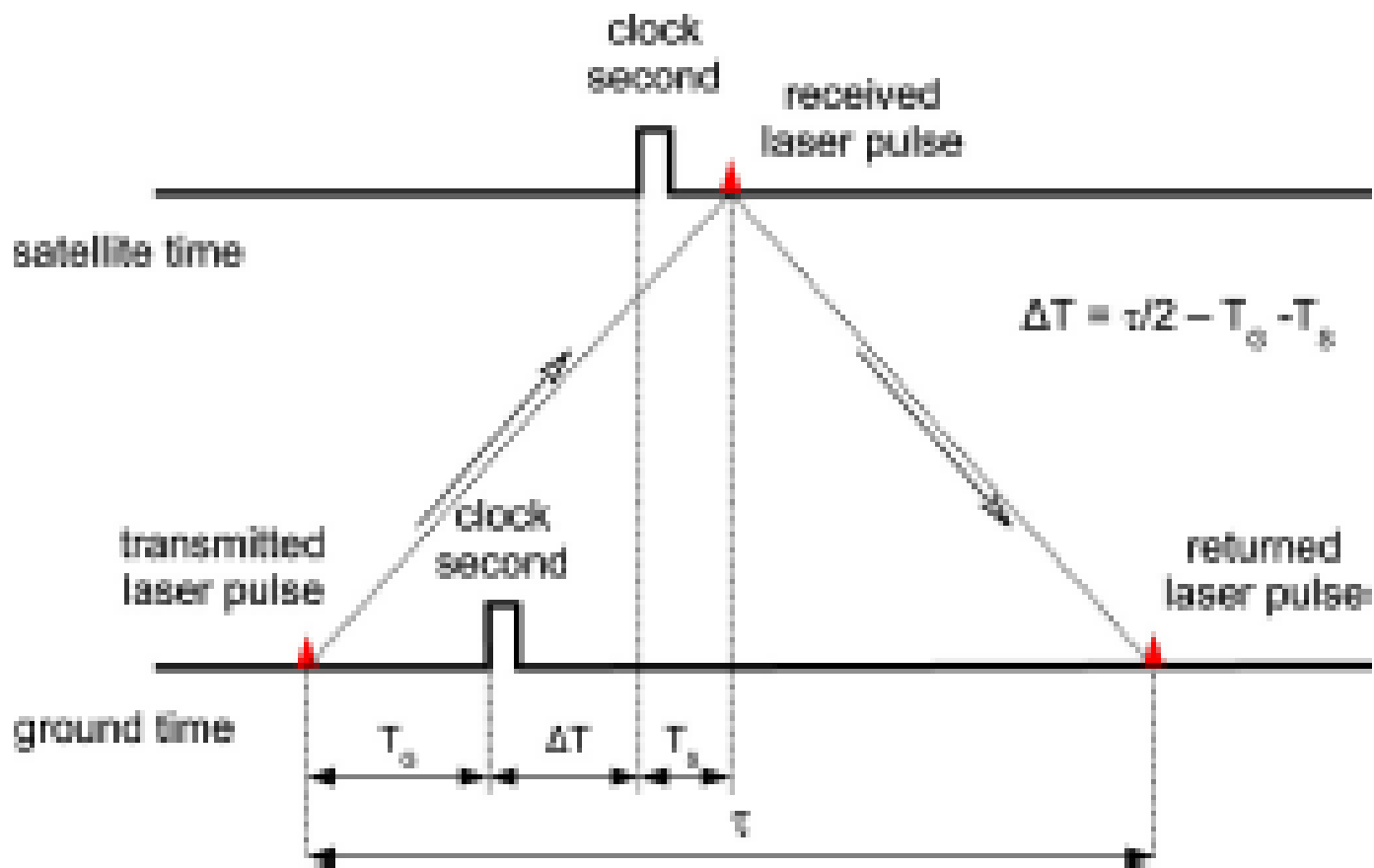




Some LLR Applications



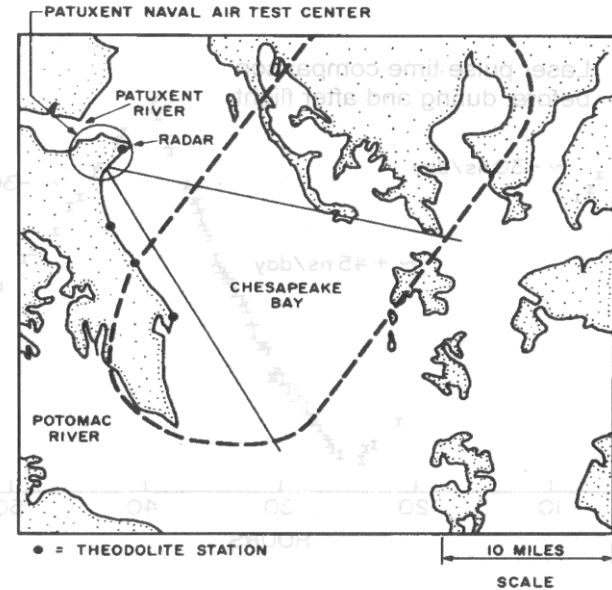
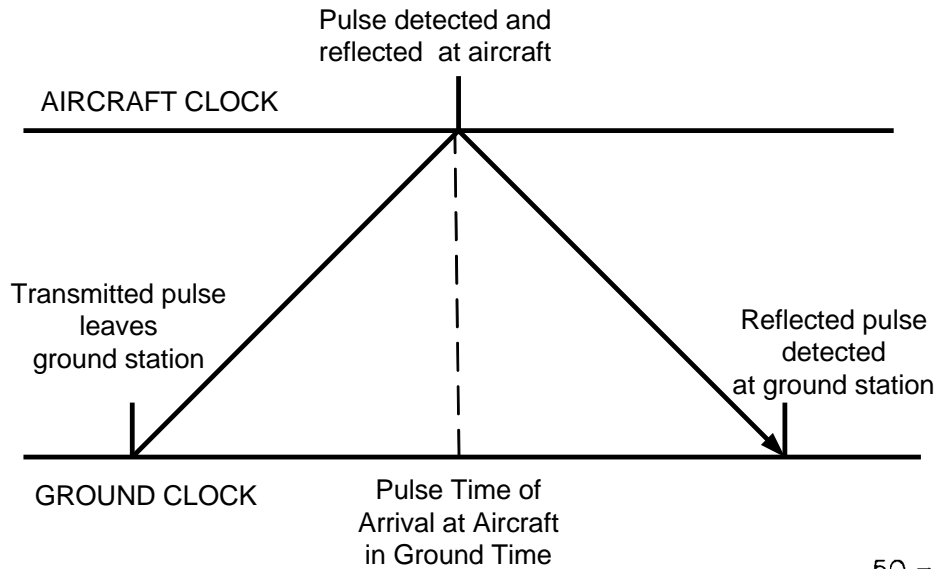
- **Lunar Physics (LLR)**
 - Centimeter accuracy lunar ephemerides
 - Lunar librations (variations from uniform rotation)
 - Lunar tidal displacements
 - Lunar mass distribution
 - Secular deceleration due to tidal dissipation in Earth's oceans
 - Measurement of $G(M_E + M_M)$
- **Solar System Reference Frame (LLR)**
 - Dynamic equinox
 - Obliquity of the Ecliptic
 - Precession constant
- **General Relativity/Fundamental Physics**
 - Test/evaluate competing gravitational and relativistic theories
 - LLR validates Einstein's Strong Equivalence Principle (SEP), which states that an object's movement in a gravitational field does not depend on its mass or composition.
 - Constrain β parameter in the Robertson-Walker Metric
 - Constrain time rate of change in G ($G\text{-dot}$)



The pulse time of arrival at the satellite coincides with the midpoint of the recorded ground start and stop times which allows one to compute the offset ΔT between the two clocks. If a second ground station performs the same experiment to the satellite, the time offset between the two ground clocks can be determined. Global laser time transfer experiments include L2T2 (France), Compass (China), ELT/ACES (ESA), SOTA (Japan).



Univ. of Maryland Airborne Atomic Clock Experiment (C. O. Alley et al, 1975)

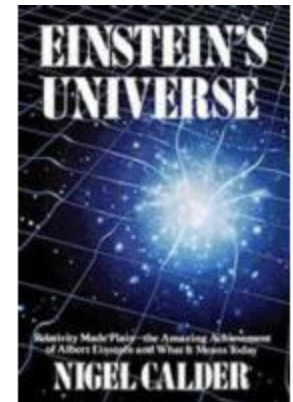
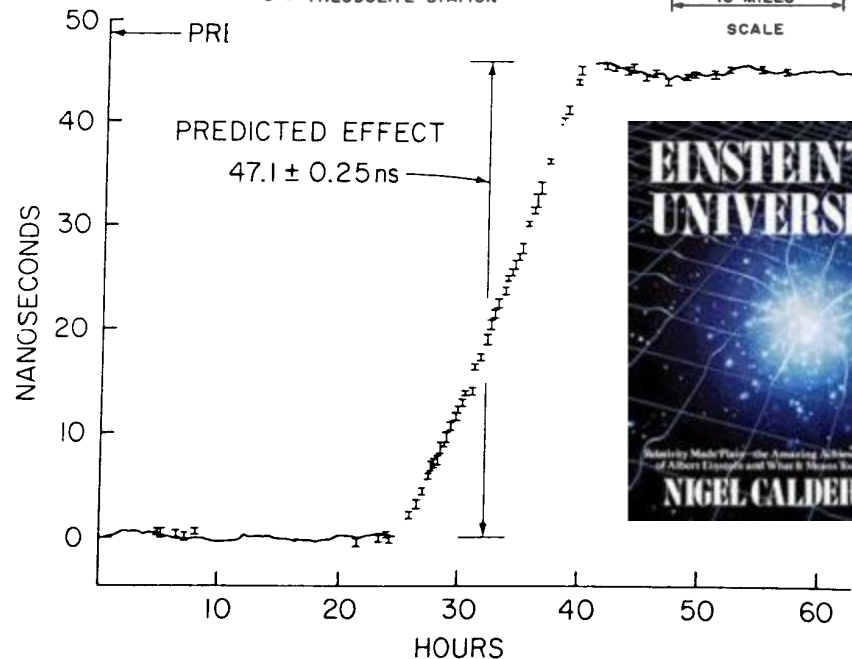


Gravitational redshift 52.8 ns

Time dilation -5.7 ns

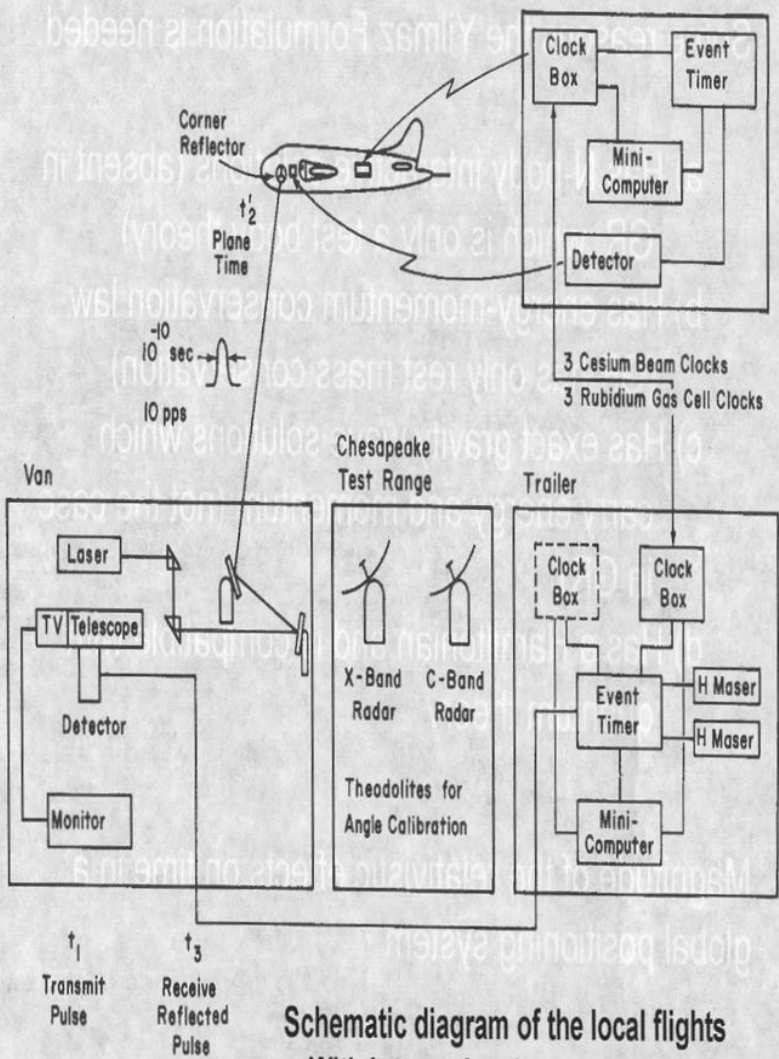
Net effect 47.1 ns

Provided validation of Einstein's theory regarding the relativistic effects of gravity and aircraft velocity on clocks over a 15 hour period!



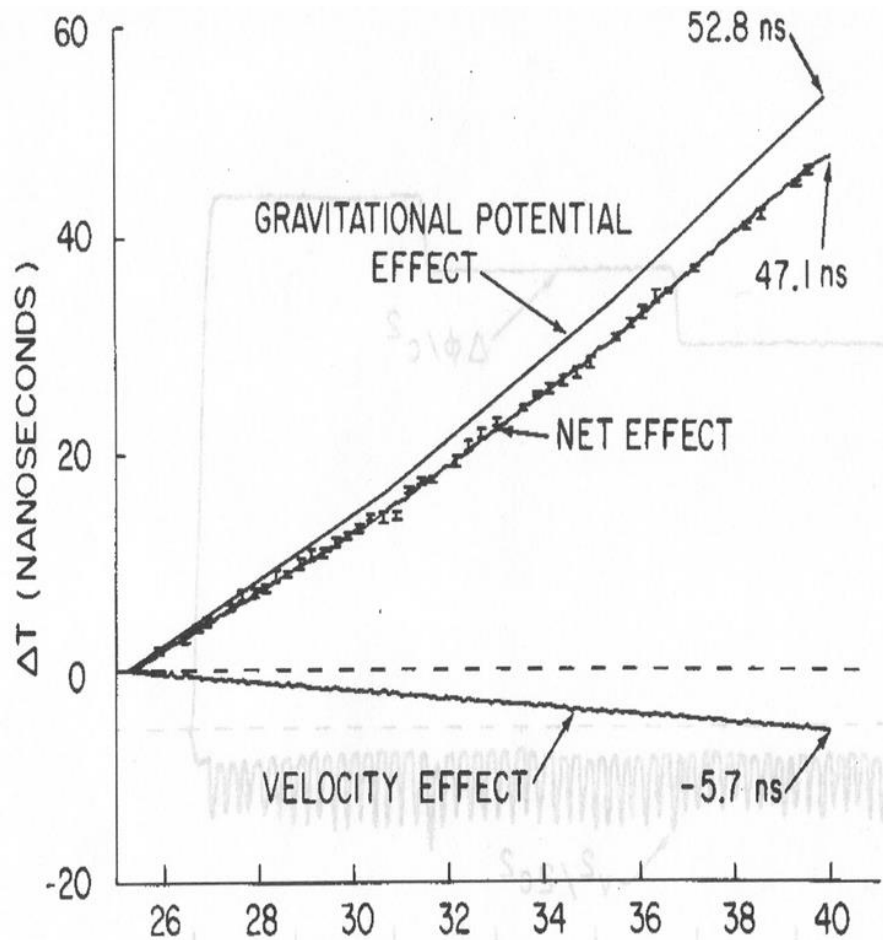


World's Most Expensive Altimeter



Schematic diagram of the local flights
With laser pulse time comparison

As the aircraft altitude increased, the gravity field weakened and the difference in the ground and airborne clocks increased!





Laser Time Transfer—operational space missions

CTU SPAD photon counters on-board of 5 satellites



China

- Compass (Beidou-2) M1
- Compass IGSO-1
- Compass IGSO-3
- Compass M3



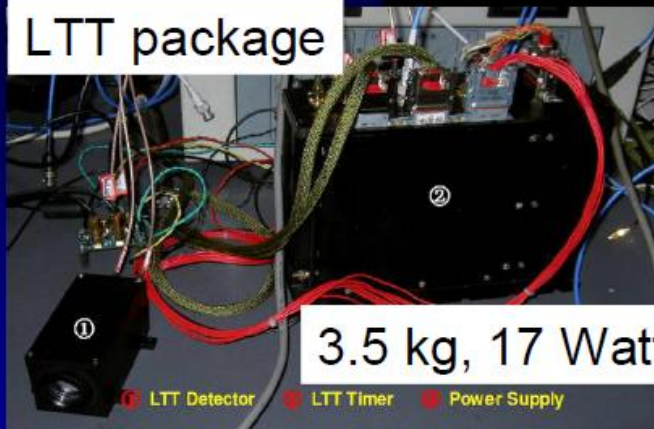
T2L2

CNES–NASA

Jason-2, 20. 6. 2008

~100 psec
absolute time
transfer

LTT package



3.5 kg, 17 Watts

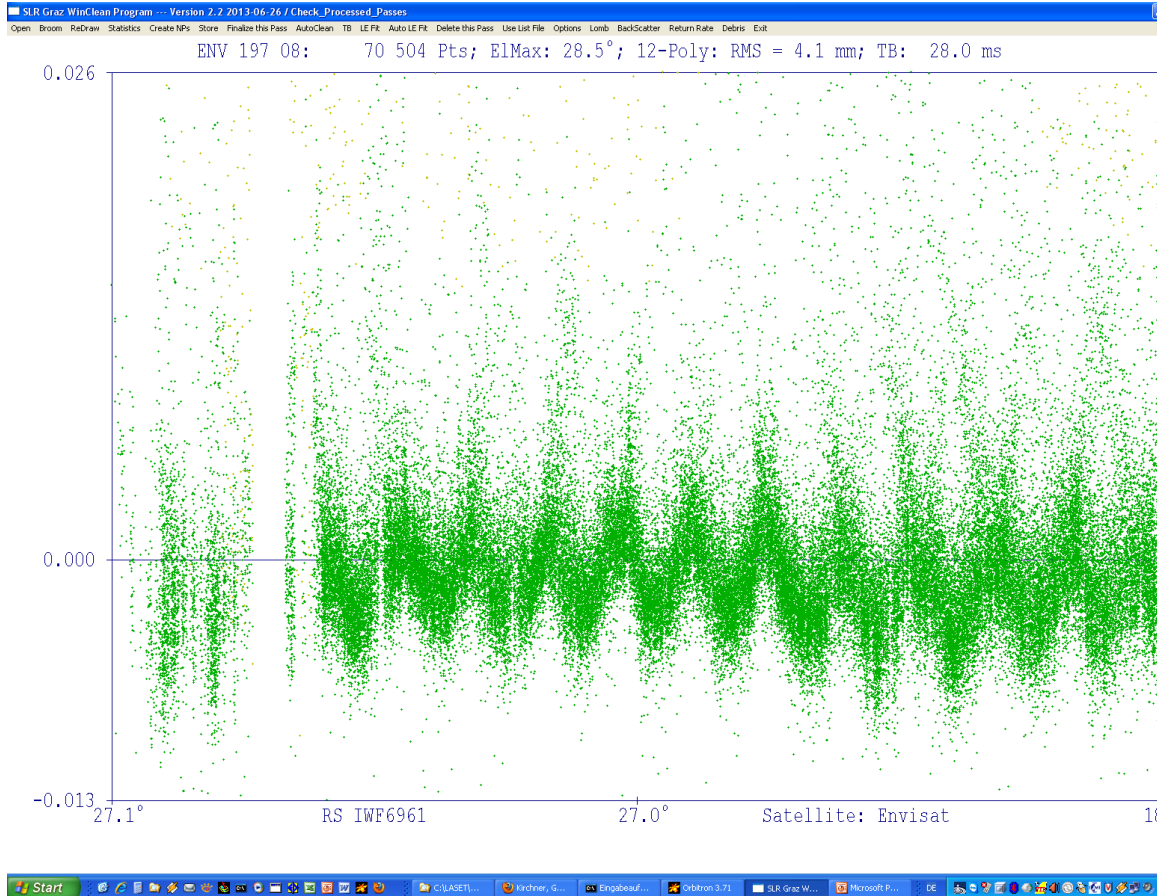
① LTT Detector ② LTT Timer ③ Power Supply





Observing Satellite Rotation with Single Photons

Courtesy: Georg Kirchner, Graz SLR, Austria



ENVISAT Retro Array

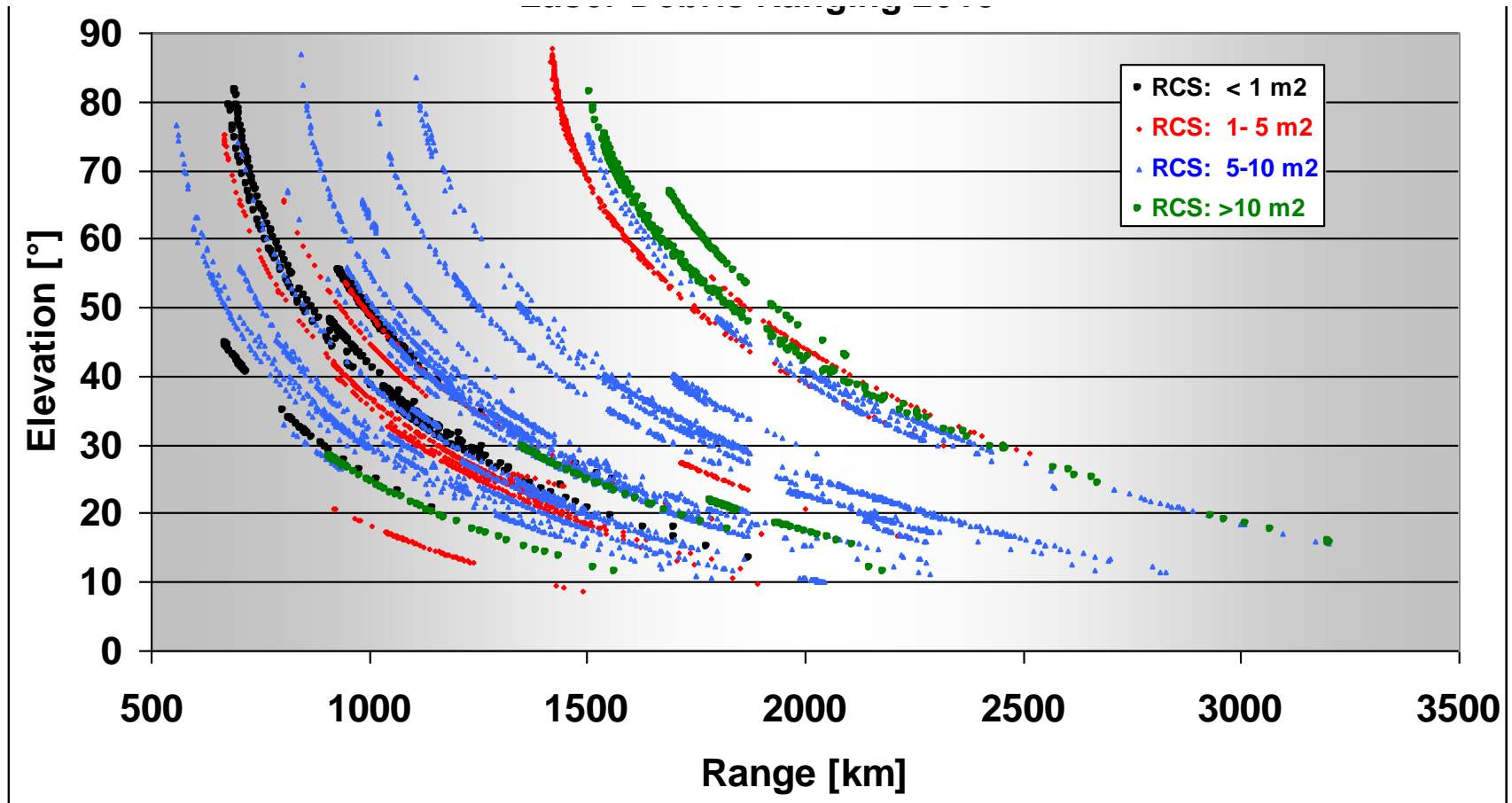
Graz Laser Characteristics:
Energy: 0.4 mJ @ 532 nm
Pulsewidth: <20 psec
Fire Rate: 2 kHz
50 cm receive telescope

Ultra short pulses at kHz rates greatly increase temporal and spatial (range) resolution and allow one to see individual retroreflectors as the satellite rotates.



Laser Debris Ranging 2013

Courtesy: Georg Kirchner, Graz, Austria



2013: In 13 Sessions – each about 2 to 3 h during early evening - >200 passes of about 60 objects measured; up to 3000 km distance . RCS = Radial Cross Section. ³³
Pulse Energy: 200 mJ; Pulsetwidth: 3 nsec; Fire Rate: 80 Hz. Flashlamp-pumped.

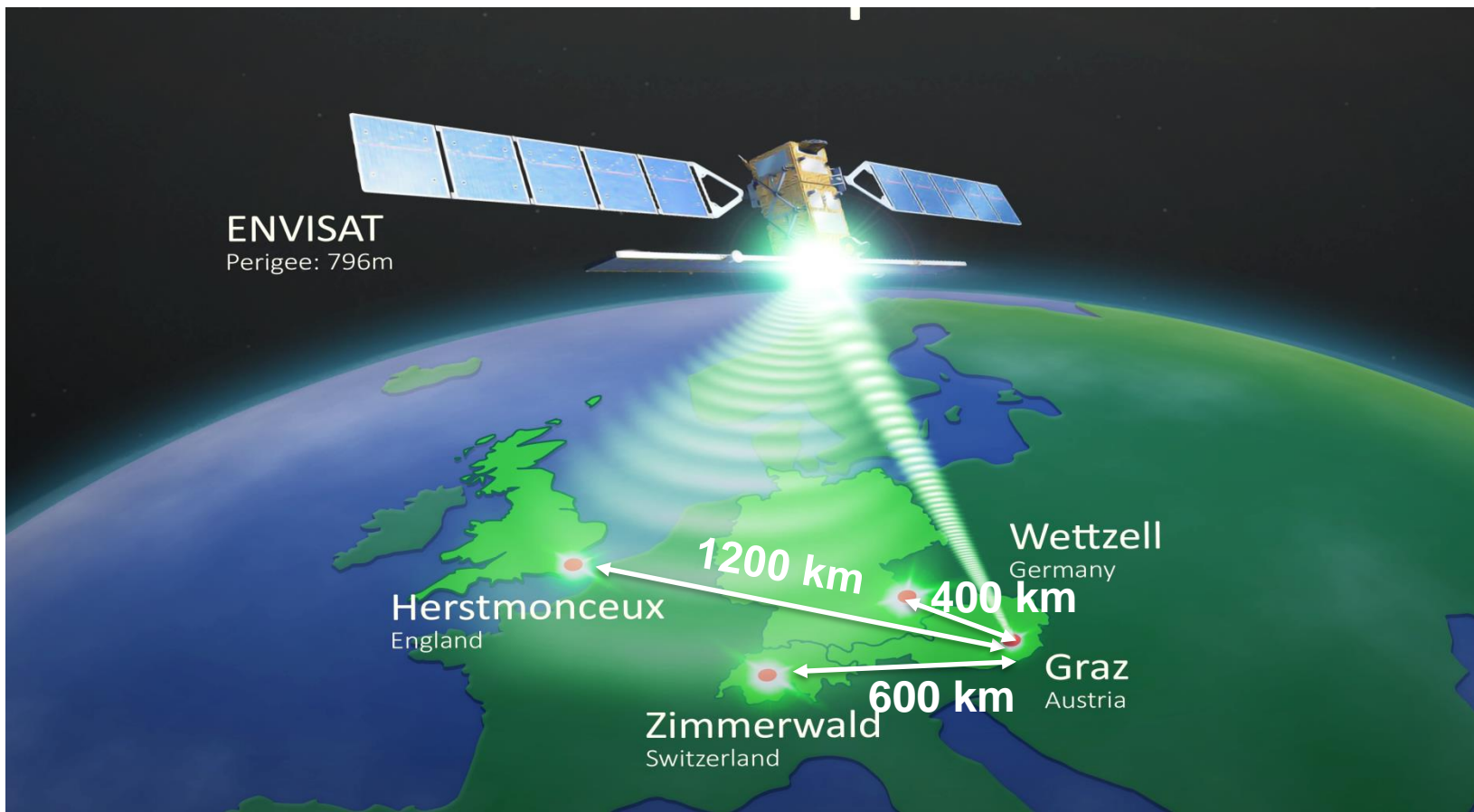


EUROPEAN MULTISTATIC EXPERIMENT

Courtesy: Georg Kirchner, Graz, Austria



Graphics: © Peter Ruzek / AIUB



SATELLITE LASER RANGING WITHOUT RETROREFLECTORS!

ONE active station (Graz) fires high energy laser pulses at a satellite with no retroreflectors. The laser photons are reflected diffusely from the satellite and the weak reflections are detected and timed at several distant passive stations equipped with single photon sensitive detectors.

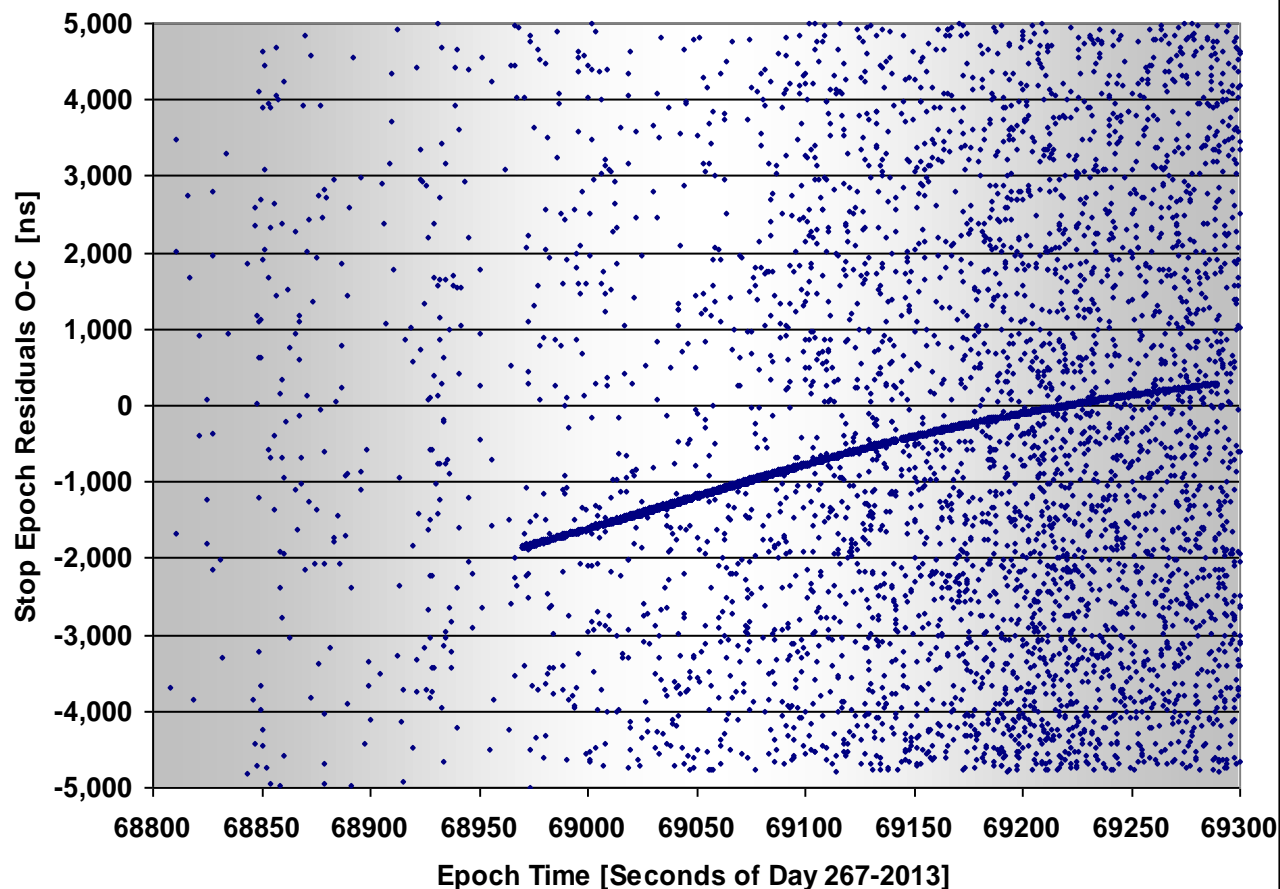


Austrian Photons off Space Debris Detected in Germany

Courtesy: Georg Kirchner, Graz SLR



WETTZELL detects Graz Photons 2013-09-24 007 / SL-16 R/B (23088); RCS: 11.2 m²



- Example: Graz fires to an old rocket body: 11 m² Radar Cross Section (RCS)
- Photons are reflected diffusely and detected in Wetzell: Clear signal visible ...
- Distance: 1800 to 2500 km
Elevation: 20° to 10° ↓
(as seen from Graz)
- Debris Laser Firing Rate: 80 Hz
- Maximum Pulse Energy 200 mJ @ 532 nm
- Laser Pulwidth: 3 nsec
- Flashlamp Pumped



Some Transponder Applications



- **Solar System Science**

- Solar Physics: gravity field, internal mass distribution and rotation
- Few mm accuracy lunar ephemerides and librations
 - Improves ranging accuracy and temporal sampling over current lunar laser ranging (LLR) operations to Apollo retroreflectors on the Moon with small, low energy, ground stations
- Decimeter to mm accuracy planetary ephemerides
- Mass distribution within the asteroid belt

- **General Relativity**

- Provides more accurate (2 to 3 orders of magnitude) tests of relativity and constraints on its metrics than LLR or microwave radar ranging to the planets, e.g.
 - Precession of Mercury's perihelion
 - Constraints on the magnitude of $G\dot{}$ (1×10^{-12} from LLR)
 - Gravitational and velocity effects on spacecraft clocks
 - Shapiro Time Delay

- **Lunar and Planetary Mission Operations**

- Decimeter to mm accuracy spacecraft ranging
- Calibration/validation/backup for Deep Space Network (DSN) microwave tracking
- Subnanosecond transfer of GPS time to interplanetary spacecraft for improved synchronization of Earth/spacecraft operations
- Transponder is a pathfinder technology for interplanetary optical communications and can serve as an independent self-locking beacon for collocated laser communications systems



Summary: Science Impact of SLR/LLR



- **Centimeter Accuracy Orbits**
 - Test/calibrate microwave navigation techniques (e.g., GPS, GLONASS, DORIS, PRARE)
 - Supports microwave and laser altimetry missions for global land topography, sea level, polar ice, and tree biomass measurements. (TOPEX/Poseidon, ERS 1&2, GFO, JASON, ICESats 1&2)
 - Support gravity missions (e.g. CHAMP, GRACE, Gravity Probe B)
- **Terrestrial Reference Frame**
 - Geocenter motion
 - Scale (GM)
 - 3-D station positions and velocities
- **Earth Gravity Field**
 - Static medium to long wavelength components
 - Time variation in long wavelength components due to mass redistributions within the solid Earth, oceans, cryosphere, and atmosphere
 - Free Air/Bouguer gravity
 - Atmospheric Drag & Radiation Pressure Models
- **Geodynamics**
 - Tectonic plate motion
 - Regional crustal deformation at plate boundaries
- **Earth Orientation Parameters (EOP)**
 - Polar motion
 - Length of Day (LOD)
- **Global Time Transfer**
- **Laser Altimetry/3D Imaging Lidar**
- **Lunar Physics (LLR)**
 - Centimeter accuracy lunar ephemerides
 - Lunar librations (variations from uniform rotation)
 - Lunar tidal displacements
 - Lunar mass distribution
 - Secular deceleration due to tidal dissipation in Earth's oceans
 - Measurement of $G(M_E + M_M)$
- **General Relativity**
 - Test/evaluate competing theories
 - Support atomic clock experiments in aircraft and spacecraft
 - LLR validates Strong Equivalence Principle (SEP)
 - Constrain β parameter in the Robertson-Walker Metric
 - Constrains time rate of change in G ($G\text{-dot}$)
 - Measure Lense-Thirring Frame Dragging Effect (LAGEOS 1 and 2)
- **Solar System Reference Frame (LLR)**
 - Dynamic equinox
 - Obliquity of the Ecliptic
 - Precession constant
- **Interplanetary Ranging, Time Transfer and Communications**
 - Two-way interplanetary ranging and time transfer for improved navigation/control of spacecraft
 - Solar System Science and improved General Relativity Experiments
 - SLR stations and constellation can also support interplanetary laser communication development